ISSN 2708-6437(Online)
2708-6429(Print)

Journal of Engineering Advancements

Editor-in-Chief:
Prof. Dr. Mohammad Mashud

Volume 02 Issue 01

SciEn

Published by:
SciEn Publishing Group

Journal of Engineering Advancements
Apt. # 6 C-D, House # 191
Road # 9/A, Dhanmondi R/A
Dhaka-1209, Bangladesh
Email: jea@scienpg.com Website: www.scienpg.com/jea/

Published in: March 2021
Published by: SciEn Publishing Group

Price: Each Issue BDT 200.00 (US$ 15) **ISSN:** 2708-6437 (Online) 2708-6429 (Print)

Journal of Engineering Advancements

Volume 02, Issue 01 March 2021

CONTENTS

Original Articles

This page is intentionally left blank.

Journal of Engineering Advancements

Published by: SciEn Publishing Group

Apt. # 6 C-D, House # 191, Road # 9/A
Dhanmondi, Dhaka-1209, Bangladesh
Email Address: jea@scienpg.com

www.scienpg.com/jea/

This page is left intentionally blank

SciEn
Journal of Engineering Advancements Vol. 02(01) 2021, pp 01-06 https://doi.org/10.38032/jea.2021.01.001

Improved Mean Shift Algorithm for Maximizing Clustering Accuracy

Chinmay Bepery[1,], Shaneworn Bhadra[1], Md. Mahbubur Rahman[1], Mihir Kanti Sarkar[2] and Mohammad Jamal Hossain[1]*

[1]Department of Computer Science and Information Technology, Patuakhali Science and Technology University, Patuakhali-8602, Bangladesh
[2]Ministry of Housing and Public Works, Bangladesh

Received: November 26, 2020, Revised: December 29, 2020, Accepted: December 31, 2020, Available Online: January 02, 2021

ABSTRACT

Clustering is a machine learning method that can group similar data points. Mean Shift (MS) is a fixed window-based clustering algorithm, which calculates the number of clusters automatically but cannot guarantee the convergence of the algorithm. The main drawback of the Mean Shift Algorithm is that the algorithm requires to set a stopping criterion (threshold point) otherwise all clusters move towards one cluster and fixed bandwidth is used here. It cannot define the upper bound of iteration numbers and need to set the iteration numbers. This paper proposed a new Mean Shift Algorithm, called Improved Mean Shift (IMS) algorithm, which overcomes the all defined pitfalls of Mean Shift Algorithm. The IMS process KD-tree data structure was used to sort the dataset and all data points as initial cluster centroids without a random selection of initial centroids. In each iteration, it shifts the variable bandwidth sliding window to the actual data point nearest to the mean using k-nearest neighbours (kNN) algorithm and finds the number of clusters automatically. Also, this paper handles the missing values using Mean Imputation (MI). The IMS algorithm produces better results than the Mean Shift Algorithm on both synthetic and real datasets.

Keywords: Clustering; Mean Shift; KD-tree; kNN; Mean Imputation.

1. Introduction

Data mining becomes a very popular decision support technique where we can extract hidden, unknown and valuable knowledge among the large amount of data [1]. Clustering must be a significant application of data mining that ensures the grouping of data points where similar groups contain mostly similar types of data points and different groups contain highly dissimilar types of data points. Nowadays, the speedily rising computer technology produced many large volume and highly dimensional datasets [2]. Clustering is an essential part of data analysis that can ensure the partition of data points where similar objects should be in the same cluster [3].

Mean Shift (MS) is an iterative, non-parametric fixed bandwidth clustering method used widely in many applications. Fukunaga and Hostetler proposed this algorithm in 1975 that introduced for locating dense areas of data points using sliding window [4]. The main advantage of Mean Shift (MS) method is that it does not want the previous knowledge about the number of clusters and does not constrain the clusters shape. Missing values in dataset become a great problem in the real world applications. Some methods are used to deal with this problem. Missing values in data are mainly caused by equipment failures, system errors, human errors, and so on [5]. The methods used for handling missing values are divided into two categories. First one is case deletion method: In this method, we need to delete all data points with missing values. If there are less instances with missing values, we can delete them, but if there are more missing values and delete them, the dataset becomes small and impacts the results [6]. The second one is missing data imputation technique: Here, we replace the missing values with the distribution's known value. Using this method, the IMS Algorithm can work better as like as a complete dataset because each missing value is replaced with known values. In this paper we handle missing values by Mean Imputation (MI) method where we have replaced the missing data values with the mean of all the instances in the dataset.

This paper focused on the improvement in the quality and accuracy of the Mean Shift Algorithm. Our proposed Improved Mean Shift method can define the upper bound of the iteration number, but this characteristic is missing in MS Method. In contrast to the MS algorithm, the proposed IMS does not require to set a stopping criterion (threshold point) and the number of iterations. Also, the Improved Mean Shift Algorithm provide the guarantee of convergence. We performed many experiments with Improved Mean Shift Algorithm (IMS) on synthetic and real datasets. Our proposed algorithm gives better clustering result on the selected datasets than Mean Shift Algorithm.

2. Related Works

Several methods have been proposed over the last few years to improve the quality and accuracy of the Mean Shift Algorithm. Most of the author used fixed bandwidth, and no one handles missing values problem. Also, no one defines the upper bound of the iteration number. Chunxia Xiao et al. [7] proposed an Efficient Mean-shift Clustering technique that used a reduced feature-space to improve the result. The reduced feature-space represents an adaptive clustering result of the original dataset using adaptive KD-tree structure in high dimensional feature space. But fixed bandwidth is used here, and for this reason, it's very complicated to get an optimal size bandwidth for the dataset of different size and dimension to get better clustering result. Bogdan Georgescu et al. [8] proposed a new technique called locality-sensitive-hashing (LSH) algorithm to minimize the computational complexity of adaptive Mean Shift process, but

*Corresponding Author Email Address: chinmay.cse@gmail.com

here we need to use pilot learning technique to discover the optimal parameters of the dataset. Vo Thi Ngoc Chau et al. [9] proposed a new clustering algorithm that has two parts. The first part is used to resolve the incompleteness of education data and the second part proposed a Mean Shift-based clustering approach using the nearest prototype strategy called MMS_nps. The main limitation is that it cannot automatically evaluate the bandwidth value h based on datasets' inherent characteristics. Dorin Comaniciu et al. [10] planned a Modified Mean Shift Algorithm for solving the automatic bandwidth problem (variable bandwidth). It can find an optimal bandwidth for dataset of different size and dimension to get better clustering result. But the convergence of the algorithm is not proven and need to set iteration number for clustering purpose. Loai AbdAllah et al. [11] proposed a new Mean Shift clustering technique that can handle missing values problem of datasets. They take a weighted distance function called MD_E distance with Mean Shift Algorithm instead of Euclidian distance to compute the distance between two points with missing attribute values. But need to set stopping criterion.

3. Improved Mean Shift Algorithm

In the case of the Mean Shift Algorithm, we need to set a stopping criterion (threshold point) and define the iteration number's upper bound. Also, it uses fixed bandwidth and cannot guarantee the convergence of algorithm. Our proposed Improved Mean Shift Algorithm (IMS) can solve these problems. IMS works with some following steps given below.

3.1 Handling missing values by Mean Imputation (MI)

Presence of missing values in the dataset are very common problem in real-world applications. If there are less instances with missing values, we can delete them. But if there are more instances with missing values and delete them, the dataset becomes small and the characteristics of datasets become change. Due to this missing value the performance and accuracy of algorithm decrease heavily. The Mean Imputation (MI) method is used here to replace the missing values to solve this problem.

Mean Imputation (MI): Replace the missing values with the mean of all the instances in each column.

3.2 KD-tree for Data Partition

KD-tree is a binary search tree where the data points are organized in K-dimensional feature space [12]. KD-tree is used in this paper in order to store and represent the dataset in a data structure. A non-leaf node in KD-tree divides the feature space into two parts where points in the left of this space are defined by left subtree of that node and points to the right of the space by the right subtree [13]. Suppose we have two Dimensional data (x,y) showing in Table 1.

Table 1 2D Dataset for KD-tree.

Data points	x	y
Data_point1	0.67	0.97
Data_point2	0.33	0.76
Data_point3	0.40	0.68
Data_point4	0.12	0.56
Data_point5	0.60	0.30
Data_point6	0.28	0.72
Data_point7	0.83	0.73

Firstly, we divide the data points into two parts by comparing each x value with root of x. Root(x) = Max(x) + Min(x)/2= (0.83 + 0.12)/2= 0.48. Next label we compare dividing two groups y values with root of y. Root(y) = Max(y) + Min(y)/2. Repeat this until fulfill the condition. Every node has three things such as (1). Dimension, (2). Value and (3). Tightest bounding box.

Table 2 Tight bounds for node _1 and node_ 2.

Tight bounds	x	y
Node _1	0.11 <= x <= 0.42	0.53 <= y <= 0.75
Node_ 2	0.54 <= x<= 0.96	0.29 <= y <= 0.93

Table 2 shows the tightest bounds area for node_1 and node_2. Similarly, divide the data structure into more parts on the basis of dimensions until each leaf node holds maximum two data points.

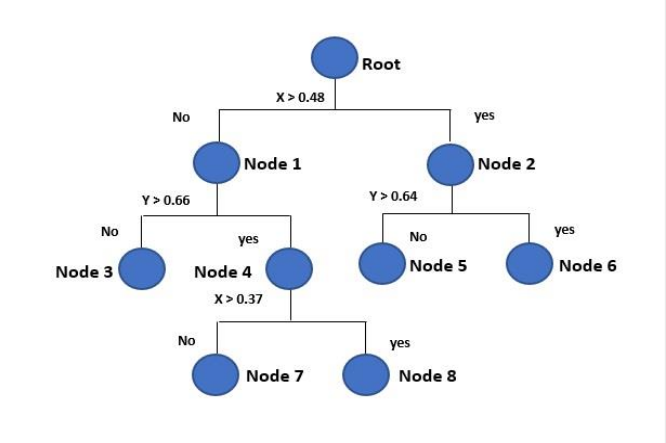

Fig. 1 KD-tree for TABLE I dataset.

Fig. 1 displays the visual representation of sorted data for Table 1. At first, the label compares x value with the root of x. Next label compares y value with the root of y. Repeat this pattern until each leaf node holds maximum two points [14].

3.3 Improved Mean Shift Clustering

In Improved Mean Shift (IMS) algorithm, we take all data points as initial cluster centres and set variable bandwidth sliding window in each data points. In each iteration, the sliding window is moved towards higher density areas by moving the initial centers to the actual data point nearest to the mean using the KNN algorithm. Multiple sliding windows overlap when they have same mean, and then data points are clustered according to the sliding window in which they reside.

KNN algorithm is used to find the nearest data point. It first loads the data points and set the number of K. Euclidean distance is used here for distance measurement purpose. Next, we need to sort the distance and get our expected nearest expected data point.

The kernel density function is used here with Improved Mean Shift (IMS) algorithm.

Given m data objects q_j, j = 1,…,m on a d-dimensional space R_d. For m number of data points, we have m initial cluster From Fig. 3 shows that in every iteration, the sliding window

shift to new centroids by moving the initial centres to the actual data point nearest to the mean using the kNN algorithm, inside the sliding window. Multiple sliding windows overlap when they have the same mean. Finally, the data points are clustered properly by the help of the sliding window.

centroids, and the algorithm become converges at most (m-1) iterations. So there is no need to set the number of iterations. Our proposed IMS algorithm can provide the upper bound of the number iterations (i.e. m − 1) for each data point. The multivariate kernel density estimation obtained with kernel K(q) and window radius $h_j \equiv h(q_j)$ is

$$f(q_j)=\frac{1}{mh_j^{\,d}}\sum_{j=1}^{m-1}K\left(\frac{q-q_j}{h_j}\right) \quad (1)$$

For radially symmetric kernels, Kernel k(q) satisfying

$$K(q)=c_{k,d^k}(||q||^2) \quad (2)$$

where $c_{k,d}$ is defined as normalization constant that guarantees $K(q) \propto 1$ and modes of K(q) are pointing at $\nabla f(q)=0$.

The gradient of density estimator (1) is

$$\nabla f\left(q_j\right)=\frac{2c_{k,d}}{mh_j^{\,d+2}}\sum_{j=1}^{m-1}(q_j-q)g\left(\left\|\frac{q-q_j}{h_j}\right\|\right)^2$$

$$=\frac{2c_{k,d}}{mh_j^{\,d+2}}\left[\sum_{j=1}^{m-1}g\left(\left\|\frac{q-q_j}{h_j}\right\|\right)^2\right]\left[\frac{\sum_{j=1}^{m-1}q_j g\left(\left\|\frac{q-q_j}{h_j}\right\|\right)^2}{\sum_{j=1}^{m-1}g\left(\left\|\frac{q-q_j}{h_j}\right\|\right)^2}-q\right] \quad (3)$$

where $g(p)=-k'(p)$. The first term of $\nabla f\left(q_j\right)$ is proportional to the density estimated at q with kernel $G(q) = c_{g,d^g}(\|q\|^2)$ and the second term is

$$m_{h_j}(q_j)=\frac{\sum_{j=1}^{m-1}q_j g\left(\left\|\frac{q-q_j}{h_j}\right\|\right)^2}{\sum_{j=1}^{m-1}g\left(\left\|\frac{q-q_j}{h_j}\right\|\right)^2}-q \quad (4)$$

defined as Improved Mean Shift with variable bandwidth hj and number of iteration (m-1). Improved Mean Shift vector always moves toward the direction of the maximum dense area.

So, the Improved Mean Shift can be obtained by

- evaluating Improved Mean Shift vector $m_{h_j}(q^t)$
- translation of sliding window $q^{t+1}=q^t+m_{h_j}(q^t)$

That provides the guarantee of convergence of the algorithm where $\nabla f\left(q_j\right)=0$.

Improved Mean Shift (IMS) mode finding process is illustrated in Fig. 2 and Fig. 3. From Fig. 2, we know that the Improved Mean Shift clustering algorithm is also a practical application of the mode finding procedure: In Improved Mean Shift clustering algorithm we first take the dataset as weighted matrix and handle the missing values using Mean imputation method. Then take all data points as initial cluster centres. Next, we should set a variable bandwidth sliding window in each data points for clustering purpose. There is no need to set the iteration numbers. For handling outliers, we also set a condition that can solve the outlier problem.

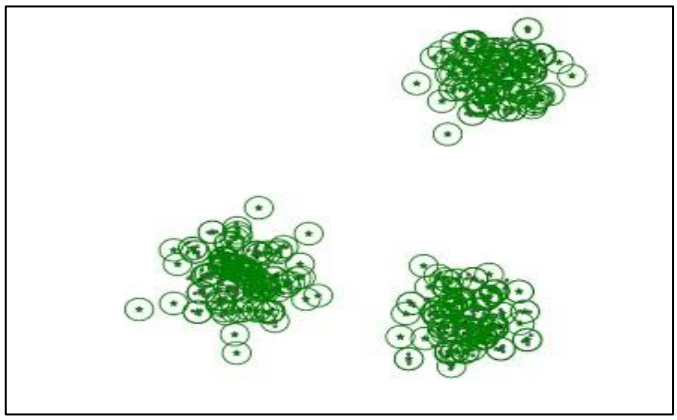

Fig. 2 Improved Mean Shift clustering procedure (take all data points as initial cluster centres).

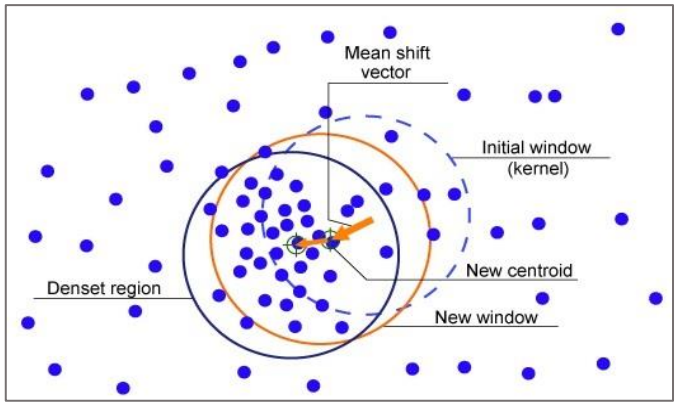

Fig. 3 Improved Mean Shift clustering procedure (shifting window).

This paper used the Gaussian KD-tree algorithm to speed up the IMS clustering process for large data sets. KD-tree algorithm partitions the datasets based on feature space in a top-down way. It begins from a root cell, and recursively split a root into two child cells adaptively along with a dimension that is alternated at successive tree levels [7].

3.4 Overview of the Algorithm

The proposed Improved Mean Shift Algorithm (IMS) works with the following steps:

Input:

A high dimensional dataset $Q=\{q_1.....q_n\}, n \geq 2$ on a d-dimensional space, Variable bandwidth h_i where i=1…n and Profile function g(q).

Output:

Clustering results $R_{1.....}R_k$, where k defined the number of clusters.

Steps:

Initialize the dataset as weighted matrix.
Use Mean Imputation for handling missing values.
Sort the dataset by KD-tree data structure.
Take all data points as initial cluster centroids.
Set variable bandwidth sliding windows in each data point.
Calculate the mean of instances lying inside the window.

Find the actual data points nearest to the mean using KNN algorithm and shift the window to that points.

Repeat till convergence and gain k number of Clusters.

Eliminate cluster that contains less than a minimum number of data points based on the condition for handling outliers.

4. Experiments

In the experimental area, we show the calculated results of our proposed IMS algorithm on synthetic and real datasets to measure IMS's performance compared with the Mean Shift Algorithm.

4.1 Datasets

The IMS algorithm operates on both synthetic and real datasets to measure the clustering output. The synthetic datasets are made by using Gaussian distribution [15]. Here we have used ten synthetic datasets of different size. The synthetic datasets are shown in Table 3. Dataset are characterized by instance number q, cluster number k and the feature number n.

Table 3 Characteristics of synthetic datasets.

Serial Number	Synthetic Dataset	Instance (q)	Feature (n)	Cluster (k)
1	S_data1	1000	2	3
2	S_data2	3000	2	3
3	S_data3	5000	2	3
4	S_data4	10000	2	5
5	S_data5	1500	5	3
6	S_data6	2500	10	5
7	S_data7	3500	15	10
8	S_data8	4500	15	10
9	S_data9	5500	15	10
10	S_data10	6500	20	10

Next phase, we select five real-world datasets downloaded from the UCI machine learning repository [15]. The real-world datasets are seen in Table 4.

Table 4 Characteristics of real datasets.

Serial Number	Real Datasets	Instance (q)	Feature (n)	Cluster (k)
1	Wine	178	13	3
2	Iris	150	4	3
3	Seed	210	7	3
4	Glass	214	10	6
5	Mammo	961	6	2

4.2 Experimental Settings and Evaluation Methods

To measure the clustering accuracy of IMS algorithm, we used two types of evaluation techniques in this paper. They are Purity and Rand Index defined as defined below:

Purity: Purity is a popular estimation technique that calculates the percentage of correctly classified objects. The purity range is between 0 and 1. Purity is defined as follows:

$$f(x)=\frac{1}{P}\sum_{j=1}^{n} max_n|Q_j \cap R_n| \quad (5)$$

Here (a). P defines the number of objects in datasets, (b). n defines cluster numbers, (c). Q_j defines the set of instances in cluster j, (d). R_n defines a set of objects in class n that has the highest number of intersections with cluster j, among all the clusters.

Rand Index: Rand Index is another popular evaluation technique where a set of m elements $Q=\{Q_1,\ldots..,Q_n\}$ divide into two partitions R and S to compare $R=\{R_1,\ldots..R_u\}$with u subsets and $S=\{S_1,\ldots..,S_v\}$with v subsets, define as following:

- e : defines the number of pairs in set S that are same for both R and S subsets.
- f : defines the number of pairs in set S that are different for both R and S subsets.
- g: defines the number of pairs in set S that are same in R subset and different in S subset.
- h: defines the number of pairs in set S that are different in R subset and same in S subset.

$$R=\frac{e+f}{e+f+g+h}=\frac{e+f}{\binom{m}{k}} \quad (6)$$

Intuitively e+f defines the number of agreements and g+h defines number of disagreements between R and S.

4.3 Experimental Results and Analysis

This section discusses and compares the experimental results between our proposed Improved Mean Shift (IMS) and Mean Shift Algorithm (MS). We take ten synthetic datasets and five real datasets to present the increment in clustering result using the IMS. In the MS algorithm, we need to set the number of iteration and a stopping criterion (a threshold point ϵ) otherwise all clusters may move toward one cluster. It also used fixed bandwidth, so it is tough to find an optimal sized bandwidth for different dataset to get better clustering result.

So, the convergence of Mean Shift is not proven. But in IMS, we use all data points as initial cluster centres, and if there are m data points, we need at most m-1 iterations to fulfil convergence criterion. Also, no need to establish a stopping criterion and iteration numbers and also handle outliers. Variable bandwidth, KD-tree and kNN algorithm are also used with IMS for better accuracy with better clustering result.

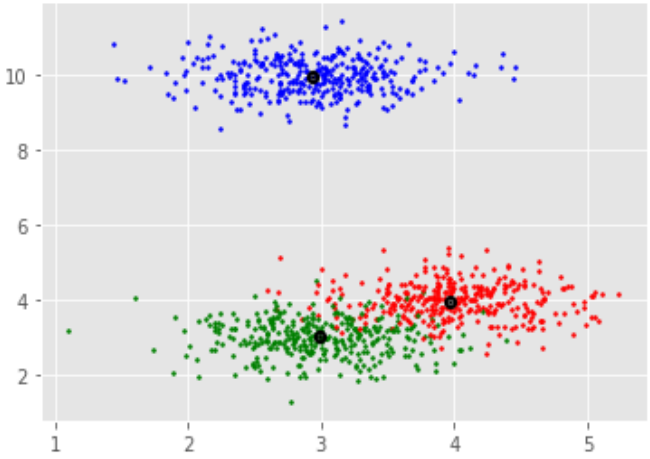

Fig. 4 Plotting of a well-distributed dataset with Mean Shift.

Fig. 4 shows the clustering results on a synthetic dataset named S_dataset1 using Mean Shift. S_dataset1 is a well-decorated dataset has 800 instances in 2D space with three clusters. We used fixed bandwidth h=1000, stopping threshold point ϵ =0.01 and number of iterations 100 for running Mean Shift Algorithm. After completing all iteration, the Mean Shift Algorithm can determine three clusters, but two clusters become ambiguous. On the contrary, in improved Mean Shift we need at most (800-1) iterations to clustered S_dataset1, and for handling outliers, we need to set a condition defined as an estimated cluster that holds more than 5 data points otherwise delete that cluster. Variable bandwidth is used here that can select bandwidth automatically.

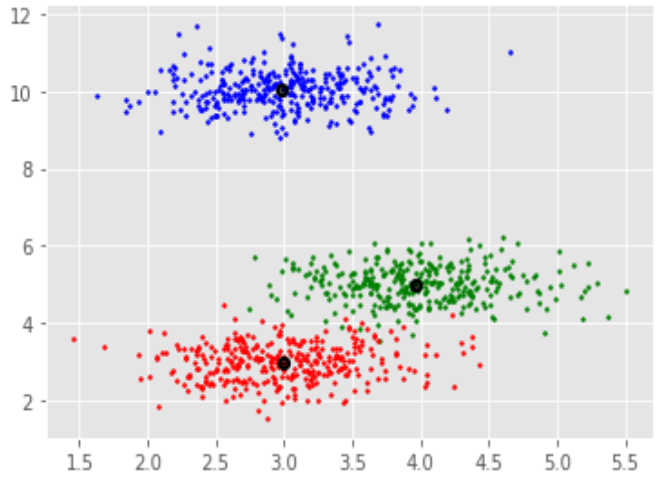

Fig. 5 Plotting of a well-distributed dataset with Improved Mean Shift.

Fig. 5 show that Improved Mean Shift can cluster the data points more correctly than the Mean Shift Algorithm. So, we can agree that IMS is far better clustering algorithm than Mean Shift.

Table 5 Comparison of clustering accuracy between Mean Shift and improved Mean Shift on synthetic datasets.

Synthetic Data	**Purity**		**Rand Index**	
	MS	***IMS***	***MS***	***IMS***
S_data1	0.791	0.802	0.789	0.810
S_data2	0.820	0.831	0.822	0.839
S_data3	0.858	0.858	0.849	0.851
S_data4	0.715	0.748	0.720	0.739
S_data5	0.775	0.789	0.768	0.780
S_data6	0.798	0.811	0.729	0.792
S_data7	0.765	0.796	0.704	0.751
S_data8	0.718	0.823	0.767	0.834
S_data9	0.709	0.799	0.818	0.851
S_data10	0.712	0.770	0.695	0.743

Table 5 presents the accuracy-test, including purity and rand index for ten synthetic datasets using both Mean Shift and Improved Mean Shift Algorithm. Here we see that S_data3 shows the almost similar result with IMS and MS. But the others show better results in accuracy test using Improved Mean Shift Algorithm than Mean Shift Algorithm. Following these explanations, it clears that our proposed IMS is far better than MS on accuracy Comparison. Python Spyder (ana) is used here for coding purpose.

Table 6 Comparison of clustering accuracy between Mean Shift and improved Mean Shift on real datasets.

Real Data	**Purity**		**Rand Index**	
	MS	***IMS***	***MS***	***IMS***
Wine	0.701	0.704	0.710	0.719
Iris	0.755	0.791	0.713	0.741
Seeds	0.696	0.719	0.633	0.674
Glass	0.661	0.679	0.512	0.552
Mammo	0.511	0.602	0.636	0.683

Table 6 presents the accuracy-test, including purity and rand index for five real datasets using both MS and IMS algorithm. Viewing these observations, we can say that our proposed IMS is far better than the Mean Shift Algorithm for these given five real datasets based on accuracy. Fig. 6 shows the comparison plot of accuracy between MS and IMS.

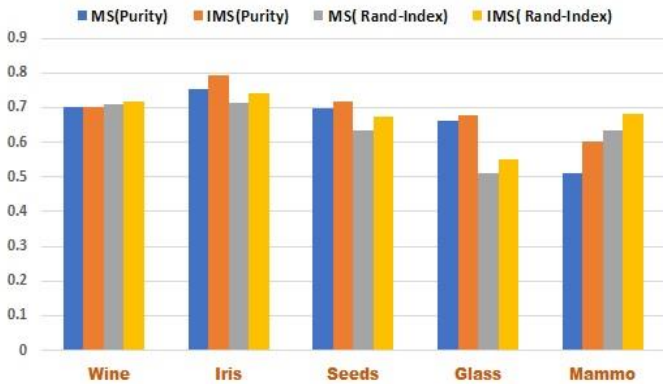

Fig. 6 Visual representation of accuracy between MS and IMS.

5. Conclusion and Future Work

Mean Shift uses fixed bandwidth, and for this reason, it is tough to find an optimal sized bandwidth for different dataset to get better clustering result. Also, it cannot guarantee the convergence of the algorithm and requires to set a stopping criterion named threshold point and the upper bound of the iteration number. But our proposed Improved Mean Shift Algorithm can solve all these problems. IMS uses all data points as initial cluster centres, and if there are n data points, we need at most m-1 iterations to being convergence. Also, set a stopping criterion is not needed here. It also eliminates cluster that contains less than a minimum number of data points based on the condition for handling outliers. Variable bandwidth sliding window, KD-tree and KNN algorithm are also used in IMS for better accuracy and better clustering results. The time complexity of our IMS is more than MS, but accuracy is much higher. So, in the future, we try to reduce our IMS algorithm's time complexity and try it on more complex datasets.

References

[1] Jiawei, H. and Micheline, K., 2005. Data Mining: Concepts and Techniques [M] Beijing. Mechanical Industry Press.

[2] Han, J. and Kamber, M., 2001."Data Mining Concepts and Techniques, Morgan Kaufmann Publishers," San Francisco, CA, pp. 335-391.

[3] Bindra, K. and Mishra, A., 2017, September. A detailed study of clustering algorithms. In *2017 6th International Conference on Reliability, Infocom Technologies and Optimization (Trends and Future Directions)(ICRITO)* (pp. 371-376). IEEE.

[4] Fukunaga, K. and Hostetler, L., 1975. The estimation of the gradient of a density function, with applications in pattern recognition. *IEEE Transactions on information theory*, *21*(1), pp.32-40.

[5] AbdAllah, L. and Shimshoni, I., A distance function for data with missing values and its applications on knn and kmeans algorithms. *Submitted to Int. J. Advances in Data Analysis and Classification*.

[6] Zhang, S., Qin, Z., Ling, C.X. and Sheng, S., 2005. "Missing is useful": missing values in cost-sensitive decision trees. *IEEE transactions on knowledge and data engineering*, *17*(12), pp.1689-1693.

[7] Xiao, C. and Liu, M., 2010. Efficient mean-shift clustering using gaussian kd-tree. In *Computer Graphics Forum* Vol. 29, No. 7, pp. 2065-2073.

[8] Georgescu, B., Shimshoni, I. and Meer, P., 2003, October. Mean shift based clustering in high dimensions: A texture classification example. In *null* (p. 456). IEEE.

[9] Chau, V.T.N., Loc, P.H. and Tran, V.T.N., 2015, November. A robust mean shift-based approach to effectively clustering incomplete educational data. In *2015 International Conference on Advanced Computing and Applications (ACOMP)* (pp. 12-19). IEEE.

[10] Comaniciu, D., Ramesh, V. and Meer, P., 2001, July. The variable bandwidth mean shift and data-driven scale selection. In *Proceedings Eighth IEEE International Conference on Computer Vision. ICCV 2001* (Vol. 1, pp. 438-445). IEEE.

[11] AbdAllah, L. and Shimshoni, I., 2014, September. Mean shift clustering algorithm for data with missing values. In *International Conference on Data Warehousing and Knowledge Discovery* (pp. 426-438). Springer, Cham.

[12] Masud, M.A., Rahman, M.M., Bhadra, S. and Saha, S., 2019, December. Improved k-means Algorithm using Density Estimation. In *2019 International Conference on Sustainable Technologies for Industry 4.0 (STI)* (pp. 1-6). IEEE.

[13] Singh, G., 2017. "Introductory guide to Information Retrieval using kNN and KDTree," *analytics vidhya.*

[14] Adams, A., Gelfand, N., Dolson, J. and Levoy, M., 2009. Gaussian kd-trees for fast high-dimensional filtering. In *ACM SIGGRAPH 2009 papers* (pp. 1-12).

[15] Masud, M.A., Huang, J.Z., Zhong, M., Fu, X. and Mahmud, M.S., 2018, November. Slice_OP: Selecting Initial Cluster Centers Using Observation Points. In *International Conference on Advanced Data Mining and Applications* (pp. 17-30). Springer, Cham.

SciEn
Journal of Engineering Advancements Vol. 02(01) 2021, pp 07-12 https://doi.org/10.38032/jea.2021.01.002

Power Performance Evaluation of a PV Module Using MPPT with Fuzzy Logic Control

Suman Chowdhury[1, *], *Dilip Kumar Das*[2] *and Md Sharafat Hossain*[3]

[1]Department of Electrical and Electronic Engineering, International University of Business Agriculture and Technology, Dhaka, Bangladesh
[2]Department of Mathematics, International University of Business Agriculture and Technology, Dhaka, Bangladesh
[3]Department of Electrical and Electronic Engineering, Dhaka University of Engineering and Technology, Gazipur, Bangladesh

Received: November 16, 2020, Revised: December 18, 2020, Accepted: December 22, 2020, Available Online: January 04, 2021

ABSTRACT

This paper exhibits performance of power of photovoltaic (PV) module in the case of shading effect. A comparison is made with performance of power of PV module void of MPPT solution. From the MATLAB simulation it is found that around 9.92% more average power generation is possible if MPPT (maximum power power point) solution is taken. To take the effect of partial shading a variation of irradiance profile has been proposed since change of irradiance causes the variation of output power to a great extent. Again to observe the performance of output power with MPPT Fuzzy logic control has been introduced for making the tracking fast and accurate. Mamdani control has been chosen as a technique for fuzzy controller. On top of this, mathematical structure of PV module has been prepared in MATLAB simulink to see output preview of PV module and this module has been linked to the fuzzy logic system to trace the peak power. In the simulation process the instantaneous power, average power and percentage power development are being analyzed with figures.

Keywords: Power, Module, MPPT, Fuzzy, PV.

1. Introduction

In the modern age renewable energy sources are playing vital role. And sun energy is treated as a best resource among all energy sources with less carbon emission [1]-[2]. That's why sun power is considered as one of big potential energy sources in earth making future aspect for consideration as inexhaustible main source of power [3]-[4]. The PV module efficiency mainly depends upon the materials used in solar cells and technical arrangement of the cells in module. At this moment, the efficiency of PV module is in range of 12 to 29% for conversion of sunlight to electricity [5]. For getting optimum energy from photovoltaic module, it is needed to run the module at maximum power using MPPT (Maximum power point tracking) followed by several common techniques like 1) perturb and observe process [6]-[8]; 2) incremental conductance process [9]-[10]; 3) fuzzy logic [11] and neural network process [12]. Implementation of fuzzy and neural networks for the control of MPPT is an outstanding field for research. These processes related to artificial intelligence are suitable for promoting the tracing capability as regard to present conventional processes [12].

Fuzzy as a part of Artificial Intelligence takes its origin by professor Lofti Zadeh who produced fuzzy set principle in 1965 [13]. Among artificial intelligence based processes fuzzy has some advantages so that the algorithm for MPPT can be obtained easily [14]. For maximization power of pv module with control of the duty cycle ratio in the profile of the PV & IV curve. Perturb and observe method [15] as well as the incremental and conductance method utilized as the common MPPT techniques inhibits step length for selection of the duty cycle [16]. So step size controls the MPPT operation to a great extent because for small step size the tracking process goes down the speed while for the large step size the fluctuation on maximum power point occurs.

For this reason to control the step size it is important to apply the intelligence technique like fuzzy logic and adaptive neuro fuzzy technique so that step size can be adapted according to the requirement [17]-[33]. Fuzzy is normally utilized to activate system as human control in an automation fact. Fuzzy is capable for controlling step size by empirical methods and professional knowledge without the necessary understanding the detailed mathematical model of the existing plant. The input_output parameters of the required system are largely responsible to enhance effectiveness of fuzzy in determination of MPPT with control of duty cycle command.

Though there are a good number of various input variables for MPPT algorithm input, slope of PV curve for photovoltaic cell is taken as the most utilized variable of input [22]-[24],[29]. Fuzzy is considered as most preferable method for seeking the maximum power of the pv system for ensuring stability and good response rate. For better output of Fuzzy control method, researchers are more intended to find MPPT solution with the Fuzzy logic in their various publications [34]-[35]. The fuzzy inherited MPPT algorithm is provided by researcher for effectiveness & robustness of PV system [36]-[37]. Actually the main problem is about to selection of the step size for MPPT tracking process in various methods of MPPT tracking system. In Fuzzy system this problem can be solved to a great extent since Fuzzy has a good platform to analyze the step size as the requirement base in decision making process.

In this paper the MPPT solution is made using Fuzzy logic to seek the power performance as well as effectiveness of the PV module having consideration of various factors. Also this paper tries to show the partial shading effect of photovoltaic module with MPPT solution followed by fuzzy logic control..

*Corresponding Author Email Address: suman@iubat.edu Published by: SciEn Publishing Group

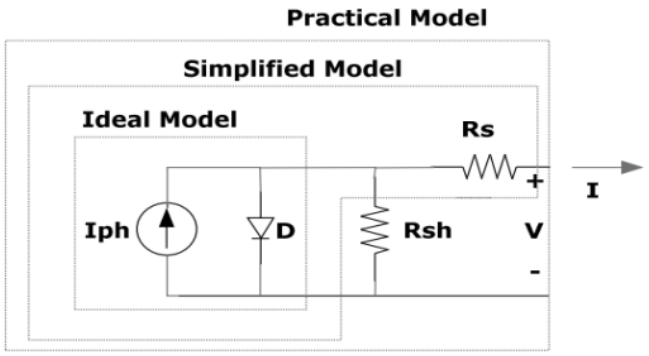

Fig. 1 Electrical equivalent circuit diagram for photovoltaic cell [40].

2. PV Cell Modeling

For the simulation process it is important to draw the electrical equivalent network. Fig. 1 explains electrical equivalent circuit for solar cell. The mathematical equation for current of photovoltaic cell is given by Equation (1) [38].

$$I = I_{ph} - I_S[\exp(\frac{q(V+IR_S)}{kT_C A}) - 1] - \frac{V+IR_S}{R_{sh}} \quad (1)$$

Where I_{ph} expresses light generated current, I_S represents dark current saturation, q is charge of electron (1.6×10^{-19} C), k is Boltzmann's constant $=1.38\times10^{-23}$J/k, T_C acts as working temperature of cell, A is ideality factor, R_{sh} is shunt resistance and R_S is series resistance.

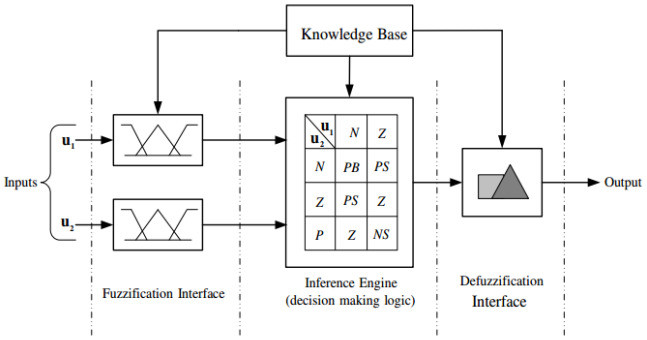

Fig. 2 Basic concept for fuzzy logic control.

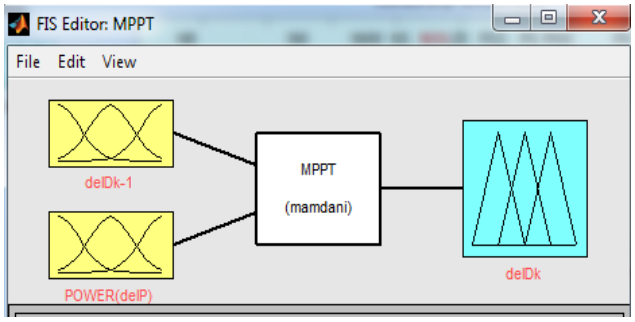

Fig. 3 Simulink model for fuzzy interface.

The photo current depending on the solar radiation and working temperature is provided by Equation (2) [38].

$$I_{ph} = [I_{SC} + K_I(T_C - T_{ref})]\frac{G}{G_n} \quad (2)$$

Where I_{SC} is the short circuit current at 25°C, K_I is the temperature coefficient of short circuit current, T_{ref} is the reference temperature and G is the solar radiation in kW/m^2 and G_n is nominal solar radiation at STC in kW/m^2. Furthermore, saturation current of cell is shown in Equation (3) [38].

$$I_S = I_{RS}(\frac{T_C}{T_{ref}})^3 \exp[\frac{qE_G(\frac{1}{T_{ref}} - \frac{1}{T_C})}{kA}] \quad (3)$$

Where I_{RS} represents the reverse saturation current at Tref, E_G is the band-gap energy.

The reverse saturation current of cell depending on Voc and Isc is given by Equation (4) [39].

$$I_{RS} = \frac{I_{SC}}{\exp(\frac{qV_{OC}}{NsKTcA}) - 1} \quad (4)$$

Where V_{OC} = the open circuit voltage of the PV cell. The Equation (5) is expressing the thermal voltage.

$$V_t = \frac{kT_C}{q} \quad (5)$$

3. PV Array Modeling

The photovoltaic array is defined as the series or parallel arrangement of the photovoltaic modules. The photovoltaic module taken for software simulation produces optimum output of 100W. For obtaining output power at expected voltage and current, the series and parallel arrangement of the photovoltaic modules needs to be observed accurately. The current equation of the photovoltaic array with N_S series and N_P parallel is provided by Equation (6).

$$I = N_P I_{ph} - N_P I_S[\exp(\frac{q(\frac{V}{N_S} + \frac{IR_S}{N_P})}{kT_C A}) - 1] - \frac{\frac{N_P V}{N_S} + IR_S}{R_{sh}} \quad (6)$$

4. MPPT using Fuzzy

For implementation of the fuzzy logic some parameters are needed to consider. Fig. 2 shows the overall concept of the fuzzy logic which is implemented to find out the duty cycle in PV system. Here Mamdani controller is used as a decision maker. And centroid method is utilized for defuzzification purpose. Two membership functions are used as the input for this fuzzy controller. These two variables are duty cycle and the power difference. Finally the output parameter is set as the update step size in terms of duty cycle.

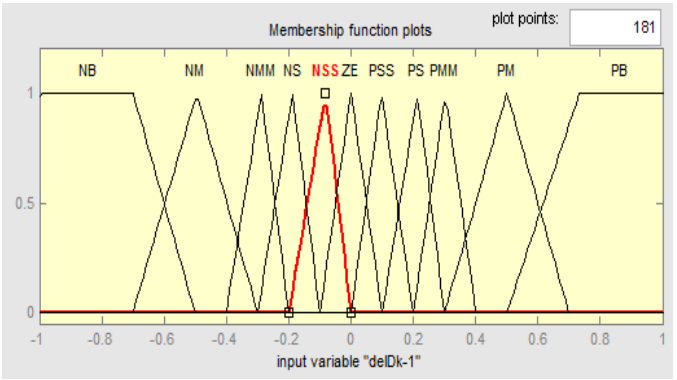

Fig. 4 Membership function of duty cycle input ΔD_{k-1}.

Fig. 3 represents the preview of fuzzy logic controller in MATLAB simulink where two input variables (Duty cycle, Power) are taken as fuzzy input and one output variable (Duty cycle) is taken as fuzzy output. All membership functions are given in Fig. 4 - Fig. 6 respectively. Fig. 4 shows that total eleven

levels are used for using as the various category of the duty cycle input variable. These levels are treated as NB (Negative big), NM (Negative medium), NMM (Negative medium medium), NS (Negative small), NSS (Negative small small), ZE (Zero), PSS (Positive small small), PS (Positive small), PMM (Positive medium medium), PM (Positive medium), PB (Positive big). Similarly Fig. 5 shows total five levels of variation used as the membership function for the input power difference. And finally Fig. 6 shows that total eleven levels of variation for the output variable as the membership function for the output duty cycle. Furthermore Table 1 shows the rules for decision maker used as Mamdani controller in this paper. The rules are read as

If ΔPk is NB and ΔDk−1 is NB then ΔDk is PM
If ΔPk is NB and ΔDk−1 is NM then ΔDk is PMM
If ΔPk is NB and ΔDk−1 is NS then ΔDk is PSS
……
If ΔPk is PB and ΔDk−1 is PB then ΔDk is PM.

Finally Fig. 7 shows the implementation of fuzzy logic in PV system in the manner of MATLAB simulink model.

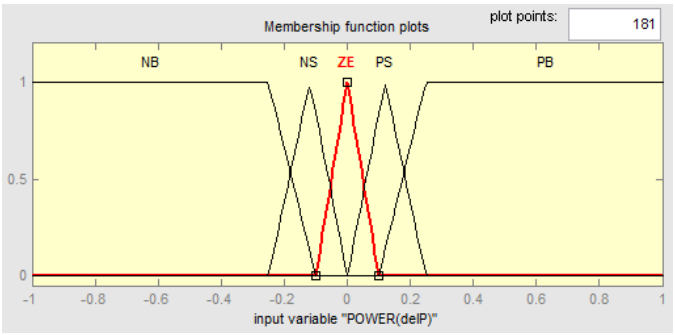

Fig. 5 Membership function of power input ΔP_k

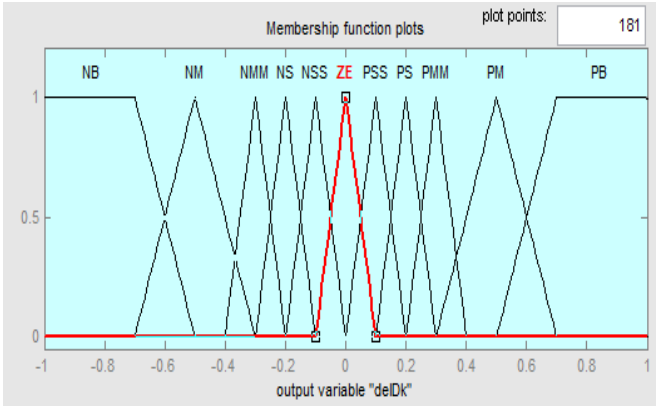

Fig. 6 The membership function of duty cycle output ΔD_k

Table 1 Rules for Fuzzy control

		$\Delta Dk-1$										
		NB	NM	NMM	NS	NSS	**ZE**	PSS	PS	PMM	PM	PB
ΔPk	NB	PM	PMM	PS	PSS	PSS	**NB**	NSS	NSS	NS	NMM	NM
	NS	PM	PMM	PS	PSS	PSS	**NS**	NSS	NSS	NS	NMM	NM
	ZE	NB	NM	NMM	NS	NSS	**ZE**	PSS	PM	PMM	PM	PB
	PS	NM	NMM	NS	NSS	NSS	**PS**	PSS	PSS	PS	PMM	PM
	PB	NM	NMM	NS	NSS	ZE	**PS**	PSS	PSS	PS	PMM	PM

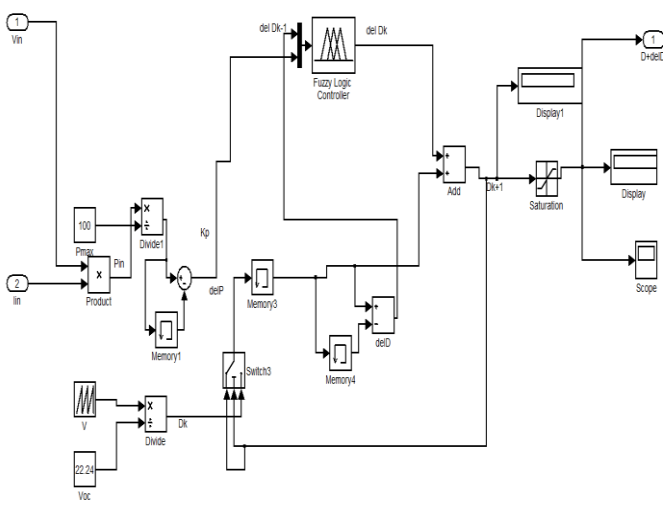

Fig. 7 Fuzzy implementation model in Simulink

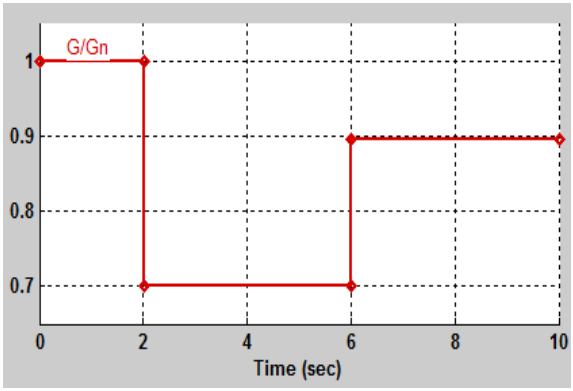

Fig. 8 Irradiance profile for producing partial shading effect.

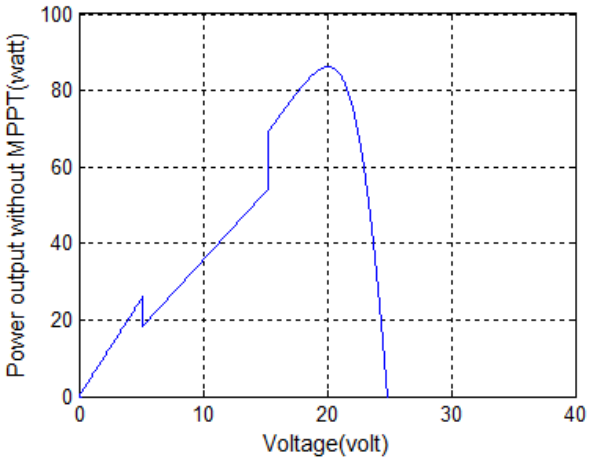

Fig. 9 Output power curve for shading effect without MPPT.

5. Results from Simulation

For purpose of simulation, CSS-MSP-100M-36 is taken as solar module. Fig. 8 is standing for showing the solar radiation preview at a certain period to produce the partial shading criteria. The power output is represented by Fig. 9 under the condition of partial shading. From the simulation it is seen that around 87 watt of power can be generated as the maximum. And at around 25 watt of power around 57 watt of power simulation shows deviation of power due to application of the partial shading effect in the PV module.

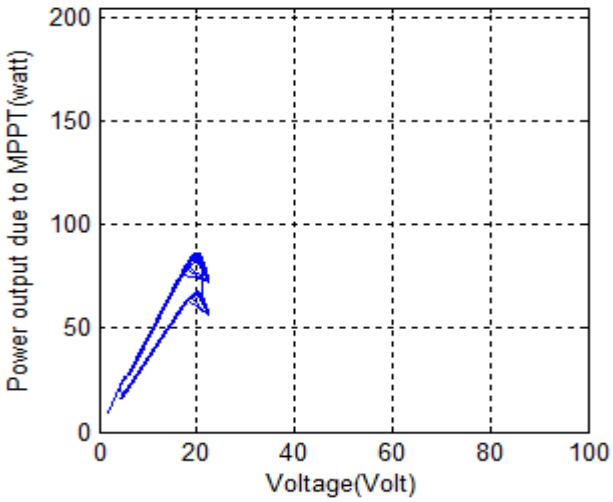

Fig. 10 Output power curve shading effect with MPPT.

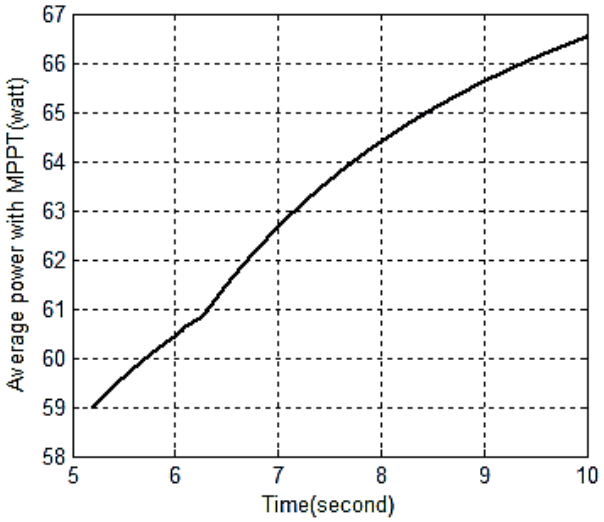

Fig. 11 Average power curve for partial shading effect with MPPT.

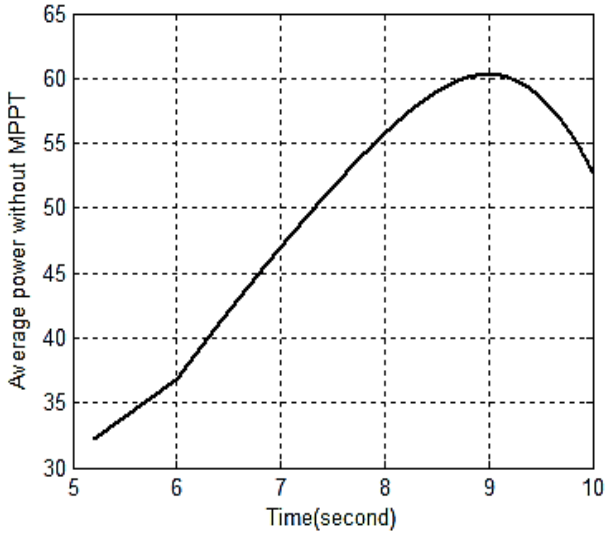

Fig. 12 Average power curve for partial shading effect without MPPT.

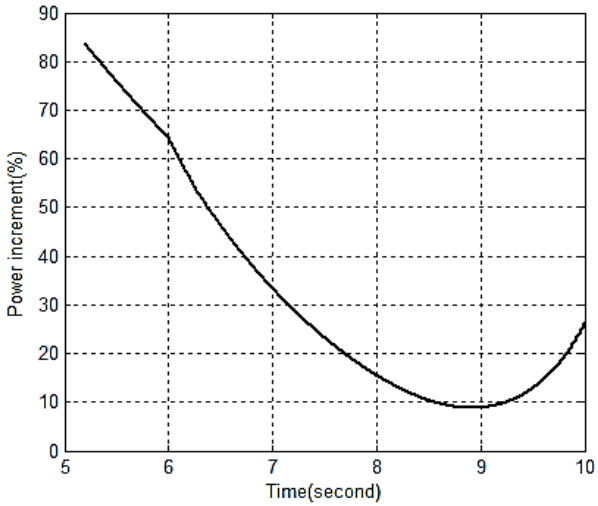

Fig. 13 Development of percentage of power under partial shading effect due to MPPT.

Whereas Fig. 10 is showing the partial shading power profile under MPPT solution handled by fuzzy controller. The simulation obtained in this figure tries to investigate the power with MPPT tracking where two power peaks are obtained at around 87 watt and at around 67 watt of power. From Fig. 11 it is seen that average power is varied in the range of 59 watt to 66.5 watt with MPPT whereas Fig. 12 shows that this range is lying in range of 33 watt to 60 watt without MPPT solution. Finally Fig. 13 represents the output power development in the terms of percentage with MPPT solution for partial shading effect. From the simulation process it is noticed that a lowest power peak is obtained at around 9% of power development.

6. Conclusion

To investigate the power performance under partial shading effect on PV module, fuzzy logic control is used as the MPPT solution. Since fuzzy has a good scope for selection of the step size as the requirement after processing the input variables in the decision making process, it is a good scope to track the maximum power from the PV module. From the MPPT solution it is found that around 84% as maximum and around 10% as minimum output power can be developed. Furthermore more research works are needed to seek power output under partial shading. A good number of factors such as temperature, series resistance of PV cell, ideality factor, clearness index etc are needed to observe the overall performance of PV module.

References

[1] Farhat, M. and Sbita, L., 2011. Advanced fuzzy MPPT control algorithm for photovoltaic systems. Science Academy Transactions on *Renewable Energy Systems Engineering and Technology*, 1(1), pp.29-36.

[2] Tafticht, T., Agbossou, K., Doumbia, M.L. and Cheriti, A., 2008. An improved maximum power point tracking method for photovoltaic systems. *Renewable energy*, 33(7), pp.1508-1516.

[3] Philibert, C., Frankl, P., Tam, C., Abdelilah, Y., Bahar, H., Marchais, Q. and Wiesner, H., 2014. Technology roadmap: solar photovoltaic energy. International Energy Agency: Paris, France.

[4] Tomabechi, K., 2010. Energy resources in the future. *Energies*, 3(4), pp.686-695.

[5] Ocran, T.A., Cao, J., Cao, B. and Sun, X., 2005. Artificial neural network maximum power point tracker for solar electric vehicle. *Tsinghua science and technology*, 10(2), pp.204-208.

[6] Hua, C. and Shen, C., 1998, February. Comparative study of peak power tracking techniques for solar storage system. *In APEC'98 Thirteenth Annual Applied Power Electronics Conference and Exposition* (Vol. 2, pp. 679-685). IEEE.

[7] Koutroulis, E., Kalaitzakis, K. and Voulgaris, N.C., 2001. Development of a microcontroller-based, photovoltaic maximum power point tracking control system. *IEEE Transactions on power electronics*, 16(1), pp.46-54.

[8] Enslin, J.H. and Snyman, D.B., 1992, November. Simplified feed-forward control of the maximum power point in PV installations. *In Proceedings of the 1992 International Conference on Industrial Electronics, Control, Instrumentation, and Automation* (pp. 548-553). IEEE.

[9] Bodur, M. and Ermis, M., 1994, April. Maximum power point tracking for low power photovoltaic solar panels. *In Proceedings of MELECON'94. Mediterranean Electrotechnical Conference* (pp. 758-761). IEEE.

[10] Sullivan, C.R. and Powers, M.J., 1993, June. A high-efficiency maximum power point tracker for photovoltaic arrays in a solar-powered race vehicle. *In Proceedings of IEEE Power Electronics Specialist Conference-PESC'93* (pp. 574-580). IEEE.

[11] Veerachary, M., Senjyu, T. and Uezato, K., 2003. Neural-network-based maximum-power-point tracking of coupled-inductor interleaved-boost-converter-supplied PV system using fuzzy controller. *IEEE Transactions on Industrial Electronics*, 50(4), pp.749-758.

[12] Ocran, T.A., Cao, J., Cao, B. and Sun, X., 2005. Artificial neural network maximum power point tracker for solar electric vehicle. *Tsinghua science and technology*, 10(2), pp.204-208.

[13] Bose, B.K., 2002. Modern power electronics and AC drives (Vol. 123). *Upper Saddle River*, NJ: Prentice hall.

[14] Balasubramanian, G. and Singaravelu, S., 2012. Fuzzy logic controller for the maximum power point tracking in photovoltaic system. *International Journal of Computer Applications*, 41(12), pp.22-28.

[15] Femia, N., Petrone, G., Spagnuolo, G. and Vitelli, M., 2005. Optimization of perturb and observe maximum power point tracking method. *IEEE transactions on power electronics*, 20(4), pp.963-973.

[16] Hussein, K.H., Muta, I., Hoshino, T. and Osakada, M., 1995. Maximum photovoltaic power tracking: an algorithm for rapidly changing atmospheric conditions. *IEE Proceedings-Generation, Transmission and Distribution*, 142(1), pp.59-64.

[17] Zainuri, M.M., Radzi, M.M., Soh, A.C. and Rahim, N.A., 2012, December. Adaptive P&O-fuzzy control MPPT for PV boost dc-dc converter. *In 2012 IEEE International Conference on Power and Energy (PECon)* (pp. 524-529). IEEE.

[18] Tian, Y., Xia, B., Xu, Z. and Sun, W., 2014. Modified asymmetrical variable step size incremental conductance maximum power point tracking method for photovoltaic systems. *Journal of Power Electronics*, 14(1), pp.156-164.

[19] Alajmi, B.N., Ahmed, K.H., Finney, S.J. and Williams, B.W., 2010. Fuzzy-logic-control approach of a modified hill-climbing method for maximum power point in microgrid standalone photovoltaic system. *IEEE transactions on power electronics*, 26(4), pp.1022-1030.

[20] Iqbal, A., Abu-Rub, H. and Ahmed, S.M., 2010, December. Adaptive neuro-fuzzy inference system based maximum power point tracking of a solar PV module. *In 2010 IEEE International Energy Conference* (pp. 51-56). IEEE.

[21] Chin, C.S., Neelakantan, P., Yoong, H.P. and Teo, K.T.K., 2011. Optimisation of fuzzy based maximum power point tracking in PV system for rapidly changing solar irradiance. *Transaction on Solar Energy and Planning*, 2, pp.130-137.

[22] Radjai, T., Gaubert, J.P. and Rahmani, L., 2014, June. The new FLC-variable incremental conductance MPPT with direct control method using Cuk converter. *In 2014 IEEE 23rd International Symposium on Industrial Electronics (ISIE)* (pp. 2508-2513). IEEE.

[23] Cheikh, M.A., Larbes, C., Kebir, G.T. and Zerguerras, A., 2007. Maximum power point tracking using a fuzzy logic control scheme. Revue des energies Renouvelables, 10(3), pp.387-395.

[24] Rahmani, R., Seyedmahmoudian, M., Mekhilef, S. and Yusof, R., 2013. Implementation of fuzzy logic maximum power point tracking controller for photovoltaic system. *American Journal of Applied Sciences*, 10, pp.209-218.

[25] Liu, C.L., Chen, J.H., Liu, Y.H. and Yang, Z.Z., 2014. An asymmetrical fuzzy-logic-control-based MPPT algorithm for photovoltaic systems. *Energies*, 7(4), pp.2177-2193.

[26] Takun, P., Kaitwanidvilai, S. and Jettanasen, C., 2010, March. Maximum power point tracking using fuzzy logic control for photovoltaic systems. *In World Congress on Engineering* 2012. July 4-6, 2012. London, UK. (Vol. 2189, pp. 986-990). International Association of Engineers.

[27] Putri, R.I., Wibowo, S. and Rifa'i, M., 2015. Maximum power point tracking for photovoltaic using incremental conductance method. *Energy Procedia*, 68, pp.22-30.

[28] Sakly, A. and Smida, B., 2012, February. M. Adequate fuzzy inference method for MPPT fuzzy control of Photovoltaic systems. *In Proceedings of the 2012 International Conference on Future Electrical Power and Energy systems, Lecture Notes in Information Technology* (Vol. 9, pp. 457-468).

[29] Mahamudul, H., Saad, M. and Ibrahim Henk, M., 2013. Photovoltaic system modeling with fuzzy logic based maximum power point tracking algorithm. *International Journal of Photoenergy*, 2013.

[30] El Khateb, A.H., Rahim, N.A. and Selvaraj, J., 2013. Type-2 fuzzy logic approach of a maximum power point tracking employing sepic converter for photovoltaic system. Journal of Clean Energy Technologies, 1(1), pp.41-44.

[31] Roy, C.P., Vijaybhaskar, D. and Maity, T., 2013, December. Modelling of fuzzy logic controller for variable-step MPPT in photovoltaic system. *In 2013 IEEE 1st International Conference on Condition Assessment Techniques in Electrical Systems (CATCON)* (pp. 341-346). IEEE.

[32] Natsheh, E.M. and Albarbar, A., 2013. Hybrid power systems energy controller based on neural network and fuzzy logic.

[33] Bos, M.J., Abhijith, S., Aswin, V., Basil, R. and Dhanesh, R., 2014. Fuzzy logic controlled PV powered buck converter with MPPT. *Int. J. Adv. Res. Electr. Electron. Instrum. Eng*, 3, pp.9370-9377.

[34] Takun, P., Kaitwanidvilai, S. and Jettanasen, C., 2010, March. Maximum power point tracking using fuzzy logic control for photovoltaic systems. *In World Congress on* Engineering 2012. July 4-6, 2012. London, UK. (Vol. 2189, pp. 986-990). International Association of Engineers.

[35] Agorreta, J.L., Reinaldos, L., Gonzalez, R., Borrega, M., Balda, J. and Marroyo, L., 2009. Fuzzy switching technique applied to PWM boost converter operating in mixed conduction mode for PV systems. *IEEE Transactions on Industrial Electronics*, 56(11), pp.4363-4373. http://dx.doi.org/10.1109/TIE.2009.2019567

[36] Alajmi, B.N., Ahmed, K.H., Finney, S.J. and Williams, B.W., 2010. Fuzzy-logic-control approach of a modified hill-climbing method for maximum power point in microgrid standalone photovoltaic system. *IEEE transactions on power electronics*, 26(4), pp.1022-1030. http://dx.doi.org/10.1109/TPEL.2010.2090903

[37] Jose, P. and Jose, P.R., 2014. Grid connected photovoltaic system with fuzzy logic control based MPPT. *International Journal of Engineering and Innovative Technology (IJEIT)*, 3(8), pp.142-148.

[38] Tsai, H.L., Tu, C.S. and Su, Y.J., 2008, October. Development of generalized photovoltaic model using MATLAB/SIMULINK. *In Proceedings of the world congress on Engineering and computer science* (Vol. 2008, pp. 1-6).

[39] Gupta, A.K., Gupta, M. and Saxena, R., 2018. Modeling and Comparative Analysis of PV Module with Improved Perturbation & Observation Based MPPT Technique for PV Applications. *Archives of Current Research International*, pp.1-12.

[40] Durago, J.G., 2011. Photovoltaic Emulator Adaptable to Irradiance, Temperature and Panel Specific IV Curves.

SciEn
Journal of Engineering Advancements Vol. 02(01) 2021, pp 13-23 https://doi.org/10.38032/jea.2021.01.003

A Review on Developments in Manufacturing Process and Mechanical Properties of Natural Fiber Composites

Md. Maruf Billah, M S Rabbi, Afnan Hasan*

Department of Mechanical Engineering, Chittagong University of Engineering & Technology, Chattogram-4349, Bangladesh

Received: January 02, 2021, Revised: January 22, 2021, Accepted: January 24, 2021, Available Online: February 03, 2021

ABSTRACT

From the last few decades, the study of natural fiber composite materials has been gaining strong attention among researchers, scientists, and engineers. Natural fiber composite materials are becoming good alternatives to conventional materials because of their lightweight, high specific strength, low thermal expansion, eco-friendly, low manufacturing cost, nonabrasive and bio-degradable characteristics. It is proven that natural fiber is a great alternative to synthetic fiber in the sector of automobiles, railway, and aerospace. Researchers are developing various types of natural fiber-reinforced composites by combining different types of natural fiber such as jute, sisal, coir, hemp, abaca, bamboo, sugar can, kenaf, banana, etc. with various polymers such as polypropylene, epoxy resin, etc. as matrix material. Based on the application and required mechanical and thermal properties, numerous natural fiber-based composite manufacturing processes are available such as injection molding, compression molding, resin transfer molding, hand lay-up, filament welding, pultrusion, autoclave molding, additive manufacturing, etc. The aim of the paper is to present the developments of various manufacturing processes of natural fiber-based composites and obtained mechanical properties.

Keywords: Natural Fiber Composites, Manufacturing Processes, Mechanical Properties.

1 Introduction

The research field of Natural Fiber Composites (NFC) has been increased due to its higher prospectus and are considering nowadays as the alternatives of carbon or glass fiber composites. Among extensive applicable fields, the demand for NFC, especially in the automotive industry is increasing comprehensively because of sound attenuation capability and lightweight, results in better fuel efficiency. NFC does not only reduce the weight of the vehicle but also lower the cost and energy needed for its production by 80% [1]. NFC can also be used to fabricate furniture, tiles, and marine piers [2]. However, the natural fiber composites have some distinct disadvantages over glass fiber composites such lower load capability, higher moisture absorption, and lower processing temperature [2],[3].

Between plant and animal fiber, the former one gives more strength and stiffness rather than the later one though silk, a plant fiber is relatively expensive [4]. The cellulose-based natural fiber such as ramie, flax, hemp can give higher mechanical properties than other. The selection of fiber for NFC depends on geography, for example, jute, flax fiber, kenaf, whereas hemp and ramie have more interest in Europe, andin Asia, sisal fiber gets the large interest. The mechanical properties of natural fiber vary with the chemical composition and chemical structure of the fiber, usually related to the fiber harvesting time, growing conditions, storage procedures, extraction method, and the chemical treatment prior to the product fabrication. Mechanical strength may be reduced by 15% when it is harvested 5 days later of optimum harvesting time [5]. In case of the extraction process, manually extracted fiber can show 20% higher strength than mechanically extracted [6]. To establish as alternatives of glass fiber, natural fiber should be collected as an optimum way in terms of time and process that can give closer strength to glass fiber.

Apart from the fiber, one of the distinctive constituents of composites is the matrix, used as the binder in the laminate. Various thermoplastic materials such as polyvinyl chloride (PVC), polypropylene (PP), polyethylene, and polyolefin are being used in NFC [7]. Thermoset polymer materials such as epoxy resin, unsaturated polyester, VE resins, and phenol-formaldehyde are used as matrices material as well though on small scale [8],[9]. Thermoset plastic exhibits better physical properties under the operating temperature of 200°C, the reason makes thermoplastics as matrices material more suitable [9].

Surface modification of fiber by coupling agent and compatibilizer is an important step for producing NFC [10].It enhances the interfacial strength between fiber and matrices. Coupling agent creates strong bond in the interface by reacting with fiber and matrices simultaneously during processing time. Besides, polymeric compatibilizer is interfacial agent which grafts fiber and matrices onto the chain of polymer [11],[12]. The mechanical properties of NFC significantly depend on which coupling agent or compatibilizer is adhered [13],[14].

The manufacturing process plays an important role on the property of NFC [15]-[17]. Fiber lengths, product size, chemical treatment of fiber are the main parameters for selecting the manufacturing process associated with NFC [18]-[20]. Long fiber and large-size products follow open mold manufacturing processes like hand lay-up, automated tape laying, etc. for better mechanical and thermal properties [1],[21]. Relatively complex and small-scale NFC product made from short fiber through closed mold process such as injection molding, compression molding, transfer molding [19],[21]. Exceptionally short fiber is used in spray up open mold processing [22]. Strong fiber dispersion provides better interfacial bonding between fiber and matrices by reducing the void at this interface [23]. For overcoming this reason higher intensive mixing process like single screw extruder and twin-screw extruder are used [24]-[26].

In this article, the developments in the manufacturing process associated with NFC are reviewed. Conventional

*Corresponding Author Email Address: rabbi@cuet.ac.bd Published by: SciEn Publishing Group

manufacturing processes for NFCs are discussed in Section 2. Section 3 depicted the comparisons of selected mechanical properties from mentioned processes. Future research work is mentioned in Section 4. Finally conclusions are drawn in Section 5.

2 Manufacturing Processes

Earlier, composite materials were produced directly by human hand [27],[28]. With the advancement of technology and increasing demand, it goes through semi-automated to automated processes like additive manufacturing. The closed mold processes are being famous in the current century because of higher precision, accuracy, and productivity [29],[30]. Injection molding, Compression molding, Resin transfer molding are the most commonly used manufacturing method of NFC material in recent days. Hand lay-up, autoclave, Pultruded, Filament wound, etc. are the special method for specific type products manufacturing. The hand lay-up process is substituted by automated tape laying process for its technological benefits [31]-[33]. In this section of the report, various manufacturing processes of NFCs are upheld with manufactured composite's mechanical properties.

2.1 Injection Molding

In injection molding process, a specific amount of fiber and molten polymer is mixed into a mold cavity by sufficient force. Various studies have been done on the injection molding process [34]-[39]. In the injection molding process, both thermosets and thermoplastics polymer are used, but the process included with thermoset is difficult to execute [40],[41]. The process parameter of thermosets such as curing time, curing temperature, injection pressure, and injection torque were investigated by Deringer et al. [42] for epoxy-based natural fiber composite. An schematic setup of injection molding process is given in Fig. 1.

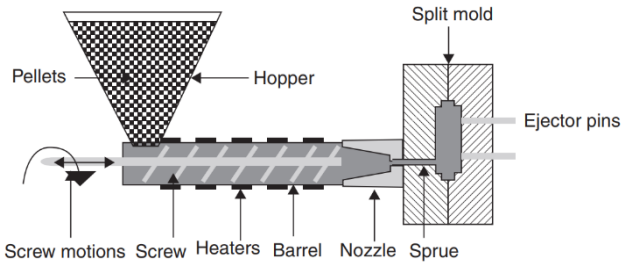

Fig. 1 Schematic setup of injection molding process [43].

In a contrast, thermoplastic polymer-based natural fiber composites production is quite easier in the injection molding process [44]. The small pellets of the thermoplastic polymer are mixed with chopped fiber and feed into a hopper. The material thus passes through high temperature and high-pressure melting section by rotating screw (single screw extruder or twin-screw extruder). High temperature is responsible for melting the material and made it viscous fluid. Finally, it goes through the sprue nozzle into mold cavities due to the above-mentioned high pressure. After solidifying, the product ejects from the mold cavities. The screw-type extruder generates the required share force for the following purpose:

(1) Generates heat to melt the pellets and reduced the friction between barrel, pellet, and screw [39],

(2) Ensures better mixing of polymer matrices and fiber [11],

(3) Push the mixture into the sprue nozzle through the mold cavities with sufficient force [11].

It has been found that the increase of temperature reduced the share viscosity of biodegradable polymers [45].

In the injection molding process, fiber length should be appropriate to transfer entire stress from matrices to fiber and better performance by following the formula [46]:

$$I_c = \frac{\sigma_{fu} d}{2\tau} \quad (1)$$

where, I_c, d, τ and σ_{fu} are critical fiber length, fiber diameter, shear stress at the interface of fiber and matrix and ultimate tensile strength of fiber respectively.

It is reported that the mechanical property of NFC is maximum at an optimum fiber length. Due to the imperfect interfacial bonding between fiber surface and matrix, the property might not reach its highest value though the critical fiber length has been obtained from equation (1) [11]. Thus, it is mandatory to choose optimum fiber length for the injection molding process. Otherwise, a predetermined critical fiber length may cause fracture in matrices.

Fiber orientation and residual stress in NFC are also important issues for unequal modulus distribution. Improper mixing, insufficient heating after injection may cause irregular fiber orientation and rapid cooling of molten polymer, excessive pressure at the mold section is accountable for growing residual stress [47]. This unexpected residual stress causes tensile stress at external surface of the product and compressive stress at intermediate region which is called injection-molded characteristic residual stress distribution[49]. Various studies have been performed in residual stress development factors [45],[48]-[50]. It has been found that non-uniform temperature distribution along with whole molten polymer, higher pressure gradient, polymer chain orientation, unequal thermal expansion coefficient between fiber and matrices are major causes of building residual stress in NFC. The geometrical parameters like mold cavities, mold shape, mold size, mold vents which help to escape air babble, and injection gate location are also responsible for stress concentration [11]. On the other hand, non-uniform fiber orientation developed due to unequal thickness of mold which causes variation in properties through the final product. For more fiber concentrated region shows fiber dominating properties and molten polymer generates a complex flow geometry on upstream [51]. Mechanical properties of NFCs which are made by injection molding process from previous literatures are listed in Table 1.

2.2 Compression Molding

Compression molding (CM) is the oldest manufacturing process among all of them. Plastic products are produced at a very early stage by CM process. In the composite manufacturing industry, it achieves huge scopes parallelly for glass fiber and natural fiber [59],[60].Both thermoplastic and thermoset matrix natural fiber composites can be produced by CM [61]. There are two mold sections, upper and lower, in the CM process. The charge is placed at the lower section of mold and during the molding time the upper section press with sufficient pressure and temperature to get the shape inside the mold cavity. The CM process can be called the combination of autoclave and hot press process. Both short and long fiber composite can be produced by this process. Prepregs of thermoplastic material are laid in a

proper sequence on mold in autoclave process. Then the laminate is bagged in negative pressure and placed inside the autoclave. The laminate goes through heat and pressure cycle and after curing the desired composite is formed [62]. On the other hand, it is not necessary of closed the mold in hot press process [63]. In close mold, precut and measured amount of natural fiber are stacked with each other and placed in the mold cavity (see Fig. 2).

Table 1 Mechanical Properties of NFC prepared by Injection molding process

Matrices	Fiber	Fiber percentage (% mass)	Tensile strength (MPa)	Flexural strength (MPa)	Young's modulus (GPa)	Flexural modulus (GPa)	Reference
PP	Hemp	40	52	86	4	4	[52]
PP	Newsprint	40	53	94	3	4	[52]
PP	Kraft	40	52	90	3	4	[52]
PP	Flax	30	52	60	5	5	[53]
PP*	Flax	30	-	70	-	6	[54]
PP	Wood BKP	40	50	78	3	3	[55]
PP	Jute	60	74	112	11	12	[56]
PA	Cordenka	30	120	-	6	-	[57]
PLA	Cordenka	25	108	-	4	-	[58]
PP	Cordenka	42	90	-	4	-	[58]

PP = Polypropylene, BKP = Bleached Kraft Pulp, PA = Polyamide, PLA = Polylactide Acid
*High molecular weightmaleic acid anhydride modified PP.

Table 2 Mechanical Properties of NFC prepared by Compression molding process

Matrices	Fiber	Fiber percentage (% mass)	Tensile strength (MPa)	Flexural strength (MPa)	Young's modulus (GPa)	Flexural modulus (GPa)	Reference
PP	Kenaf	30	46	58	5	4	[10]
UP	PALF	30	53	80	2	3	[65]
Epoxy	Harakeke	45	136	155	11	10	[66]
Epoxy	Hemp	50	105	126	9	8	[66]
Epoxy	Hemp	65	113	145	18	10	[67]
Epoxy	Hemp	65	165	180	17	9	[67]
PP	Hemp	46	-	127	-	11	[68]
PLA	Hemp	30	83	143	11	7	[67]
PLA	Kenaf	40	82	126	8	7	[69]
PHB	Kenaf	40	70	101	6	7	[69]
PLA	Hemp	30	77	101	10	7	[69]
PLA	Kenaf	80	223	254	23	22	[70]
Epoxy	Sisal	73	410	320	6	27	[71]
Epoxy	Sisal	77	330	290	10	22	[71]
Epoxy	Harakeke	55	223	223	17	14	[72]
Epoxy	Harakeke	52	211	-	15	-	[73]
PLA	Harakeke	30	102	-	8	-	[66]
Epoxy	Flax	50	290	248	24	22	[42]
Epoxy	Flax	40	34	90	-	-	[74]
Epoxy	Bamboo	40	23	58	-	-	[74]
UP	Flax	58	304	-	30	-	[75]
PP	Flax	50	40	-	7	-	[76]
UP	PALF	30	53	80	2	3	[65]
PHB	Lyocell	30	66	105	5	5	[69]

UP = Unsaturated Polyester, PLAF = Pineapple Leaf Fiber, PHB = Poly (3-Hydroxybutyrate).

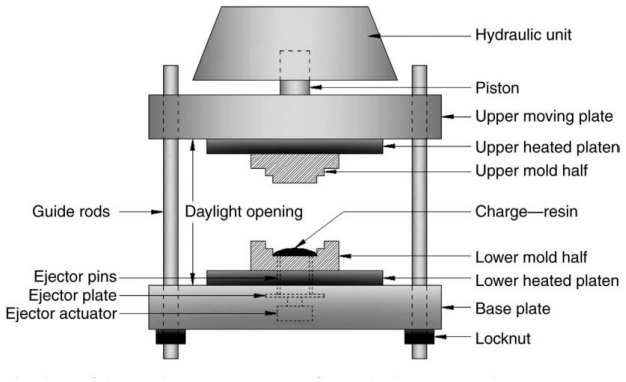

Fig. 2 Schematic setup of compression molding process [64].

In the CM process, BMCs and SMCs are the consecutive initial charge of this molding process. Around 30 to 70% of the lower mold cavity is filled up by this initial charge [62]. Sufficient pressure is applied before getting high temperature. In that case, some fiber may fracture when excessive pressure is applied before molten of matrices. After applying heat, it gets cool and removed from the mold cavity. Lots of studies had been done to find out the prospects of using renewable polymer and natural fiber composite as a new form of bio-composite by compression molding process [34]-[37]. Zero shear stress, proper placing of fiber in the mold cavity, unwanted motion during processing ensure minimum fiber damage. To make large volume fraction of fiber, long fiber can be used. And for better reinforcement and lower shrinkage of molten material, short fiber and compound should be mixed with each other[11]. Mechanical properties of NFCs which are made by the CM process from previous literatures are listed in Table 2.

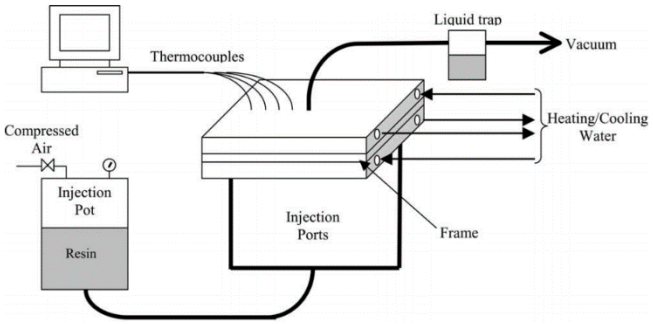

Fig. 3 Schematic setup of resin transfer molding process [84].

2.3 Resin Transfer Molding

Table 3.

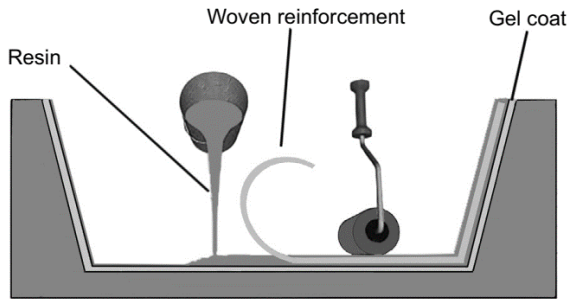

Fig. 4 Schematic setup of hand lay-up process [96].

In resin transfer molding (RTM), thermoset resin is used as matrices which is injected in mold cavity containing fiber (see Fig. 3). To avoid leakage, two halves of matching molds are clamped together with sufficient pressure. Generally, continuous or long fiber is used in the RTM process [30],[77]. Various studies have been done to find out the prospects of resin transfer molding process [29],[78]-[82]. The process parameter of thermosets such as curing time, curing temperature, heat flow, and degree of cure were investigated by Rouison et al. [30] for unsaturated polyester resin-based natural fiber composite. Dominating criteria of RTM are injection pressure, temperature, perform architecture of fiber, resin viscosity, fiber mat permeability, and mold configuration [11]. The main advantages of RTM over the other processes are requirement of lower temperature and abstinence of thermomechanical degradation [83]. Natural fibers have lower compaction than glass fibers which made an effect on the NFC properties of low density in the RTM process [83]. RTM is suitable for large volume production which is also cost-effective compared to other manufacturing processes [11]. Higher injection temperature and pressure reduces the RTM manufacturing cycle time. Though excessive pressure may deform the mold shape and excessive temperature may cause premature resign formation.

In the RTM process, little clearance should be maintained between mold edges and fiber which adjust the fiber perform deformation. At the beginning stage of injection process, higher velocity difference exists which is reduced with respect to the time difference. The flow resistance is accountable for reducing this velocity difference [60]. Without increasing injection pressure, resin flow can be faster by using multiple injection gates. But, a large number of gates creates the process more complex and creates numerous bubbles in the meet point of flow fronts [85]. This void content area reduces the mechanical properties remarkably. To reduce the void in the product, the injection pot and mold need to remain vacuum before starting injection process.

Besides, higher flow resistance creates an obstacle in flow path and flow goes into lower resistance channel for injection pressure hence the effect is escalated. Therefore, the required time at edge flow of bottom is increased which creates adverse effect to format spillage and dry spots [86].The average velocity field of resin flow may look smooth but the local velocity field can be varied point to point at microscopic scale. Local capillary pressure, permeability, non-uniform microstructures are the main reason for local velocity field roughness [87]. Mechanical properties of NFCs which are made by resin transfer molding process from previous literatures are listed in

Mechanical properties of NFCs which are made by resin transfer molding process from previous literatures are listed in Table 4.

2.4 Hand Lay-up

Hand lay-up is older open mold manufacturing technic of natural fiber reinforcement composites compared to others [93]. Long and continuous natural, glass or carbon fiber composite materials can be prepared easily by this process for wide range size of products [27]. Hand lay-up has wide variation to orient fiber in different directions such as unidirectional, inclined or woven. Hybrid composites are made step by step in this process that types of composite gains strong attention in composites industry because of its less directional dependency and resistance to multiple types of stress [94].

In this process, antiadhesive agent is treated at mold surface to prevent polymer sticking and to release it easily [95]. In bottom and top section of the mold plate, a plastic sheet is placed to get smooth surface [96]. Then gel coat of matrix material is applied to the lower mold surface and the fiber which is in various orientation and chemically treated, is kept immediately on coat as shown in Fig. 4. Then, little amount of pressure is created by roller to removed trapped air bubbles from it. Fiber, matrix or both need to mix with ingredients which ensure stronger interfacial bond on this different material [97]. After fully cured of base material the hardened product is removed from mold cavity [78].

Table 3 Mechanical Properties of NFC prepared by Resin transfer molding process

Matrices	Fiber	Fiber percentage (% mass)	Tensile strength (MPa)	Flexural strength (MPa)	Young's modulus (GPa)	Flexural modulus (GPa)	Reference
UP	Flax	39	61	91	6	5	[88]
UP	Jute	35	50	103	8	7	[88]
Bio-epoxy	Cellulose	-	92	727	9	27	[89]
VE	Flax yarn	35	111	128	10	10	[89]
VE	Flax yarn	24	248	-	24	-	[90]
UP	Flax yarn	34	143	198	14	17	[90]
Epoxy	Flax	37	132	-	15	-	[91]
Epoxy	Flax	46	280	-	35	-	[92]
Epoxy	Flax	54	279	-	39	-	[92]
Epoxy	Sisal	48	211	-	20	-	[91]
Epoxy	Sisal	37	183	-	15	-	[91]

VE = Vinyl Ester

Table 4 Mechanical Properties of NFC prepared by Hand lay-up molding process

Matrices	Fiber	Fiber percentage (% mass)	Tensile strength (MPa)	Flexural strength (MPa)	Young's modulus (GPa)	Flexural modulus (GPa)	Reference
Epoxy	Jute	36	102	53	3.8	4	[98]
Polyester	Jute	20	36	64	-	-	[99]
Polyester	Jute	30	41	71	-	-	[99]
Polyester	Jute	40	46	82	-	-	[99]
UP	Jute	14	23	-	4	-	[100]
PLA	Bamboo	40	115	-	6	-	[101]
UP	Bamboo	15	22	-	4	-	[100]
UP	Kenaf	13	28	-	5	-	[100]
Epoxy	Banana	40	108	72	-	-	[102]
Epoxy	Banana	50	113	65	-	-	[102]
Epoxy	Banana	60	98	77	-	-	[102]
Epoxy	Banana	-	37	128	-	-	[103]
Epoxy	Coir	30	24	25	1	-	[104]
Epoxy	Coir	40	21	14	1	-	[104]
Epoxy	Coir	50	18	6	2	-	[104]
Polyester	Rattan	10	16	48	-	-	[105]
Polyester	Rattan	18	12	31	-	-	[105]
Epoxy	Rattan	13	13	131	-	-	[103]
Epoxy	Flax	31	160	190	15	15	[90]

2.5 Other Processes

Depends on shape of the products, different types of processes are used to produce NFCs. Pultrusion, Filament wounding, Autoclave molding, and Vacuum bag molding are the most popular among the numerous methods.

Pultrusion was developed at the middle of the twentieth century. The pulled fiber is impregnated by formulated resin in this process (see Fig. 5). Hollow cylindrical shape products are

mostly produced by pultrusion process. During the manufacturing process, the fiber experiencing high tension and thus results in higher production rate and great fiber orientation [106]. The long/continuous fibers are immersed in resin bath and goes through shaping die, here the curing of impregnated resin occurred [107]. Traditionally this process has higher consistency in quality, distribution, impregnation, and alignment of reinforcing fiber [108],[109]. Mechanical properties of NFCs which are made by pultrusion process from previous literatures are listed Table 5.

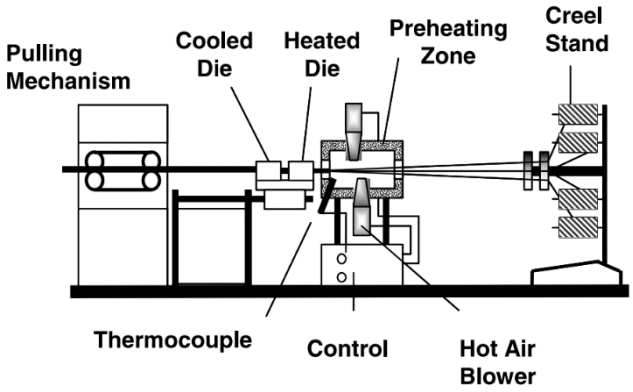

Fig. 5 Schematic setup of pultrusion process [110].

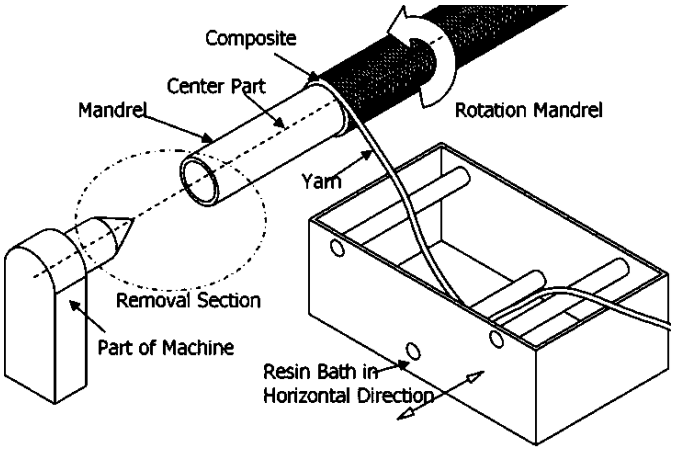

Fig. 6 Schematic setup of filament wounding process [118].

Filament wounding (see Fig. 6) is another open molded manufacturing process which is most preferable for rotationally symmetric products from continuous fiber composites. This process is mostly used for glass and carbon fiber. Recently various study conducted to prove the ability of natural fiber uses too [111]-[116]. Mechanical properties of NFCs which are made by filament wounding process from previous literatures are listed in Table 5. A rotating mandril creats wounding of fiber on it which may be simple or helical. Helical and cross filament wounding provide better mechanical properties compared with simple one [117].

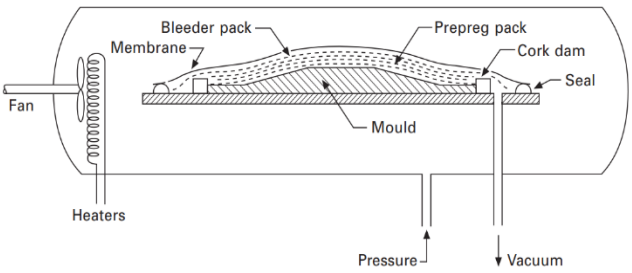

Fig. 7 Schematic setup of autoclave molding process [119].

Autoclave molding ensure higher accuracy and surface finish which is mostly used in aerospace industry from prepregs. A smooth polyester ply covers the both sides of laminates which enhances the surface quality of products (see Fig. 7). A good sealing of whole assembly is provided by non-porous membrane where a porous film covers the top surface of laminate. To remove porosity and volatility of mold, vacuum pressure is crated inside membrane cover where temperature and pressure are controlled to provide exact cure and thermal equilibrium inside the mold. The process is cost intensive and slower compared to other process [119].

Mechanical properties of NFCs which are made by pultrusion, filament wounding, and autoclave molding process from previous literatures are listed in Table 5.

Table 5 Mechanical Properties of NFC

Matrices	Fiber	Fiber percentage (% mass)	Tensile strength (MPa)	Flexural strength (MPa)	Young's modulus (GPa)	Flexural modulus (GPa)	Process	Reference
Polyurethane	Hemp	30	122	145	18	12	Pultrusion	[106]
Epoxy	Flax hackled	28	-	182	-	20	Pultrusion	[90]
PP	Flax yarn	30	89	-	7	-	Pultrusion	[110]
Epoxy	Flax	52	191	-	28	-	Filament wounding	[112]
EpoBioX	Flax	48	152	-	2	-	Filament wounding	[112]
PP	Flax yarn	72	321	-	29	-	Filament wounding	[120]
Epoxy	Flax yarn	45	133	218	28	18	Autoclave	[121]

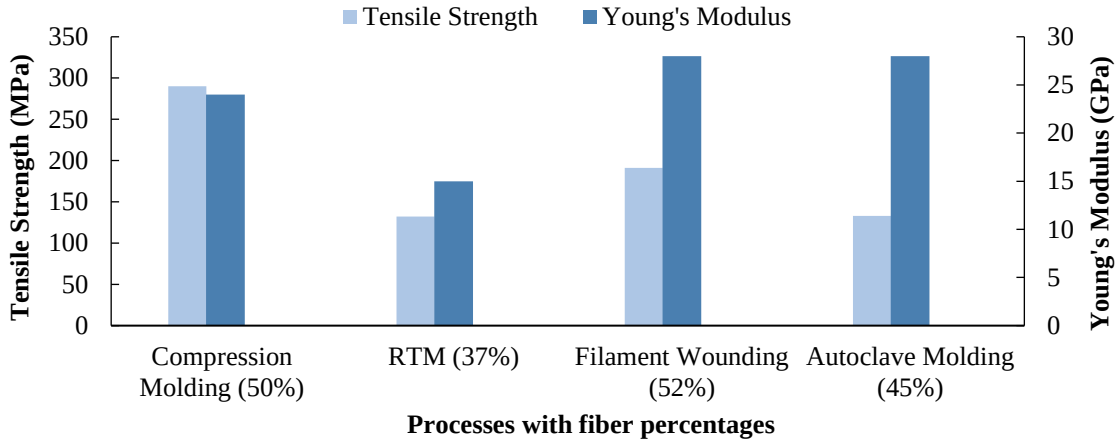

Fig. 8 Comparative Tensile strength and Young's Modulus of epoxy-flax composite from different processes.

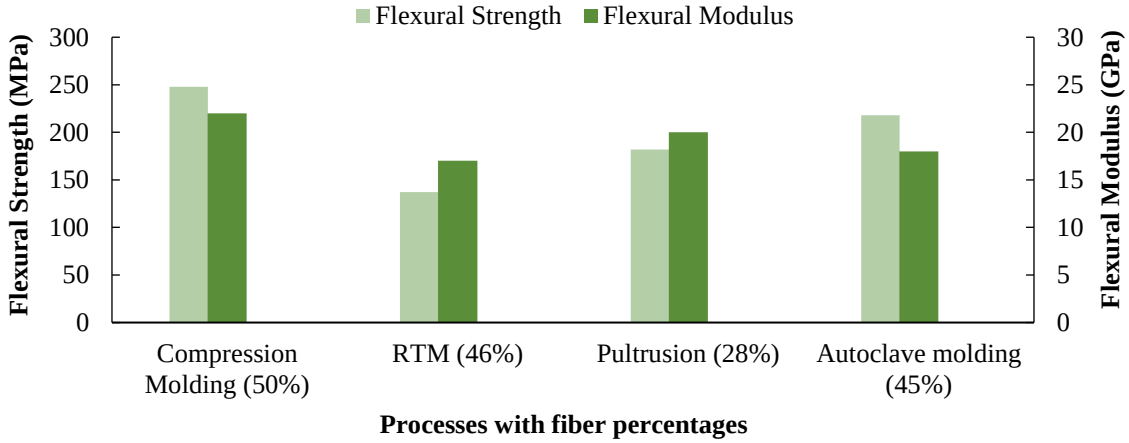

Fig. 9 Comparative Flexural strength and Flexural Modulus of Epoxy-Flax composite from different processes.

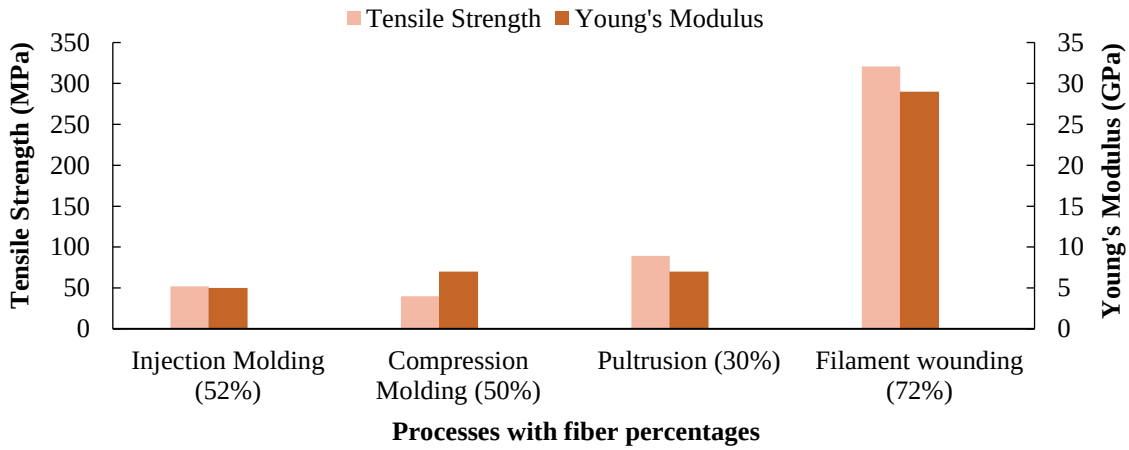

Fig. 10 Comparative Tensile strength and Young's Modulus of polypropylene-flax composite from different processes.

3 Comparisons of Mechanical Properties

Among all of the discussed natural fiber, flax fiber gives the highest mechanical properties. Consequently, the flax-based NFCs from various processes have more strength compared to others and utmost research has been done associated with it. In this article, adequate mechanical properties of flax-based NFCs with thermoplastics and thermosets binding have been upheld for comparison.

Epoxy as a thermoset has higher mechanical properties but the process associated with it is little complex than thermoplastics. The properties are shown in Fig. 8 and Fig. 9 of epoxy-flax composites with various fiber percentages which are prepared from Compression Molding, Resin Transfer Molding, Filament Wounding, and Autoclave Molding.

Short fiber composites behave like quasi-isotropic material additionally the mechanical properties in a random direction are slightly higher than long fiber composites. Contrastingly, long fiber composites have slightly lower mechanical properties with having strong directional dependency. As a result, compression molding short fiber composite has higher tensile strength than the other three processes. Pure epoxy has tensile strength of 82-115MPa [122] and flax fiber can show maximum 1500MPa tensile strength while the minimum is 88MPa [123]. The fiber percentage can play a tremendous effect where the higher

strength flax fibers are used. Approximately similar fiber percentages are used in compression molding, filament wounding, and autoclave molding. Among all of them, compression molding gives the highest tensile strength which is 51% higher than filament wounding. Contrastingly, Young's modulus remains near about similar at every process except Resin transfer molding because of its lower fiber percentage.

Besides, compression molding composite has comparative flexural strength with compared to others except pultrusion process. Though pultrusion process has lower fiber percentage, it shows comparatively higher flexural strength and flexural modulus. Approximately similar fiber percentages are used in compression molding, resin transfer molding and autoclave molding. Among all of them, compression molding gives higher flexural strength which is 13-36% higher than pultrusion and autoclave molding process.

Polypropylene as a thermoplastic has lower mechanical properties but the process associated with thermoplastics is little easier than thermosets. The properties are shown in Fig. 10 of polypropylene-flax composites with various fiber percentages which are prepared from Injection molding, Compression molding, Pultrusion, and Filament wounding.

The results show similar properties except Filament wounding because of the higher percentage of flax on it. The orientation of fiber in filament wounding is closely packed and orientated rather than compression molding and injection molding. Pultrusion process deal with long fiber which creates directional dependency but gives more strength compared to similar percentages of fiber in compression and injection molding. Pure polypropylene has only tensile strength of 35MPa [124] and flax fiber can show maximum 1500MPa tensile strength while the minimum is 88MPa [123]. The fiber percentage can play a tremendous effect on mechanical properties because of the higher properties of flax fiber compared to polypropylene. With increasing 1.5 times of fiber percentages from pultrusion to filament wounding tensile strength increased 2.6 times as well as the tensile modulus.

4 Future work

Currently, natural fiber reinforced composites are suffering from lower mechanical strength, lower heat resistance, lower water, and moisture resistance. These properties are strongly dependent on adhesion between matrix and fiber. More the adhesion ensures more mechanical strength, more thermal resistance, more water, and moisture resistance. Suitable manufacturing processes, chemical, and physical treatments of fiber can enhance these properties of NFCs. The above mentioned conventional manufacturing process can give better properties when optimum process parameters and effective physical and chemical treatments of fibers are applied.

5 Conclusion

The advancement of natural fiber reinforced composite has become attractive for eco-friendly production. Uses of NFCs have been growing firstly in outdoor and as well as load-bearing applications because of its lightweight and higher specific strength. The manufacturing process associated with it, is developing for suitable and cost-effectiveness. Though it is uncertain to say which process and chemical treatment of fiber are most suitable for a specific product. This article addresses recent developments and issues associated with different natural fiber reinforced composite conventional manufacturing processes. However, researchers are trying to develop economic and effective manufacturing process like additive manufacturing for case dependent simultaneously trying to reduce the production time and to find the most suitable process parameters of individual case. This article addresses recent developments and issues associated with different natural fiber reinforced composite conventional manufacturing processes. Advance composite production is being enriched by injection and compression molding processes where complex geometrical shape can be manufactured with higher mechanical strength compared to others. Rely on this report, it can be remarked that, natural fibers are compatible for reinforcing various polymer for enhancing mechanical properties of it which can be used in wide range of sectors like automotive, housing, packaging, infrastructure etc.

References

[1] Pickering, K.L., Efendy, M.A. and Le, T.M., 2016. A review of recent developments in natural fibre composites and their mechanical performance. *Composites Part A: Applied Science and Manufacturing*, 83, pp.98-112.

[2] Malkapuram, R., Kumar, V. and Negi, Y.S., 2009. Recent development in natural fiber reinforced polypropylene composites. *Journal of Reinforced Plastics and Composites*, 28(10), pp.1169-1189.

[3] Saheb, D.N. and Jog, J.P., 1999. Natural fiber polymer composites: a review. Advances in Polymer Technology: *Journal of the Polymer Processing Institute*, 18(4), pp.351-363.

[4] Shah, D.U., Porter, D. and Vollrath, F., 2014. Can silk become an effective reinforcing fibre? A property comparison with flax and glass reinforced composites. *Composites Science and Technology*, 101, pp.173-183.

[5] Pickering, K.L., Beckermann, G.W., Alam, S.N. and Foreman, N.J., 2007. Optimising industrial hemp fibre for composites. *Composites Part A: Applied Science and Manufacturing*, 38(2), pp.461-468.

[6] Bos, H.L., Van Den Oever, M.J.A. and Peters, O.C.J.J., 2002. Tensile and compressive properties of flax fibres for natural fibre reinforced composites. *Journal of Materials Science*, 37(8), pp.1683-1692.

[7] Dos Santos, P.A., Giriolli, J.C., Amarasekera, J. and Moraes, G., 2008, September. Natural fibers plastic composites for automotive applications. In *8th Annual automotive composites conference and exhibition (ACCE 2008)*. Troy, MI: SPE Automotive & Composites Division (pp. 492-500).

[8] Holbery, J. and Houston, D., 2006. Natural-fiber-reinforced polymer composites in automotive applications. *Jom*, 58(11), pp.80-86.

[9] Summerscales, J., Dissanayake, N.P., Virk, A.S. and Hall, W., 2010. A review of bast fibres and their composites. Part 1–Fibres as reinforcements. *Composites Part A: Applied Science and Manufacturing*, 41(10), pp.1329-1335.

[10] Zampaloni, M., Pourboghrat, F., Yankovich, S.A., Rodgers, B.N., Moore, J., Drzal, L.T., Mohanty, A.K. and Misra, M., 2007. Kenaf natural fiber reinforced polypropylene composites: A discussion on manufacturing problems and solutions. *Composites Part A: Applied Science and Manufacturing*, 38(6), pp.1569-1580.

[11] Ho, M.P., Wang, H., Lee, J.H., Ho, C.K., Lau, K.T., Leng, J. and Hui, D., 2012. Critical factors on manufacturing processes of natural fibre composites. *Composites Part B: Engineering*, 43(8), pp.3549-3562.

[12] Vallejos, M.E., Espinach, F.X., Julian, F., Torres, L., Vilaseca, F. and Mutje, P., 2012. Micromechanics of hemp strands in polypropylene composites. *Composites Science and Technology*, 72(10), pp.1209-1213.

[13] Matuana, L.M., Balatinecz, J.J., Sodhi, R.N.S. and Park, C.B., 2001. Surface characterization of esterified cellulosic fibers by XPS and FTIR spectroscopy. *Wood Science and Technology*, 35(3), pp.191-201.

[14] Sun, Z.Y., Han, H.S. and Dai, G.C., 2010. Mechanical properties of injection-molded natural fiber-reinforced polypropylene composites: formulation and compounding processes. *Journal of Reinforced Plastics and Composites*, 29(5), pp.637-650.

[15] Ramesh, M., Palanikumar, K. and Reddy, K.H., 2013. Mechanical property evaluation of sisal–jute–glass fiber reinforced polyester composites. *Composites Part B: Engineering*, 48, pp.1-9.

[16] Masoodi, R. and Pillai, K.M., 2011. Modeling the processing of natural fiber composites made using liquid composite molding. *Handbook of Bioplastics and Biocomposites Engineering Applications*, ed. by S. Pilla, Scrivener-Wiley.

[17] Mohanty, A.K., Wibowo, A., Misra, M. and Drzal, L.T., 2004. Effect of process engineering on the performance of natural fiber reinforced cellulose acetate biocomposites. *Composites Part A: applied science and manufacturing*, 35(3), pp.363-370.

[18] Drzal, L.T. and Madhukar, M., 1993. Fibre-matrix adhesion and its relationship to composite mechanical properties. *Journal of Materials Science*, 28(3), pp.569-610.

[19] Pandey, J.K., Ahn, S.H., Lee, C.S., Mohanty, A.K. and Misra, M., 2010. Recent advances in the application of natural fiber based composites. *Macromolecular Materials and Engineering*, 295(11), pp.975-989.

[20] Medina, L., Schledjewski, R. and Schlarb, A.K., 2009. Process related mechanical properties of press molded natural fiber reinforced polymers. *Composites Science and Technology*, 69(9), pp.1404-1411.

[21] Elanchezhian, C., Ramnath, B.V., Ramakrishnan, G., Rajendrakumar, M., Naveenkumar, V. and Saravanakumar, M.K., 2018. Review on mechanical properties of natural fiber composites. *Materials Today: Proceedings*, 5(1), pp.1785-1790.

[22] Cho, D., Seo, J.M., Lee, H.S., Cho, C.W., Han, S.O. and Park, W.H., 2007. Property improvement of natural fiber-reinforced green composites by water treatment. *Advanced Composite Materials*, 16(4), pp.299-314.

[23] Bongarde, U.S. and Shinde, V.D., 2014. Review on natural fiber reinforcement polymer composites. International Journal of Engineering *Science and Innovative Technology*, 3(2), pp.431-436.

[24] Feldmann, M., Heim, H.P. and Zarges, J.C., 2016. Influence of the process parameters on the mechanical properties of engineering biocomposites using a twin-screw extruder. *Composites Part A: Applied Science and Manufacturing*, 83, pp.113-119.

[25] Sui, G., Fuqua, M.A., Ulven, C.A. and Zhong, W.H., 2009. A plant fiber reinforced polymer composite prepared by a twin-screw extruder. *Bioresource Technology*, 100(3), pp.1246-1251.

[26] Ariffin, A. and Ahmad, M.S.B., 2011. Single screw extruder in particulate filler composite. *Polymer-Plastics Technology and Engineering*, 50(4), pp.395-403.

[27] Sanjay, M.R. and Yogesha, B., 2017. Studies on natural/glass fiber reinforced polymer hybrid composites: An evolution. *Materials Today: Proceedings*, 4(2), pp.2739-2747.

[28] Prasad, V., Hunize, C.M., Abhiraj, R.I., Jospeh, M.A., Sekar, K. and Ali, M., 2019. Mechanical properties of flax fiber reinforced composites manufactured using hand layup and compression molding—a comparison. In *Advances in Industrial and Production Engineering* (pp. 781-789). Springer, Singapore.

[29] Williams, G.I. and Wool, R.P., 2000. Composites from natural fibers and soy oil resins. *Applied Composite Materials*, 7(5), pp.421-432.

[30] Rouison, D., Sain, M. and Couturier, M., 2003. Resin-transfer molding of natural fiber–reinforced plastic. I. Kinetic study of an unsaturated polyester resin containing an inhibitor and various promoters. *Journal of Applied Polymer Science*, 89(9), pp.2553-2561.

[31] Haiyan, L., Yong, L., Jun, X. and Dajun, H., 2009. Research on Automatic Tape-laying Technique for Composites-Calculation Method of Tape-laying Path on Free-form Surfaces [J]. *Acta Aeronautica Et Astronautica Sinica*, 9.

[32] Yao, J., Sun, D., Yao, Z.Q., Zhang, P., Zhang, M.C. and Shi, R.H., 2011. Current situation and research progress of automated tape-laying technology for composites. Ji Xie She Ji Yu Yan Jiu(*Machine Design and Research*), 27(4), pp.60-65.

[33] Grimshaw, M.N., Grant, C.G. and Diaz, J.M.L., 2001, May. Advanced technology tape laying for affordable manufacturing of large composite structures. In *International sampe symposium and exhibition* (pp. 2484-2494). SAMPE; 1999.

[34] Serizawa, S., Inoue, K. and Iji, M., 2006. Kenaf-fiber-reinforced poly (lactic acid) used for electronic products. *Journal of Applied Polymer Science*, 100(1), pp.618-624.

[35] Huda, M.S., Mohanty, A.K., Drzal, L.T., Schut, E. and Misra, M., 2005. "Green" composites from recycled cellulose and poly (lactic acid): physico-mechanical and morphological properties evaluation. *Journal of Materials Science*, 40(16), pp.4221-4229.

[36] Huda, M.S., Drzal, L.T., Misra, M. and Mohanty, A.K., 2006. Wood-fiber-reinforced poly (lactic acid) composites: evaluation of the physicomechanical and morphological properties. *Journal of Applied Polymer Science*, 102(5), pp.4856-4869.

[37] Huda, M.S., Drzal, L.T., Misra, M., Mohanty, A.K., Williams, K. and Mielewski, D.F., 2005. A study on biocomposites from recycled newspaper fiber and poly (lactic acid). *Industrial & Engineering Chemistry Research*, 44(15), pp.5593-5601.

[38] Huda, M.S., Drzal, L.T., Mohanty, A.K. and Misra, M., 2006. Chopped glass and recycled newspaper as reinforcement fibers in injection molded poly (lactic acid)(PLA) composites: a comparative study. *Composites Science and Technology*, 66(11-12), pp.1813-1824.

[39] Nyström, B., 2007. Natural fiber composites: optimization of microstructure and processing parameters (*Doctoral dissertation*, Luleå tekniska universitet).

[40] Thomason, J.L. and Rudeiros-Fernández, J.L., 2018. A review of the impact performance of natural fiber thermoplastic composites. *Frontiers in Materials*, 5, p.60.

[41] Rowell, R.M., 1998. Economic opportunities in natural fiber-thermoplastic composites. In *Science and Technology of Polymers and Advanced Materials* (pp. 869-872). Springer, Boston, MA.

[42] Deringer, T., Gröschel, C. and Drummer, D., 2018. Influence of mold temperature and process time on the degree of cure of epoxy-based materials for thermoset injection molding and prepreg compression molding. *Journal of Polymer Engineering*, 38(1), pp.73-81.

[43] Leong, Y.W., Thitithanasarn, S., Yamada, K. and Hamada, H., 2014. Compression and injection molding techniques for natural fiber composites. In *Natural Fibre Composites* (pp. 216-232). Woodhead Publishing.

[44] Farsi, M., 2012. Thermoplastic matrix reinforced with natural fibers: a study on interfacial behavior. *Some critical issues for injection molding*, pp.225-250.

[45] Fang, Q. and Hanna, M.A., 1999. Rheological properties of amorphous and semicrystalline polylactic acid polymers. *Industrial Crops and Products*, 10(1), pp.47-53.

[46] Geethamma, V.G., Joseph, R. and Thomas, S., 1995. Short coir fiber-reinforced natural rubber composites: effects of fiber length, orientation, and alkali treatment. *Journal of Applied Polymer Science*, 55(4), pp.583-594.

[47] Santos, J.D., Fajardo, J.I., Cuji, A.R., García, J.A., Garzón, L.E. and López, L.M., 2015. Experimental evaluation and simulation of volumetric shrinkage and warpage on polymeric composite reinforced with short natural fibers. *Frontiers of Mechanical Engineering*, 10(3), pp.287-293.

[48] Kim, S.K., Lee, S.W. and Youn, J.R., 2002. Measurement of residual stresses in injection molded short fiber composites considering anisotropy and modulus variation. *Korea-Australia Rheology Journal*, 14(3), pp.107-114.

[49] Lee, K.S., Lee, S.W., Youn, J.R., Kang, T.J. and Chung, K., 2001. Confocal microscopy measurement of the fiber orientation in short fiber reinforced plastics. *Fibers and Polymers*, 2(1), pp.41-50.

[50] White, J.R., 1985. On the layer removal analysis of residual stress. *Journal of Materials Science*, 20(7), pp.2377-2387.

[51] Folkes, M.J. and Russell, D.A.M., 1980. Orientation effects during the flow of short-fibre reinforced thermoplastics. *Polymer*, 21(11), pp.1252-1258.

[52] Sain, M., Suhara, P., Law, S. and Bouilloux, A., 2005. Interface modification and mechanical properties of natural fiber-polyolefin composite products. *Journal of Reinforced Plastics and Composites*, 24(2), pp.121-130.

[53] Bledzki, A.K., Mamun, A.A., Lucka-Gabor, M. and Gutowski, V.S., 2008. The effects of acetylation on properties of flax fibre and its polypropylene composites. *Express Polymer Letters*, 2(6), pp.413-422.

[54] Snijder, M.H. and Bos, H.L., 2000. Reinforcement of polypropylene by annual plant fibers: optimisation of the coupling agent efficiency. *Composite Interfaces*, 7(2), pp.69-75.

[55] Li, H. and Sain, M.M., 2003. High stiffness natural fiber-reinforced hybrid polypropylene composites. *Polymer-Plastics Technology and Engineering*, 42(5), pp.853-862.

[56] Rana, A.K., Mandal, A. and Bandyopadhyay, S., 2003. Short jute fiber reinforced polypropylene composites: effect of compatibiliser, impact modifier and fiber loading. *Composites Science and Technology*, 63(6), pp.801-806.

[57] Feldmann, M. and Bledzki, A.K., 2014. Bio-based polyamides reinforced with cellulosic fibres–processing and properties. *Composites Science and Technology*, 100, pp.113-120.

[58] Fink, H.P. and Ganster, J., 2006, December. Novel Thermoplastic Composites from Commodity Polymers and Man-Made Cellulose Fibers. In *Macromolecular Symposia* (Vol. 244, No. 1, pp. 107-118). Weinheim: WILEY-VCH Verlag.

[59] Adekunle, K., Åkesson, D. and Skrifvars, M., 2010. Biobased composites prepared by compression molding with a novel thermoset resin from soybean oil and a natural-fiber reinforcement. Journal of Applied Polymer Science, 116(3), pp.1759-1765.

[60] Idicula, M., Sreekumar, P.A., Joseph, K. and Thomas, S., 2009. Natural fiber hybrid composites—A comparison between compression molding and resin transfer molding. *Polymer Composites*, 30(10), pp.1417-1425.

[61] Milanese, A.C., Cioffi, M.O.H. and Voorwald, H.J.C., 2011. Mechanical behavior of natural fiber composites. *Procedia Engineering*, 10, pp.2022-2027.

[62] Mallick, P.K., 2007. Fiber-reinforced composites: materials, manufacturing, and design. *CRC press*.

[63] Hu, R. and Lim, J.K., 2007. Fabrication and mechanical properties of completely biodegradable hemp fiber reinforced polylactic acid composites. *Journal of Composite Materials*, 41(13), pp.1655-1669.

[64] Tatara, R.A., 2017. Compression molding. In *Applied plastics engineering handbook* (pp. 291-320). William Andrew Publishing.

[65] Devi, L.U., Bhagawan, S.S. and Thomas, S., 1997. Mechanical properties of pineapple leaf fiber-reinforced polyester composites. *Journal of Applied Polymer Science*, 64(9), pp.1739-1748.

[66] Le, T.M., 2016. Harakeke fibre as reinforcement in epoxy matrix composites and its hybridisation with hemp fibre (*Doctoral dissertation*, University of Waikato).

[67] Islam, M.S., Pickering, K.L. and Foreman, N.J., 2011. Influence of alkali fiber treatment and fiber processing on the mechanical properties of hemp/epoxy composites. *Journal of Applied Polymer Science*, 119(6), pp.3696-3707.

[68] Zhang, L. and Miao, M., 2010. Commingled natural fibre/polypropylene wrap spun yarns for structured thermoplastic composites. *Composites Science and Technology*, 70(1), pp.130-135.

[69] Graupner, N. and Müssig, J., 2011. A comparison of the mechanical characteristics of kenaf and lyocell fibre reinforced poly (lactic acid)(PLA) and poly (3-hydroxybutyrate)(PHB) composites. *Composites Part A: Applied Science and Manufacturing*, 42(12), pp.2010-2019.

[70] Ochi, S., 2008. Mechanical properties of kenaf fibers and kenaf/PLA composites. *Mechanics of Materials*, 40(4-5), pp.446-452.

[71] Rong, M.Z., Zhang, M.Q., Liu, Y., Yang, G.C. and Zeng, H.M., 2001. The effect of fiber treatment on the mechanical properties of unidirectional sisal-reinforced epoxy composites. *Composites Science and Technology*, 61(10), pp.1437-1447.

[72] Le, T.M. and Pickering, K.L., 2015. The potential of harakeke fibre as reinforcement in polymer matrix composites including modelling of long harakeke fibre composite strength. *Composites Part A: Applied Science and Manufacturing*, 76, pp.44-53.

[73] Newman, R.H., Le Guen, M.J., Battley, M.A. and Carpenter, J.E., 2010. Failure mechanisms in composites reinforced with unidirectional Phormium leaf fibre. *Composites Part A: Applied Science and Manufacturing*, 41(3), pp.353-359.

[74] Sathish, S., Kumaresan, K., Prabhu, L. and Vigneshkumar, N., 2017. Experimental investigation on volume fraction of mechanical and physical properties of flax and bamboo fibers reinforced hybrid epoxy composites. *Polymers and Polymer Composites*, 25(3), pp.229-236.

[75] Hughes, M., Carpenter, J. and Hill, C., 2007. Deformation and fracture behaviour of flax fibre reinforced thermosetting polymer matrix composites. *Journal of Materials Science*, 42(7), pp.2499-2511.

[76] Oksman, K., 2000. Mechanical properties of natural fibre mat reinforced thermoplastic. *Applied Composite Materials*, 7(5), pp.403-414.

[77] Rouison, D., Sain, M. and Couturier, M., 2006. Resin transfer molding of hemp fiber composites: optimization of the process and mechanical properties of the materials. *Composites Science and Technology*, 66(7-8), pp.895-906.

[78] Sreekumar, P.A., Joseph, K., Unnikrishnan, G. and Thomas, S., 2007. A comparative study on mechanical properties of sisal-leaf fibre-reinforced polyester composites prepared by resin transfer and compression moulding techniques. *Composites Science and Technology*, 67(3-4), pp.453-461.

[79] Ferland, P., Guittard, D. and Trochu, F., 1996. Concurrent methods for permeability measurement in resin transfer molding. *Polymer Composites*, 17(1), pp.149-158.

[80] Kim, S.K. and Daniel, I.M., 2003. Determination of three-dimensional permeability of fiber preforms by the inverse parameter estimation technique. *Composites Part A: Applied Science and Manufacturing*, 34(5), pp.421-429.

[81] Ikegawa, N., Hamada, H. and Maekawa, Z., 1996. Effect of compression process on void behavior in structural resin transfer molding. *Polymer Engineering & Science*, 36(7), pp.953-962.

[82] Warrior, N.A., Turner, T.A., Robitaille, F. and Rudd, C.D., 2003. Effect of resin properties and processing parameters on crash energy absorbing composite structures made by RTM. *Composites Part A: Applied Science and Manufacturing*, 34(6), pp.543-550.

[83] Francucci, G., Rodríguez, E.S. and Vázquez, A., 2012. Experimental study of the compaction response of jute fabrics in liquid composite molding processes. *Journal of Composite Materials*, 46(2), pp.155-167.

[84] Rouison, D., Sain, M. and Couturier, M., 2004. Resin transfer molding of natural fiber reinforced composites: cure simulation. *Composites Science and Technology*, 64(5), pp.629-644.

[85] Kang, M.K., Jung, J.J. and Lee, W.I., 2000. Analysis of resin transfer moulding process with controlled multiple gates resin injection. *Composites Part A: Applied Science and Manufacturing*, 31(5), pp.407-422.

[86] Richardson, M.O.W. and Zhang, Z.Y., 2000. Experimental investigation and flow visualisation of the resin transfer mould filling process for non-woven hemp reinforced phenolic composites. *Composites Part A: Applied Science and Manufacturing*, 31(12), pp.1303-1310.

[87] Rodriguez, E., Giacomelli, F. and Vazquez, A., 2004. Permeability-porosity relationship in RTM for different fiberglass and natural reinforcements. *Journal of Composite Materials*, 38(3), pp.259-268.

[88] Rodríguez, E., Petrucci, R., Puglia, D., Kenny, J.M. and Vazquez, A., 2005. Characterization of composites based on natural and glass fibers obtained by vacuum infusion. *Journal of Composite Materials*, 39(3), pp.265-282.

[89] Felline, F., Pappada, S., Gennaro, R. and Passaro, A., 2013. Resin transfer moulding of composite panels with bio-based resins. *SAMPE Journal*, 49(3), pp.20-24.

[90] Goutianos, S., Peijs, T., Nystrom, B. and Skrifvars, M., 2006. Development of flax fibre based textile reinforcements for composite applications. *Applied Composite Materials*, 13(4), pp.199-215.

[91] Oksman, K., Wallström, L., Berglund, L.A. and Filho, R.D.T., 2002. Morphology and mechanical properties of unidirectional sisal–epoxy composites. *Journal of Applied Polymer Science*, 84(13), pp.2358-2365.

[92] Oksman, K., 2001. High quality flax fibre composites manufactured by the resin transfer moulding process. *Journal of Reinforced Plastics and Composites*, 20(7), pp.621-627.

[93] Davidovits, J., 2015. Geopolymer Chemistry and Applications. 4-th edition. J. Davidovits.–*Saint-Quentin*, France.

[94] Noorunnisa Khanam, P., Mohan Reddy, M., Raghu, K., John, K. and Venkata Naidu, S., 2007. Tensile, flexural and compressive properties of sisal/silk hybrid composites. *Journal of Reinforced Plastics and Composites*, 26(10), pp.1065-1070.

[95] Kornmann, X., Rees, M., Thomann, Y., Necola, A., Barbezat, M. and Thomann, R., 2005. Epoxy-layered silicate nanocomposites as matrix in glass fibre-reinforced composites. *Composites Science and Technology*, 65(14), pp.2259-2268.

[96] Raji, M., Abdellaoui, H., Essabir, H., Kakou, C.A. and Bouhfid, R., 2019. Prediction of the cyclic durability of woven-hybrid composites. In Durability and Life Prediction in Biocomposites, *Fibre-Reinforced Composites and Hybrid Composites* (pp. 27-62). Woodhead Publishing.

[97] Li, X., Tabil, L.G. and Panigrahi, S., 2007. Chemical treatments of natural fiber for use in natural fiber-reinforced composites: a review. *Journal of Polymers and the Environment*, 15(1), pp.25-33.

[98] Mishra, V. and Biswas, S., 2013. Physical and mechanical properties of bi-directional jute fiber epoxy composites. *Procedia Engineering*, 51, pp.561-566.

[99] Bindal, A., Singh, S., Batra, N.K. and Khanna, R., 2013. Development of glass/jute fibers reinforced polyester composite. *Indian Journal of Materials Science*, 2013.

[100] Hojo, T., Xu, Z., Yang, Y. and Hamada, H., 2014. Tensile properties of bamboo, jute and kenaf mat-reinforced composite. *Energy Procedia*, 56, pp.72-79.

[101] Sukmawan, R., Takagi, H. and Nakagaito, A.N., 2016. Strength evaluation of cross-ply green composite laminates reinforced by bamboo fiber. *Composites Part B: Engineering*, 84, pp.9-16.

[102] Ramesh, M., Atreya, T.S.A., Aswin, U.S., Eashwar, H. and Deepa, C., 2014. Processing and mechanical property evaluation of banana fiber reinforced polymer composites. *Procedia Engineering*, 97, pp.563-572.

[103] Islam, M.S., Azmy, S. and Almamun, A., 2019. Comparative study on mechanical properties of banana and rattan fiber reinforced epoxy composites. *American Journal of Engineering Research (AJER)*, 8(2), pp.1-6.

[104] Obele, C. and Ishidi, E., 2015. Mechanical properties of coir fiber reinforced Epoxy resin composites for helmet shell. *Industrial Engineering Letters*, 5(7).

[105] Rachchh, N.V., Ujeniya, P.A. and Misra, R.K., 2014. Mechanical characterisation of rattan fibre polyester composite. *Procedia Materials Science*, 6, pp.1396-1404.

[106] Peng, X., Fan, M., Hartley, J. and Al-Zubaidy, M., 2012. Properties of natural fiber composites made by pultrusion process. *Journal of Composite Materials*, 46(2), pp.237-246.

[107] Nguyen-Chung, T., Friedrich, K. and Mennig, G., 2007. Processability of pultrusion using natural fiber and thermoplastic matrix. *Research Letters in Materials Science*, 2007.

[108] Van de Velde, K. and Kiekens, P., 2001. Thermoplastic pultrusion of natural fibre reinforced composites. *Composite structures*, 54(2-3), pp.355-360.

[109] Akil, H.M., Cheng, L.W., Ishak, Z.M., Bakar, A.A. and Abd Rahman, M.A., 2009. Water absorption study on pultruded jute fibre reinforced unsaturated polyester composites. *Composites Science and Technology*, 69(11-12), pp.1942-1948.

[110] Angelov, I., Wiedmer, S., Evstatiev, M., Friedrich, K. and Mennig, G., 2007. Pultrusion of a flax/polypropylene yarn. *Composites Part A: Applied Science and Manufacturing*, 38(5), pp.1431-1438.

[111] Bobba, S., Leman, Z., Zainudin, E.S. and Sapuan, S.M., 2020, October. Characterisation of the tensile and fracture properties of filament wound natural fibre rings. In *AIP Conference Proceedings* (Vol. 2284, No. 1, p. 020015). AIP Publishing LLC.

[112] Lehtiniemi, P., Dufva, K., Berg, T., Skrifvars, M. and Järvelä, P., 2011. Natural fiber-based reinforcements in epoxy composites processed by filament winding. *Journal of Reinforced Plastics and Composites*, 30(23), pp.1947-1955.

[113] Goutianos, S., Peijs, T., Nystrom, B. and Skrifvars, M., 2007. Textile reinforcements based on aligned flax fibres for structural composites. *Composites Innovation*.

[114] Gassan, J. and Bledzki, A.K., 1999. Possibilities for improving the mechanical properties of jute/epoxy composites by alkali treatment of fibres. *Composites Science and Technology*, 59(9), pp.1303-1309.

[115] Lee, S.M. ed., 1992. Handbook of composite reinforcements. *John Wiley & Sons*.

[116] Gohil, P.P. and Shaikh, A.A., 2010. Experimental investigation and micro mechanics assessment for longitudinal elastic modulus in unidirectional cotton-polyester composites. *International Journal of Engineering and Technology*, 2(2), pp.111-118.

[117] Munro, M., 1988. Review of manufacturing of fiber composite components by filament winding. *Polymer Composites*, 9(5), pp.352-359.

[118] Salit, M.S., Jawaid, M., Yusoff, N.B. and Hoque, M.E. eds., 2015. Manufacturing of natural fibre reinforced polymer composites (pp. 1-383). New York, USA: *Springer International Publishing*.

[119] Halley, P.J., 2012. Rheology of thermosets: the use of chemorheology to characterise and model thermoset flow behaviour. In Thermosets (pp. 92-117). *Woodhead Publishing*.

[120] Madsen, B. and Lilholt, H., 2003. Physical and mechanical properties of unidirectional plant fibre composites—an evaluation of the influence of porosity. *Composites Science and Technology*, 63(9), pp.1265-1272.

[121] Van de Weyenberg, I., Ivens, J., De Coster, A., Kino, B., Baetens, E. and Verpoest, I., 2003. Influence of processing and chemical treatment of flax fibres on their composites. *Composites Science and Technology*, 63(9), pp.1241-1246.

[122] Yang, J.P., Chen, Z.K., Yang, G., Fu, S.Y. and Ye, L., 2008. Simultaneous improvements in the cryogenic tensile strength, ductility and impact strength of epoxy resins by a hyperbranched polymer. *Polymer*, 49(13-14), pp.3168-3175.

[123] Jawaid, M.H.P.S. and Khalil, H.A., 2011. Cellulosic/synthetic fibre reinforced polymer hybrid composites: A review. Carbohydrate polymers, 86(1), pp.1-18.

[124] Arib, R.M.N., Sapuan, S.M., Ahmad, M.M.H.M., Paridah, M.T. and Zaman, H.K., 2006. Mechanical properties of pineapple leaf fibre reinforced polypropylene composites. Materials & Design, 27(5), pp.391-396.

SciEn
Journal of Engineering Advancements Vol. 02(01) 2021, pp 24-34 https://doi.org/10.38032/jea.2021.01.004

Mathematical Analysis of Improving the System Capacity and Signal to Interference Ratio in Cellular Mobile Communication

Md. Ariful Islam[1], Amena Begum[2] and Md. Rakib Hasan[2]*

[1]Dept. of Robotics & Mechatronics Engineering, University of Dhaka, Dhaka, Bangladesh
[2]Dept. of Information & Communication Technology, Comilla University, Cumilla, Bangladesh

Received: January 01, 2021, Revised: January 28, 2021, Accepted: January 30, 2021, Available Online: February 06, 2021

ABSTRACT

The most important index for Quality of Service (e.g. reliability, performance) is call drop which has not been accurately discussed before. Sometimes the network disconnects while talking on the phone, this disconnection is called a dropped call. The level of call drop of mobile operators in the every country has increased significantly lately. As a result, thousands of mobile phone users are suffering. To reduce call drop, at first the factors causing call drop have been identified in this paper. Based on these factors, a dropped call model has developed to find out the parameters associated with call drop. Then some existing techniques have analyzed mathematically to improve the different parameters of these factors to reduce call drop. Three main factors have been identified from the developed dropped call model causing call drops such as the lack of available channels, the poor signal quality and the handover failure. In this paper, mathematical analysis of cell splitting, cell sectoring and microcell zone concept have been provided to support extra connecting demand, ongoing service and to improve the signal to interference ratio. Also queuing handoff will be analyzed mathematically with justification to avoid disturbing service call drop. Simulation of a mathematical model of these call drop reduction techniques has performed using MATLAB software.

Keywords: Cell Splitting; Cell Sectoring, Microcell Zone Concept, Quality of Service, Capacity, Signal to Interference Ratio.

1. Introduction

Mobile companies cannot afford a large amount of network demands with increasing population density day by day [1]. For these reasons force termination of calls has to be implemented to support the traffic-congested area. So, now-a-days call drop reduction becomes our the main goal to ensure the best service in the wireless communication system. For call drop reduction, at first the factors causing call drop will have to be investigated. With the help of this investigation, the solution of call drop will be provided with mathematical proof. This research may help steer the mobile operators to improve the quality of the service with existing techniques that they will provide.

Puru Gaur [1] published a paper on a review of menace of call drops in India and possible ways to minimize it. In that paper, they demonstrated the overall condition of call drops and possible ways such as cell splitting, cell sectoring, dynamic channel allocation and hybrid channel allocation were provided to minimize the call drops. But they did not give any mathematical proof analysis of their proposed methods. Ohaneme C.O, Onoh G.N, Ifeagwu E.N and Eneh [2] presented cell splitting as a technique of improving channel capacity and reducing blocking probability. But any solution regarding the signal to interference ratio problem was not provided. Jatin and Karishan Kumar [3] analyzed call dropping and handover problem in the cellular system. But any solution based on a mathematical model was not mentioned. This paper deals with various techniques such as cell splitting, cell sectoring, micro-cell zone concept and queuing handoffs mechanism with a view to minimizing call drop probability within high density traffic area. The service coverage area has been maximized and interference has minimized in this work. The existing techniques will be verified mathematically.

2. Methodology

2.1 Identify factors causing call drop

To develop a model to reduce call drop, the factors causing call drop have to be identified. The factors which are responsible casing call drop are given as follows.

2.1.1 Increasing demand of wireless cellular connectivity

The blocking probability increases with increasing the offered traffic intensity. This relationship can be found from Erlang B formula [4] given by equation (1)

$$B(M,A) = \frac{A^M/A!}{\sum_{i=0}^{M}\left(\frac{A^i}{i!}\right)} \Rightarrow M = \frac{log[B(M,A)\sum_{i=0}^{M}(\frac{A^i}{i!})]}{logA} \times A! \quad (1)$$

Where, $B(M,A)$ is the lost call probability, A is the traffic intensity which is offered in Erlangs and M is the available number of channels.

2.1.2 Handover Failure

According to Hong and Rappaport model [5] the handoff rate is given by equation (2)

$$\lambda_{HAR} = \frac{P_{NCOH}(1 - B_{originating})}{1 - P_{SHC}(1 - P'_{failure})}\lambda_{originatig} \quad (2)$$

*Corresponding Author Email Address: arif_eeedu@yahoo.com Published by: SciEn Publishing Group

Where, λ_{HAR} is the handoff arrival rate, P_{NCOH} is the probability of a new call required at least one handoff, P_{SHC} is the probability of successfully handed call required another call, $B_{originating}$ is the originating call blocking probability, $P'_{failure}$ is the handoff failure probability, $\lambda_{originating}$ is the originating arrival call rate. If proper handover cannot be ensured, call drop occurs. Basically handover failure can be occurred due to mismanagement of cell allocation scheme of incoming requested call to be switched into another base station cell.

2.1.3 Lack of signal strength

When a user enters an area which is out of coverage or having inadequate signal strength or the place where the signals are interfered, interrupted or jammed may cause call drop [1].

2.1.4 Co-channel Interference

The signal to interference ratio may be reduced due to co-channel interference which can be realized from the equation (3) [1].

$$\frac{S}{I} = \frac{(3N)^{\gamma/2}}{6} \Rightarrow \frac{S}{I} = \frac{1}{\sum_{l=1}^{6}(\frac{D_l}{R})^{-\gamma}} \Rightarrow \frac{S}{I} = \frac{1}{6(q)^{-\gamma}} = \frac{q^{\gamma}}{6} \quad (3)$$

Where, D_l is the distance between l^{th} interfering cell and mobile station, N is the cluster size, R is the cell radius, γ is the path loss exponent and q is the frequency reuse ratio.

2.2 Dropped call model

Now dropped call model can be developed considering the factors that have previously discussed. Let, κ_t is the total entering traffic. A fraction of this entering traffic will be dropped which is known as dropped call probability denoted by P_{drop}.Then the relation between the dropped call rate and dropped call probability [6] can be shown by equation (4)

$$D_r = \kappa_t \times P_{drop} \quad (4)$$

The channel utilization factor ϱ is the ratio of traffic intensity to the number of channels and it can be found [6] by equation (5)

$$\varrho = \frac{\kappa_t}{M} \quad (5)$$

The dropped call probability P_{drop} can be modeled [4] as given in equation (6)

$$P_{drop} = 1 - \frac{1}{e^{\varrho} - 1}\sum_{l=1}^{\infty}\frac{\varrho^l}{l!}\int_0^{\infty} f_T(t)e^{-\frac{D_r t}{l}}dt \quad (6)$$

The model has revealed that the dropped call probability depends on the dropped call rate D_r, the utilization factor ϱ and the probability density function $f_T(t)$ of call duration which is normally terminated.

Dropped call rate and Dropped call probability can be calculated with the help of equations (4) and (6). According to equation (4) and (6), the relationship between dropped call rate, dropped call probability and network traffic can be established shown in Fig. 1. As the network traffic increases, the dropped call rate and probability increase gradually.

With different number of active users, the dropped call probability can be calculated from equation (6). For reducing Dropped Cal Probability, the capacity should be increased to support large number of users. According to equation (6), the dropped call probability increases as the number of active user increases gradually shown in Fig. 2.

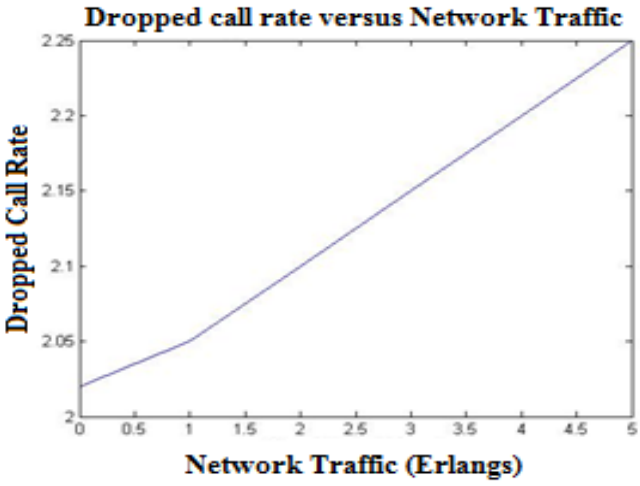

(a)

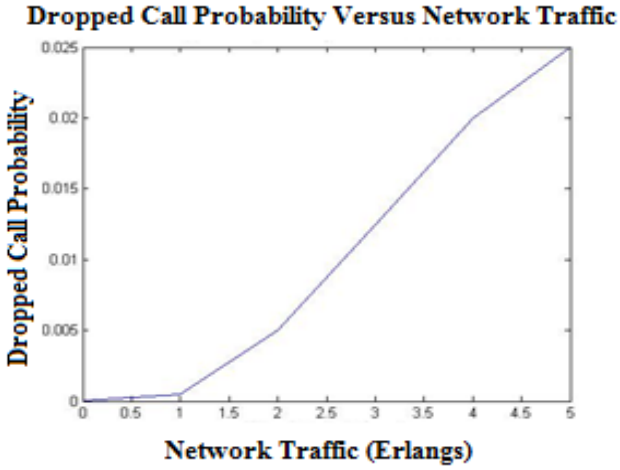

(b)

Fig. 1 Graph of (a) Dropped call rate versus Network traffic, (b) Dropped call probability versus Network traffic.

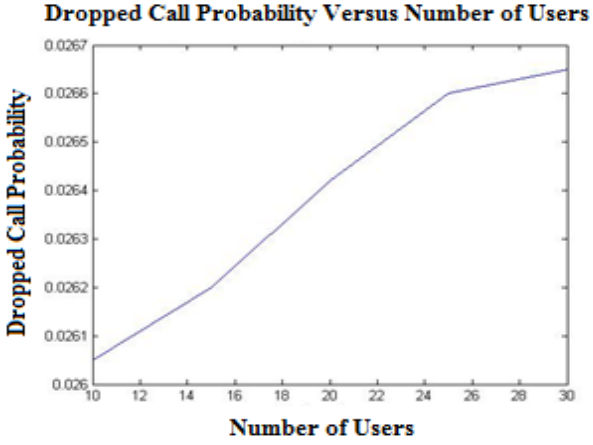

Fig. 2 Dropped call probability versus number of active users.

Channel Utilization Factors can be found from equation (5) and with channel utilization factor (ϱ), the dropped call probability can be calculated from equation (6). From equation (5), the channel utilization factor depends on the total traffic. As the traffic intensity increases, the channel utilization factor also increases with the given number of channels and as a result the dropped call probability decreases which can be evaluated from the equation (6) shown in Fig. 3.

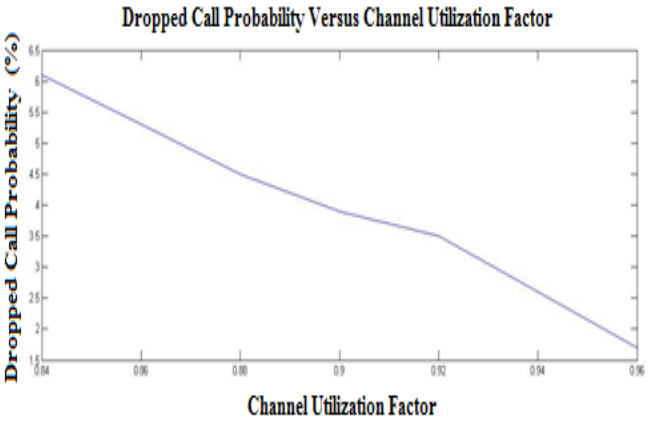

Fig. 3 Dropped call probability versus channel utilization factor.

2.3 Analysis of Techniques to reduce call drop

Based on the dropped call probability model, different techniques such as cell splitting, cell sectoring and microcell zone concept can be applied to reduce the call drop. Here, the mathematical justification of these techniques have analyzed so that a network designer can design a cellular network based on this study.

2.3.1 Cell Splitting

When a large congested cell is subdivided into smaller cells with its own base station, the antenna height and transmitting power will be reduced. This process is known as cell splitting shown in Fig. 4. In cell splitting, the congested cells are subdivided into micro, pico and femto cells with own base station [4].

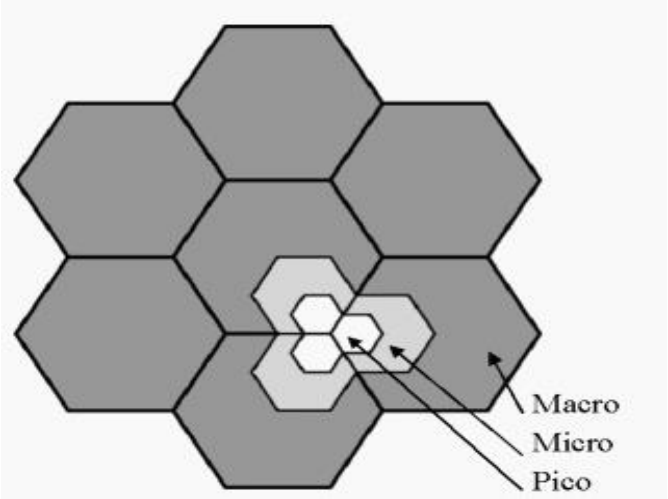

Fig. 4 Cell splitting [4].

A base station covers the radio area which is known as cell. Cell can be in different shapes shown in Fig. 5.

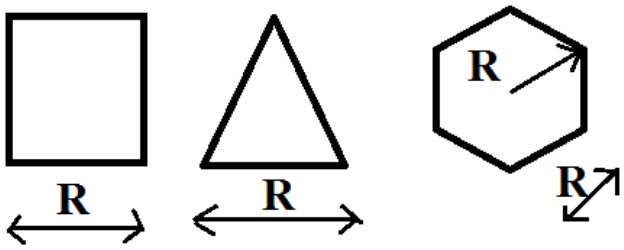

Fig. 5 Different cell model [4].

In most modeling and simulation, hexagonal cells [4] are used. The area of hexagon can be found by

$$Area_{hexagon} = \frac{3\sqrt{3}\,R^2}{2}$$

Two shift parameters i and j (values can be $0, 1, 2\ldots., n.$) are used to find out the location of co-channel cell located in the neighborhood region separated by 60^0 shown in Fig. 6 and Fig. 7.

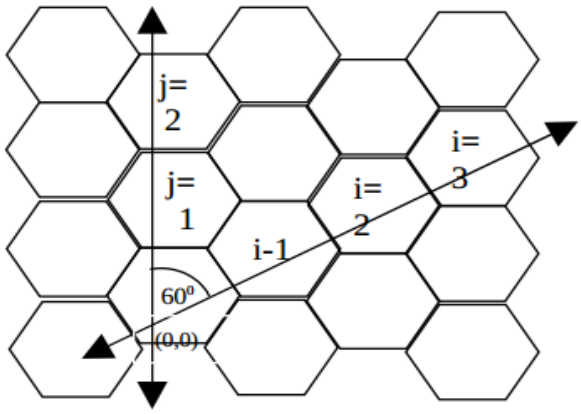

Fig. 6 Shift Parameters i and j in hexagonal network.

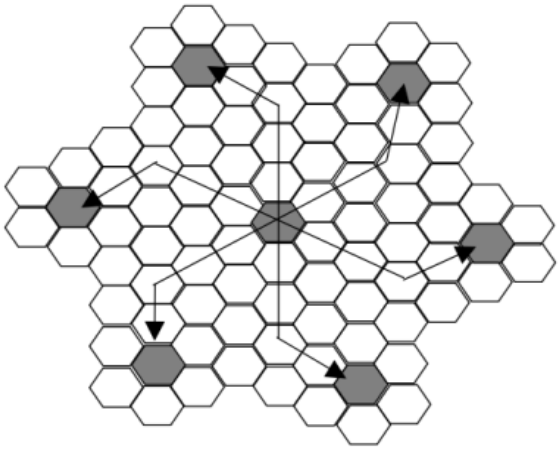

Fig. 7 Locating co-channel cells when i=3 & j=2.

To develop the relationship between cluster size and shifting parameters i *and* j, let R be the distance between the center of a regular hexagon to any of its vertex and d be the distance between the centre of two neighboring hexagons, and following steps are followed while calculating the size of a cluster N.

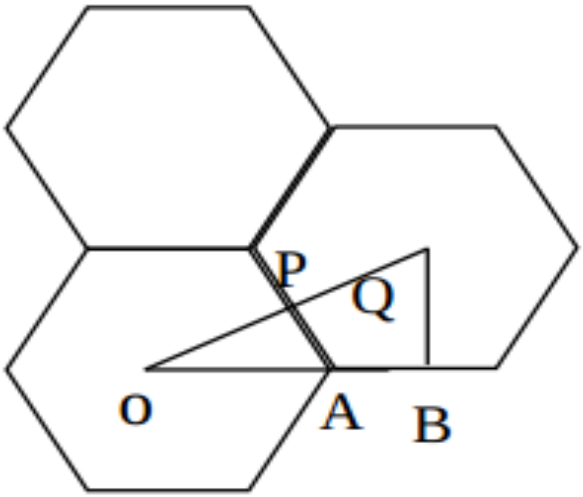

Fig. 8 Distance between two adjacent cells.

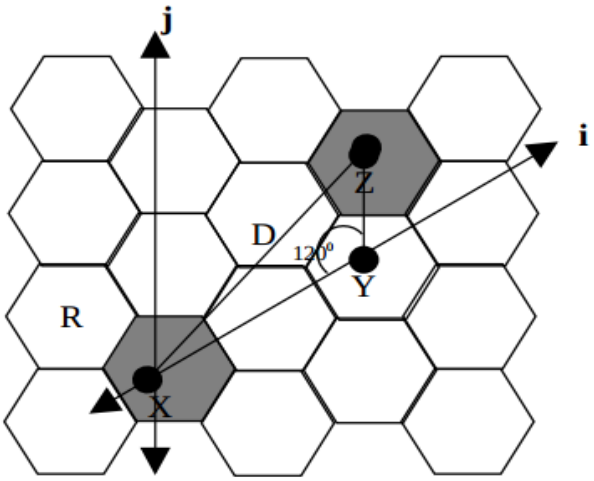

Fig. 9 Relationship between N and shift parameters (i & j).

From the geometry of the Fig. 8, $OA = R$ and $AB = R/2$. Then, $OB = OA + AB = R + R/2 = 3R/2$. In right-angled $\Delta OAP, OP = OA\ sin60^0 = \frac{\sqrt{3}}{2}R$. Let the distance between the centers of two neighboring hexagonal cells, OQ, be denoted by d, then, $OQ = OP + PQ\ (where\ OP = PQ)$.

Therefore, $d = [\frac{\sqrt{3}}{2}R + \frac{\sqrt{3}}{2}R] = \sqrt{3}\,R$.

The area of a hexagonal cell with radius R is given as $A_{small\ hexagon} = (\frac{3\sqrt{3}}{2})R^2$. Using cosine formula ΔXYZ in Fig. 9, we have, $XZ^2 = XY^2 + YZ^2 - 2(XY)(YZ)cos120^0$

$$\Rightarrow D^2 = (i \times d)^2 + (j \times d)^2 - 2(i \times d)(j \times d)\left(-\frac{1}{2}\right) = 3R^2(i^2 + j^2 + i \times j) \quad (7)$$

Where, D is the distance between a particular cell and nearest co-channel cells. To find the area of a large hexagon, $A_{large\ hexagon}$, joining the centers of the six nearest neighboring co-channel cells, a large hexagon is formed with radius equal to D, which is also the co-channel cell separation shown in Fig. 10.

The area of the large hexagon having a radius of D can be given as

$$A_{large\ hexagon} = (\frac{3\sqrt{3}}{2}) \times R^2 = (\frac{3\sqrt{3}}{2}) \times D^2 = (\frac{3\sqrt{3}}{2}) \times 3R^2(i^2 + j^2 + i \times j)$$

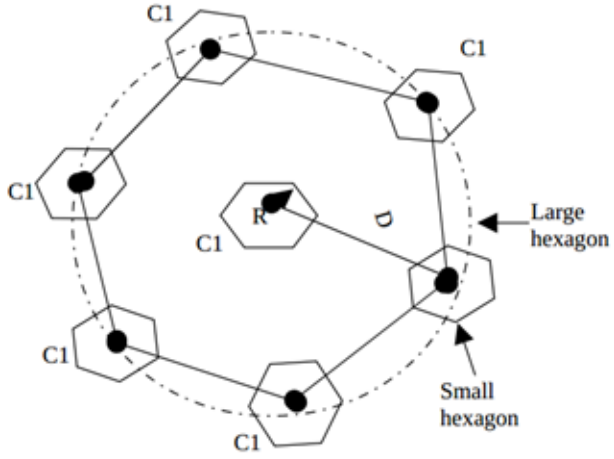

Fig. 10 Larger hexagon in the first tie [4].

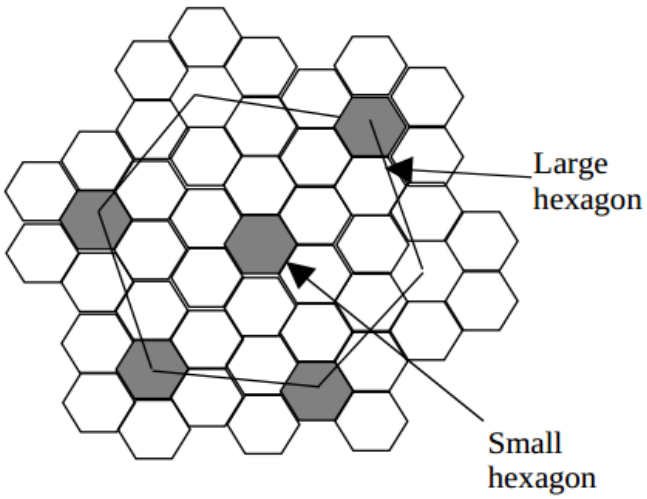

Fig. 11 Number of clusters in the first tier for N=7.

Number of cells in large hexagon,

$$L = \frac{A_{large}}{A_{small}} = \frac{(\frac{3\sqrt{3}}{2}) \times 3R^2(i^2 + j^2 + i \times j)}{(\frac{3\sqrt{3}}{2}) \times R^2} = 3(i^2 + j^2 + i \times j)$$

It can be seen from Fig. 11, the total number of cells enclosed by the larger hexagon is

$$L = N + 6 \times [\frac{1}{3} \times N] = N + 2N = 3N = 3(i^2 + j^2 + i \times j)$$

$$\Rightarrow N = (i^2 + j^2 + i \times j) \quad (8)$$

Where, i and j are the shift parameters and N is the cluster size. The co-channel interference depends on the frequency reuse ratio shown in Fig. 12 and is given [6] by equation (10).

$$q = \frac{D}{R} \quad (9)$$

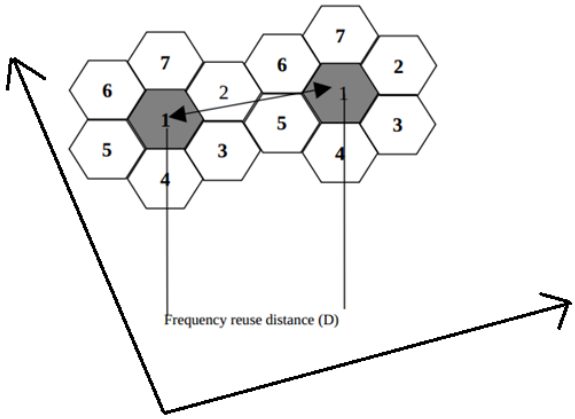

Fig. 12 Frequency reuse distance.

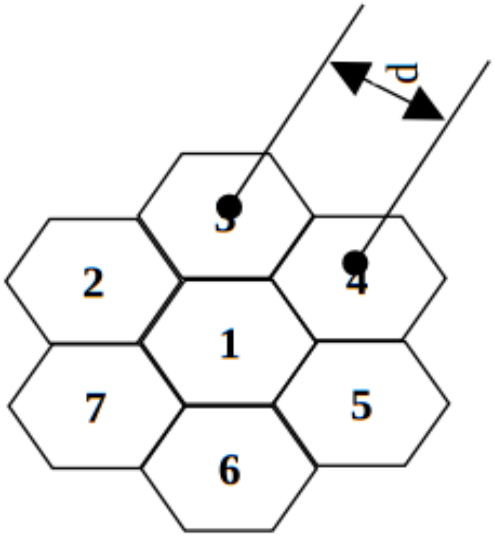

Fig. 13 Distance between two adjacent cells [4].

Let d be the distance between two cell centers of neighboring cells shown in Fig. 13. Therefore, putting $d = \sqrt{3}R$ and the relationship between $D, d,$ and shift parameters is

$$D^2 = 3R^2(i^2 + j^2 + i \times j) = 3R^2N \quad (10)$$

$$\Rightarrow 3N = \frac{D^2}{R^2} = (\frac{D}{R})^2 = q^2 \Rightarrow q = \sqrt{3N}$$

2.3.2 Cell Sectoring

The radio signals with equal power strength are transmitted to all directions in omni-directional antennas. But it is arduous to design this type of antennas. The directional antennas can be implemented to cover a region of 60 degrees or 120 degrees shown in Fig. 14.

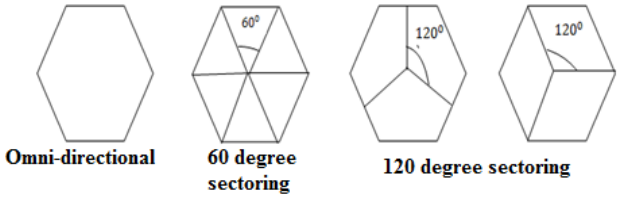

Fig. 14 Cell sectoring [5].

The cells which are served by them are called sectored cells. There are two cases for observing the SIR performance with cell sectoring methods. In omni-directional case, the signal to interference ratio can be written [4] by equation (11).

$$\frac{S}{I} = \frac{R^{-\delta}}{2(D-R)^{-\delta} + 2D^{-\delta} + 2(D+R)^{-\delta}} \quad (11)$$

Where, δ is the exponent of path loss. In three-sector case, the cell is divided into three sectors with three 120 degree directional antennas. Two interferers can be occurred in this case. Then, the signal to interference ratio can be written as equation (12).

$$\frac{S}{I} = \frac{R^{-\delta}}{D^{-\delta} + (D+0.7R)^{-\delta}} \quad (12)$$

For six sector case, the cell is divided into six sectors with six 120 degree directional antennas. Only one interferer can be occurred in this case. Then, the signal to interference ratio will be as given in equation (13).

$$\frac{S}{I} = \frac{R^{-\delta}}{(D+0.7R)^{-\delta}} \quad (13)$$

2.3.3 Microcell Zone Concept

The problem of sectoring can be addressed by another technique called the microcell zone concept shown in Fig. 15. A cell can be subdivided into micro cells per zone in this concept. Each microcell is coupled to the same base station unlike cell splitting through fiber optic line or microwave link. A directional antenna is used by each zone. When a cell phone makes a journey from one zone to another, the same channel will be retained. As a result no handoff is done.

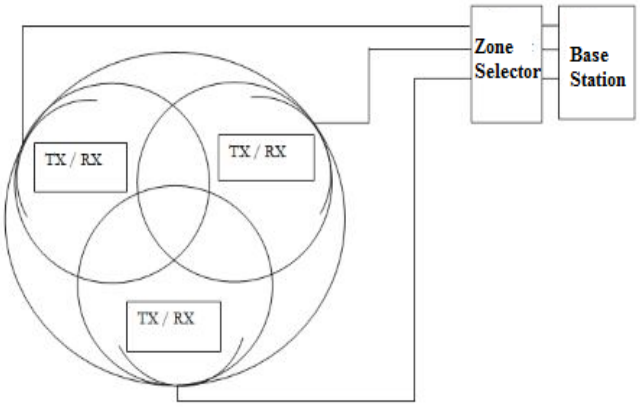

Fig. 15 Microcell zone concept [4].

In microcell zone method, no handoff is needed, because all zones are connected to the same Base-station (BS). Moreover, antennas use lesser transmitting power and they are directional. Thus Co-channel Interference (CCI) is decreased and signal quality and capacity ~~is~~ are improved. Thus call drop can be reduced. The base station is just switching from one microcell to another. By microcell zone technique, the system capacity can be defined by equation (14).

$$System\ capacity = Capacity\ increase\ factor \times number\ of\ subscriber \quad (14)$$

2.3.4 Queuing of handoffs:

Instead of rejecting the handoff request calls, the request can be queued, when the new cell sites will busy. It is more fruitful algorithm than two-level handoff algorithm [4].

Let, $\frac{1}{\xi}$ is the mean calling time involving new requesting call and existing call for handoff expressed in seconds, κ_1 is the coming rate for originating calls, κ_2 is the coming rate for requesting calls of handoff, Q_1 is the queue size of originating calls, Q_2 is the queue size of requesting calls of handoff, and M is the number of audio channels [4].

$$A = \frac{\kappa_1+\kappa_2}{\xi},\ a_1 = \frac{\kappa_1}{\xi},\ a_2 = \frac{\kappa_2}{\xi}$$

To observe the enhancement of handoff administration, the following three cases can be considered.

Case-1: When the originating calls and the requested handoff calls have no queue policy, then the blocking probability of originating and requested handoff calls will be [4]

$$B_o = \frac{A^M}{M!}P(0);\ P(0) = \left(\sum_{m=0}^{M}\frac{a^M}{m!}\right)^{-1} \quad (15)$$

Case-2: When the originating calls are queued but the handoff calls are not queued, the blocking probability of originating calls [4] will be

$$B_{oq} = \left(\frac{a_1}{M}\right)^{Q_1} P_{queue}(0);\ P_{queue}(0) = [M!\sum_{m=0}^{M-1}\frac{A^{m-N}}{m!} + \frac{1-(\frac{a_1}{M})^{Q_1+1}}{1-(\frac{a_1}{M})}]^{-1} \quad (16)$$

Also the blocking probability of requested handoff calls will be

$$B_{oh} = \frac{1-\left(\frac{a_1}{M}\right)^{Q_1+1}}{1-\left(\frac{a_1}{M}\right)} P_{queue}(0);\ P_{queue}(0) = [M!\sum_{m=0}^{M-1}\frac{A^{m-M}}{m!} + \frac{1-(\frac{a_1}{M})^{Q_1+1}}{1-(\frac{a_1}{M})}]^{-1} \quad (17)$$

Case-3: When the requested handoff calls are queued but the originating calls are not queued, then the blocking probability of requested handoff calls [4] will be

$$B_{hq} = \left(\frac{a_2}{M}\right)^{Q_2} P_{queue}(0);\ P_{queue}(0) = [M!\sum_{m=0}^{M-1}\frac{a^{m-M}}{m!} + \frac{1-(\frac{a_1}{M})^{Q_1+1}}{1-(\frac{a_1}{M})}]^{-1} \quad (18)$$

Also the blocking probability of originating calls will be

$$B_{ho} = \frac{1-\left(\frac{a_2}{M}\right)^{Q_2+1}}{1-\left(\frac{a_2}{M}\right)} P_{queue}(0);\ P_{queue}(0) = [M!\sum_{m=0}^{M-1}\frac{A^{m-M}}{m!} + \frac{1-(\frac{a_1}{M})^{Q_1+1}}{1-(\frac{a_1}{M})}]^{-1} \quad (19)$$

3. Result and Discussion

Dropped call rate and dropped call probability has been calculated using equations (4) and (6) shown in Table 1.

Table 1 Dropped call rate and dropped call probability versus network traffic.

Network Traffic, λ_t	Dropped Call Rate, V_d	Dropped Call Probability, P_d
0	2.02	2×10^{-5}
1	2.05	5×10^{-4}
2	2.1	5×10^{-3}
3	2.15	2.5×10^{-2}
4	2.2	2×10^{-2}
5	2.25	1.25×10^{-2}

With different number of active users, the dropped call probability can be calculated from equation (6) shown in Table 2.

Table 2 Dropped call probability versus number of users.

Number of Users, k	Dropped Call Probability, P_d
10	2.605×10^{-2}
15	2.620×10^{-2}
20	2.642×10^{-2}
25	2.660×10^{-2}
30	2.665×10^{-2}

Channel utilization factors can be found from equation (5) and with channel utilization factor (ρ), the dropped call probability can be calculated from equation (6) shown in Table 3.

Table 3 Dropped call probability versus channel utilization factor.

Channel Utilization Factor, ρ	Dropped Call Probability, P_d
0.96	1.7 %
0.92	3.5 %
0.90	3.9 %
0.88	4.5 %
0.86	5.3 %
0.84	6.1 %

3.1 Mathematical analysis of cell splitting

Let, the total coverage area is $2000\ km^2$, total available channel is 320, call holding time is 120 seconds, path loss exponent is 4. Let the cell radius is 8 km and the frequency pattern is (2,1).

From equation (7), the distance between a particular cell and the nearest co-channel, $D = 36.66\ km \approx 37\ km$. The frequency reuse ratio is $q = \frac{D}{R} = \frac{37}{8} = 4.58$. Area of small hexagon $A_{small} = \frac{3\sqrt{3}}{2}R^2 = \frac{3\sqrt{3}}{2}\times 8^2 = 166.2768\ km^2$

For seven cells cluster, area of cluster $= 166.3 \times 7 = 1164.1\ \text{km}^2$. Number of clusters for covering total area $= \frac{2000\ km^2}{1164.1\ km^2} = 1.718 \approx 2$.

System Capacity $= number\ of\ cluster \times available\ channels = 640$

The signal to interference ratio from equation (3), $\frac{S}{I} = \frac{(3N)^{\gamma/2}}{6} = \frac{(3\times2)^{4/2}}{6} = 7.78\ dB$

Number of channels per cell site $= \frac{320}{2} = 160$

From the Erlang B traffic table [7], for 160 channels, $Traffic\ load = 146.6\ erlangs$

The number of calls per hour per cell is $\frac{N_{call}\times120}{3600} = (1-0.02)\times146.6\ erlangs$

$$\Rightarrow N_{call} = 4310.04 \approx 4310$$

Average call arrival rate, $\lambda = \frac{4310\ requests}{3600}\times120 = 143.667$.

From Erlang B traffic table [7], Number of serving channels, N=162.

Blocking probability from equation (1), $B(N,A) = \frac{A^N/_{A!}}{\sum_{i=0}^{N}(\frac{A^i}{i!})} = 1.2\%$ and

The performance of cell splitting for this system can be summarized using equations from (7) to (10) as shown in Table 4.

Table 4 Performance of cell splitting technique.

Parameters to be found	**Cell radius**		
	R=8 km	R=4 km	R=2 km
Area of Clusters	1164.1 km^2	290.983 km^2	72.74 km^2
Number of Clusters	2	7	28
Signal to Interference ratio (SIR)	7.78 dB	18.66 dB	30.70 dB
Blocking Probability	1.2%	0.9%	0.02%
System Capacity	640	2240	6960

From Table 4, the performance of cell splitting technique can be discussed.

The blocking probability decreases (see Fig. 16), as the number of channels increase. Thus the cellular capacity is increased that reduces the call drop. For 40 call requests, the blocking probability is increased compared to the 30 call requests with the same number of channels. If we further increase the number of channels with 40 call requests, the blocking probability will be decreased.

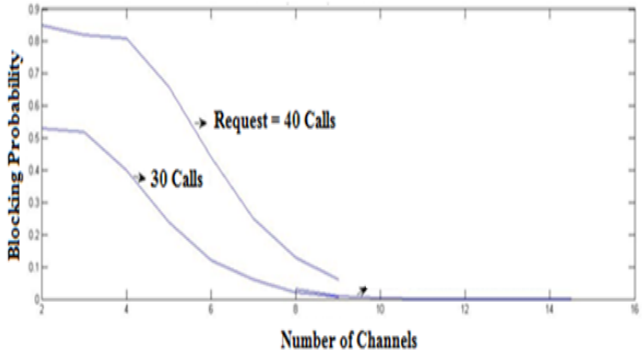

Fig. 16 Blocking probability versus number of channels.

Thus the handover failure rate can be successfully reduced in terms of call drop reduction method.

The capacity of a cellular system can be found. As the number of cells increase, the capacity increases (see Fig. 17). Using cell splitting technique, the number of cells can be increased.

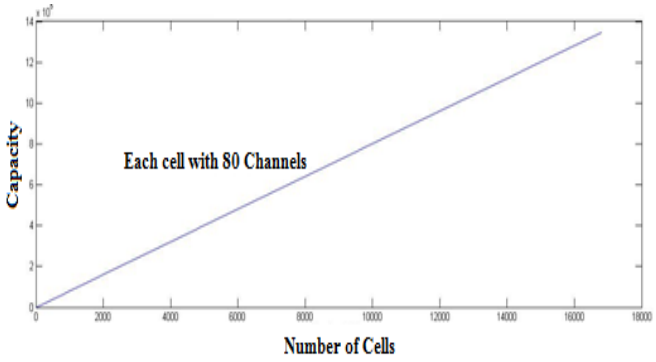

Fig. 17 Capacity versus number of cells.

With smaller size of the cell, a large number of users can use the cells. Thus higher capacity can be ensured in cell splitting technique. With increasing the number of cells, the number of clusters will be increased and hence the number of channels and capacity will be increased.

According to equation (3), signal to interference ratio (SIR) in cellular network can be analyzed. As the cell radius increases, the cell reuse factor decreases and so the signal to interference ratio is reduced (see Fig. 18). If the cell is divided into many smaller cells, the cell radius is decreased and thus the signal to interference ratio is improved.

There is restricted interference with small cells but there is huge interference with larger cells. As cell radius decreases, signal to interference ratio increases. So in a particular dense populated area, this technique can be used to improve the signal to interference ratio and reduces the effect of call drop.

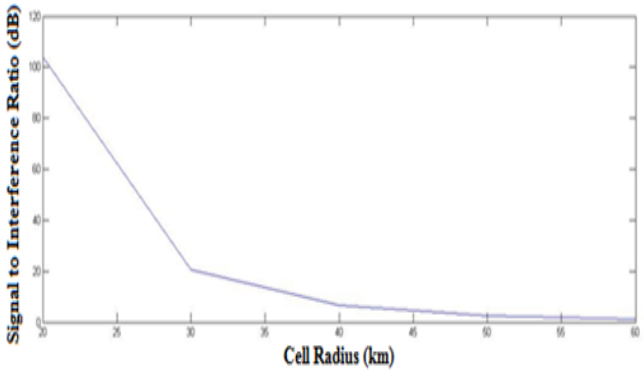

Fig. 18 SIR versus cell radius.

3.2 Mathematical analysis of Cell Sectoring

Assume that the frequency reuse pattern is $(i=2, j=1)$, path loss exponent $\gamma = 4$ and the radius of the cell is 2 km. From equation (7), the distance between a particular cell and the nearest co-channel, $D = 9.165\ km$. Frequency reuse ratio,

$$q = \frac{D}{R} = \frac{9.165\ km}{2\ km} = 4.5825$$

From equation (11), with omni-directional antenna, the S/I ratio can be given as

$$\frac{S}{I} = \frac{R^{-\gamma}}{2(D-R)^{-\gamma}+2D^{-\gamma}+2(D+R)^{-\gamma}} \Rightarrow \frac{1}{2(q-1)^{-4}+2q^{-4}+2(q+1)^{-4}} = 18.7\ dB$$

From equation (12), with 120^0 sectored antenna, the S/I ratio will be

$$\frac{S}{I} = \frac{R^{-\gamma}}{D^{-\gamma}+(D+0.7R)^{-\gamma}} = 24.48\ dB$$

From equation (13), with 60^0 sectored antenna, the S/I ratio will be

$$\frac{S}{I} = \frac{R^{-\gamma}}{(D+0.7R)^{-\gamma}} = 29\ dB$$

Assume traffic per user is 40 mErl or 0.04 Erl, the grade of service (GOS) is 2% and the total number of traffic channels is 320.

For omni-directional antenna with N=7:

Voice channels per sector [6] $= \frac{Allocated\ channels}{Cluster\ size \times number\ of\ antenna} = \frac{320}{7\times1} = 45.714$

Offered traffic load per cell [6]

$= number\ of\ antenna \times offered\ traffic\ load\ per\ sector\ with\ 2\%\ blocking = 1 \times 36.1 = 36.5$

The traffic load will be $\frac{N_{call}\times120}{3600} = (1-.02)\times 36.5$, or $N_{call} = 358$

Offered traffic load (5), $A = \frac{traffic\ request}{3600} \times call\ holding\ time = \frac{358}{3600}\times 120 = 11.933$

From the Erlang-B traffic table [7], Number of serving channels, $N = 20$

Blocking probability (from equation (1)), $B(N,A) = \frac{A^N/_{A!}}{\sum_{i=0}^{N}(\frac{A^i}{i!})} = 2\%$

No of channels per cell=320/7=46.

With 2% blocking, traffic supported per cell = 36.5 Erl and total no of users supported per cell= (36.5/0.04)=913.

Assume that a cellular service provider decides to use a digital TDMA scheme which can tolerate a signal to interference ratio of 15 dB in the worst case. The optimal value of N can be calculated for omni-directional antennas, 120° sectored antennas and 60° sectored antennas. Assume a path loss exponent $\gamma = 4$.

3.2.1 With omni-directional antenna

Assuming six interferers from the first tire of co-channel cells.

The value of N is $\frac{S}{I} = \frac{(\frac{D}{R})^{\gamma}}{I_0} = \frac{(\sqrt{3N})^{\gamma}}{I_0} \Rightarrow N = 4.592.$

Since we have to choose higher possible value to satisfy the S/I requirement,

With $N = 7$, $\frac{S}{I} = \frac{(\sqrt{3N})^{\gamma}}{I_0} = \frac{(\sqrt{3\times7})^4}{6} = 18.66\ dB.$

Where 18.66 dB is better than the requirement. In this type of antenna, choose $N = 7$

3.2.2 With 120° Sectored antenna

With 120° sectoring and N=4, there are 2 interferers in the first tier of co channel cells.

Taking $I_0 = 2$ in the expression, $\frac{S}{I} = \frac{(\sqrt{3N})^n}{I_0} = \frac{(\sqrt{3\times4})^4}{2} = 18.57\ dB$ With 120° sectoring, the S/I obtained is better than required; so $N = 4$ can be used.

We have to again check for the frequency reuse pattern $(i = 1, j = 1) and\ N = 3.$

Taking $I_0 = 3$ in the expression, $\frac{S}{I} = \frac{(\sqrt{3N})^n}{I_0} = \frac{(\sqrt{3\times3})^4}{3} = 14.314\ dB$. Since it is lower than the required value; so $N = 3$ cannot be used.

3.2.3 With 60° Sectored antenna

With 60° sectoring and N=4, there are 1 interferer in the first tier of co-channel cells.

Taking $I_0 = 1$ in the expression, $\frac{S}{I} = \frac{(\sqrt{3N})^n}{I_0} = \frac{(\sqrt{3\times4})^4}{1} = 21.57\ dB$. With 60° sectoring, the S/I obtained is better than required. So N=4 can be used.

We have to again check for the frequency reuse pattern $(i = 1, j = 1) and\ N = 3.$

Taking $I_0 = 2$ in the expression, $\frac{S}{I} = \frac{(\sqrt{3N})^n}{I_0} = \frac{(\sqrt{3\times4})^4}{2} = 16.074\ dB$

Since it is higher than the required value, N=3 can be used.

Table 5 Optimization of cluster size, N.

With 120 ° sectored antenna (N=4)	**With 60 ° sectored antenna (N=3)**
➢ No of channels per cell=420/4=105	➢ No of channels per cell=420/3=140
➢ No of channels per sector=105/3=35	➢ No of channels per sector=140/6=23.33≈23
With 2% blocking,	With 2% blocking,
➢ Traffic supported by one sector = 26.44 Erl	➢ Traffic supported by one sector = 15.76 Erl
➢ Traffic supported by one cell = 26.44*3=79.32	➢ Traffic supported by one cell = 15.76*6=94.56
➢ Total no of users supported per cell = (79.32/0.04)=1983	➢ Total no of users supported per cell = (94.56/0.04)=2364

For the given number of channels in the system, 60° sectoring with N=3 gives the largest capacity shown in Table 5. With this optimum value of N, the performance of cell sectoring can be analyzed shown in

Table 6.

Table 6 Performance of cell sectoring with optimum value.

Type of antenna	Omni-directional antenna	120° sectoring	60° sectoring
Number of interferers in the first tier co-channel cells	6	2	1
Optimum value of N for S/I= 15dB	7	4	3
System Capacity with optimum value of N	913	1983	2364

Assume that the frequency reuse pattern is $(i = 2, j = 1)$, path loss exponent $\gamma = 4$ and the radius of the cell is 2 km. The performance of cell sectoring for this system can be summarized from equation (11), (12) and (13) as shown in Table 7.

Table 7 Performance of cell sectoring.

Parameters to be found	Omni-directional Antenna	Three sectored Antenna	Six sectored Antenna
Blocking Probability	2%	1.5%	0.2%
System Capacity	913	2663	4575
Signal to interference ratio	18.7 dB	24.48 dB	29 dB

From equations (11), (12) and (13), the signal to interference ratio can be analyzed with respect to cluster size given in Fig. 19.

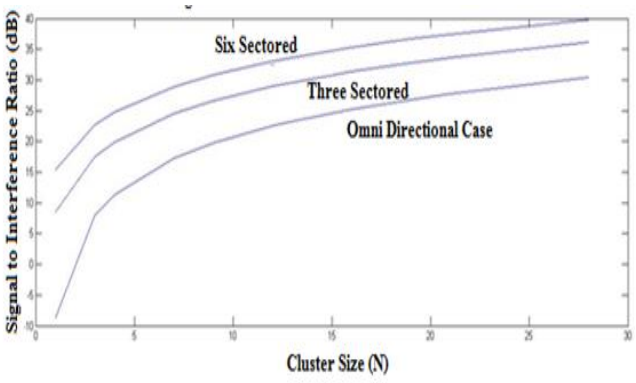

Fig. 19 SIR versus cluster size.

60 degree sectored configuration can be used under heavy traffic to reduce co-channel interference according to equation (13) (See Fig. 10). It can be concluded that the 60 degree sectored configuration with N=3 will give the largest capacity.

3.3 Mathematical analysis of Microcell Zone Concept

According to microcell zone concept, consider three zones within one cell created. Thus the supported number of subscribers can be increased without making any interference problem. According to equation (14), the system capacity can be increased by microcell zone technique. As the size of the cluster decreases, the system capacity increases linearly (see Fig. 20). Thus the supported number of subscribers can be increased without making any interference problem. Same channel will be kept for the call progress by the cell phone user, when users move from one zone to another zone. So, there is no need of handoff within the microcell zone.

Assume that the desired Signal-to-interference ratio is 18 dB, the number of subscriber is 1000 and the path loss exponent γ is 4. For simplicity consider the three zones per cell. To achieve Signal-to-interference ratio of 18 dB, the cluster size N should be 7. According to microcell zone concept, three zones within one cell created.

For new cluster size N=3, Capacity increase factor $= \frac{7}{3} = 2.33$

By microcell zone technique (from equation (14))

System Capacity $= Capacity\ increase\ factor \times number\ of\ subscriber = 2.33 \times 1000 = 2330$

Thus the supported number of subscribers can be increased without making any interference problem.

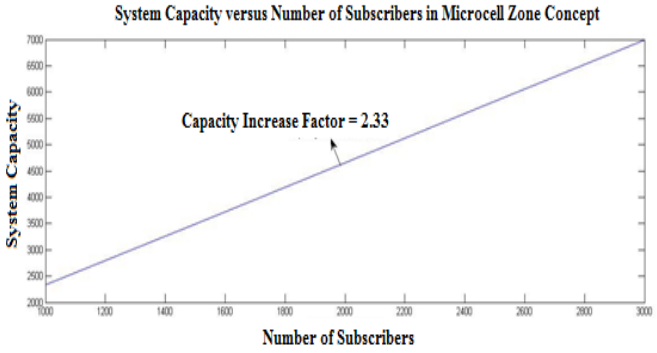

Fig. 20 System capacity with the number of subscribers.

3.4 Mathematical analysis of Queuing Handoffs

Consider the number of channels at the cell site is 70, the call holding time is 101s, the number of originating calls attempted per hour is 2270 and the number of handoff calls attempted per hour is 80. Then, $A = \frac{\lambda_1+\lambda_2}{\mu} = (2270 + 80) \times \frac{101}{3600} = 65.80$, $b_1 = \frac{\lambda_1}{\mu} = 2270 \times \frac{101}{3600} = 63.60$, $b_2 = \frac{\lambda_2}{\mu} = 80 \times \frac{101}{3600} = 2.245$

3.4.1 Queuing the originating calls but not the handoff calls

Let the size of the queue for originating calls is 16. Using MATLAB simulation,

From equation (15), the blocking probability for originating calls is $P_q(0) = [N! \sum_{n=0}^{N-1} \frac{a^{n-N}}{n!} + \frac{1-(\frac{b_1}{N})^{M_1+1}}{1-(\frac{b_1}{N})}]^{-1} = 0.04$ and $B_{oq} = \left(\frac{63.60}{70}\right)^{16} \times 0.04 = 0.012$

From equation (16), the blocking probability for handoff calls is $B_{oh} = \frac{1-\left(\frac{b_1}{N}\right)^{M_1+1}}{1-\left(\frac{b_1}{N}\right)} P_q(0) = \frac{1-\left(\frac{63.60}{70}\right)^{16+1}}{1-\left(\frac{63.60}{70}\right)} \times 0.04 = 0.3534$

Let the size of the queue for originating calls is 10. Using MATLAB simulation,

The blocking probability for originating calls is $P_q(0) = [N!\sum_{n=0}^{N-1}\frac{a^{n-N}}{n!} + \frac{1-(\frac{b_1}{N})^{M_1+1}}{1-(\frac{b_1}{N})}]^{-1} = 0.044$ and $B_{oq} = \left(\frac{63.60}{70}\right)^{10} \times 0.044 = 0.016$

The blocking probability for handoff calls is $B_{oh} = \frac{1-\left(\frac{b_1}{N}\right)^{M_1+1}}{1-\left(\frac{b_1}{N}\right)} P_q(0) = \frac{1-\left(\frac{63.60}{70}\right)^{10+1}}{1-\left(\frac{63.60}{70}\right)} \times 0.044 = 0.3186$

3.4.2 Queuing the handoff calls but not the originating calls

Let the size of the queue for handoff calls is 2. Using MATLAB simulation,

$$P_q(0) = [N!\sum_{n=0}^{N-1}\frac{a^{n-N}}{n!} + \frac{1-(\frac{b_1}{N})^{M_1+1}}{1-(\frac{b_1}{N})}]^{-1} = 0.058$$

From equation (18), the blocking probability for handoff calls is $B_{hq} = \left(\frac{b_2}{N}\right)^{M_2} P_q(0) = 0.0000593$

From equation (19), the blocking probability for originating calls is $B_{ho} = \frac{1-\left(\frac{b_2}{N}\right)^{M_2+1}}{1-\left(\frac{b_2}{N}\right)} P_q(0) = \frac{1-\left(\frac{2.24}{70}\right)^{2+1}}{1-\left(\frac{2.24}{70}\right)} \times 0.058 = 0.05938$

Let the size of the queue for handoff calls is 3. Using MATLAB simulation, $P_q(0) = [N!\sum_{n=0}^{N-1}\frac{a^{n-N}}{n!} + \frac{1-(\frac{b_1}{N})^{M_1+1}}{1-(\frac{b_1}{N})}]^{-1} = 0.058$

The blocking probability for handoff calls is $B_{hq} = \left(\frac{2.24}{70}\right)^3 \times 0.058 = 0.000001900$

The blocking probability for originating calls is $B_{ho} = \frac{1-\left(\frac{b_2}{N}\right)^{M_2+1}}{1-\left(\frac{b_2}{N}\right)} P_q(0) = \frac{1-\left(\frac{2.24}{70}\right)^{3+1}}{1-\left(\frac{2.24}{70}\right)} \times 0.058 = 0.05991$

According to equation (16) and (17), the blocking probability of new originating calls and the blocking probability of requested handoff calls can be found (see Fig. 21 and Fig. 22).

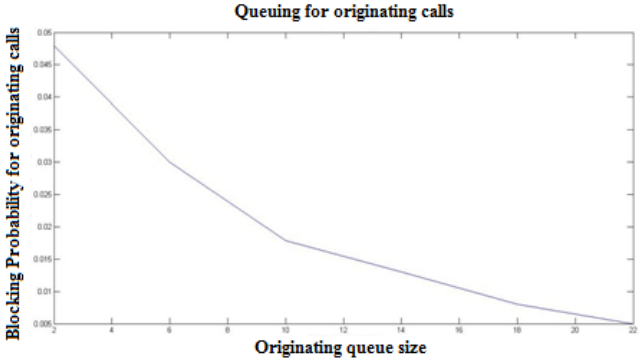

Fig. 21 Blocking probability of originating call, when only the originating calls are queued.

According to equation (18), the blocking probability of requested handoff calls and the blocking probability of new originating calls can be found (see Fig. 23 and Fig. 24).

The blocking probability of requested handoff calls will increase with the queuing of new originating calls. In case of call drop, this is the main problem. The blocking probability of requested handoff calls will decrease with the queuing of requested handoff calls (see Fig. 14). Also it does not affect the blocking probability of new originating calls (see Fig. 15). It can be concluded that the queuing of requested handoff calls is more important than the queuing of new originating call. Because customers become more upset for call drop than call blockings.

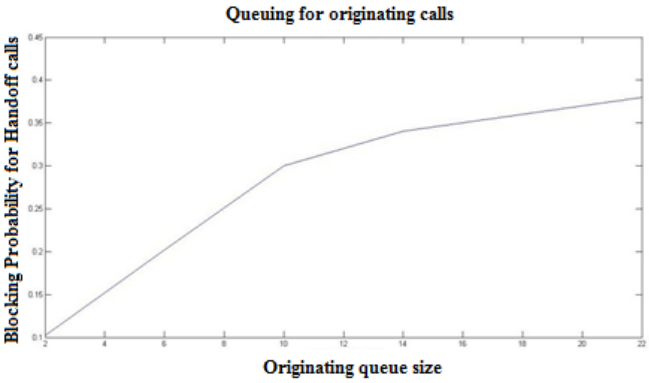

Fig. 22 Blocking probability of requested handoff calls, when only the originating calls are queued.

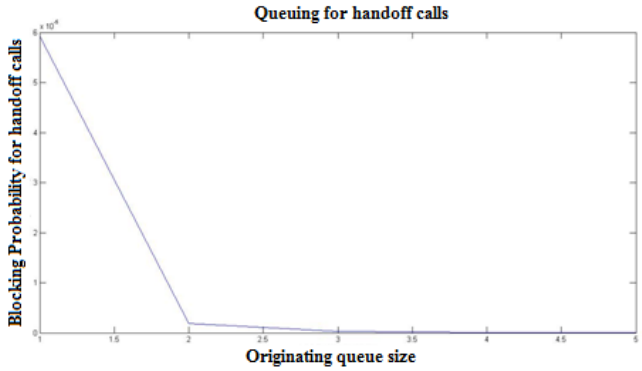

Fig. 23 Blocking probability of requested handoff calls, when only the requested handoff calls are queued.

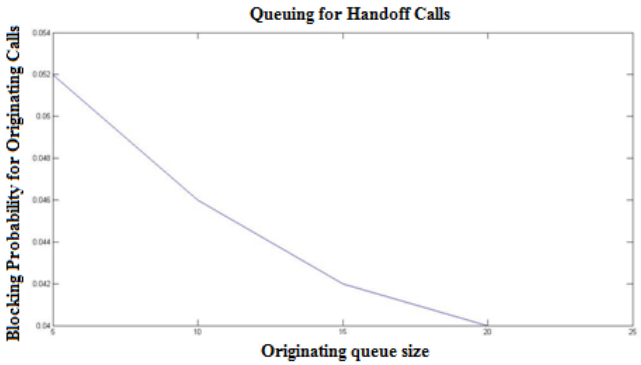

Fig. 24 Blocking probability of new originating calls, when only the requested handoff calls are queued.

4. Conclusion

To reduce dropped call probability in cellular network, a mathematical model has developed in this paper considering different factors causing call drop incidents. Then the parameters have been identified by which call drop probability can be minimized by improving those. In this paper, some efficient techniques such as cell splitting, cell sectoring, micro cell zone

concept have analyzed mathematically to increase the system capacity and signal to interference ratio. In cell splitting technique, the cellular capacity will be increased with increasing number of channels which can be increased by splitting the larger cell into smaller cell. As a result the cell radius has decreased which in turns improve the signal to interference ratio. In cell sectoring technique, co-channel interference has reduced by introducing 60 degree sectored configuration cell under heavy traffic. Mathematically it has proven that the 60 degree sectored configuration with cluster size of 3 has given the largest capacity which in turns improved the cellular network. In microcell zone concept, due to decrease ~~of~~ the cluster size, also the system capacity has increased linearly. Thus subscriber numbers have increased without making any interference problem. The same channel has kept for the call progress by the cell phone user, when users move from one zone to another zone. So, there is no need of handoff within the microcell zone. In handoff queuing methods, the blocking probability of requested handoff calls has increased with increasing the queuing of new originating calls. The blocking probability of requested handoff calls will decrease with increasing the queuing of requested handoff calls. Also it does not affect the blocking probability of new originating calls. It has concluded that the queuing of requested handoff calls is more important than the queuing of new originating call. This work will help the network designer to implement an analytical model with better performance in terms of system capacity and signal quality.

References

[1] Gaur, P., 2016. A review of menace of call drops in India and possible ways to minimize it. *Int. J. Math. Eng. Manag. Sci*, *1*(3), pp.130-138.

[2] Ohaneme, C.O., Onoh, G.N., Ifeagwu, E.N. and Eneh, I.I., 2012. Improving channel capacity of a Cellular system using Cell Splitting. *International Journal of Scientific and Engineering Research*, *3*(5), pp.1-8.

[3] Jatin, K., 2016. Study and Analysis of Call dropping and Handover Problem in cellular system. *International Journal of Advanced Research in Computer Engineering & Technology*, *5*(6), pp.1776-1777.

[4] Garg, V., 2010. *Wireless communications & networking*. Elsevier.

[5] Agrawal, D.P. and Zeng, Q.A., 2015. *Introduction to wireless and mobile systems*. Cengage learning.

[6] Boggia, G., Camarda, P. and D'alconzo, A., 2007. Modeling of call dropping in well-established cellular networks. *EURASIP Journal on Wireless Communications and Networking*, *2007*, pp.1-11.

[7] Angus, I., 2001. An introduction to Erlang B and Erlang C. *Telemanagement*, *187*, pp.6-8.

SciEn
Journal of Engineering Advancements Vol. 02(01) 2021, pp 35-40 https://doi.org/10.38032/jea.2021.01.005

Trust Concerns regarding Health-Related Smartphone Apps in collecting Personally Identifiable Information throughout COVID-19-like Zoonosis

Molla Rashied Hussein[1], *Md. Ashikur Rahman*[1], *Md. Jahidul Hassan Mojumder*[1], *Shakib Ahmed*[1], *Ehsanul Hoque Apu*[2]

[1]Department of Computer Science & Engineering (CSE), University of Asia Pacific (UAP), Dhaka, Bangladesh
[2]Department of Biomedical Engineering, Michigan State University, East Lansing, MI, USA

Received: November 19, 2020, Revised: February 10, 2021, Accepted: February 13, 2021, Available Online: February 22, 2021

ABSTRACT

Coronavirus disease 2019 or COVID-19 is a zoonosis, which means a disease that contaminates from the animals to the humans. Since it is very highly epizootic, it has forced the public health experts to implement smartphone-based applications to trace its swift transmission trajectory as well as the affected individuals. For this, the individuals' personally identifiable information is utilized. Nonetheless, these information may hamper privacy and cyber security, especially the trust concerns, if not handled properly. If the issues are not resolved at this very moment, the consequences will induce the mass level population to use the health-related applications in their smartphones inadequately. Therefore, a catastrophe will be imminent for another COVID-19-like zoonosis to come. So, to mitigate, an extensive study was required to address this severe issue, namely, trust concern. This paper has studied the needed by discussing the recently designed and developed health-related applications region by region across the world. Moreover, it has analyzed the benefits and drawbacks. The trust defiance is recognized and inspected from the perspective of an end-user. Some recommendations are advised in the later part of this paper to leverage and collaborate the awareness campaign between the Government, the App Developers and the common individuals.

Keywords: Trust, Smartphone Application, COVID-19, Personally Identifiable Information, Awareness, Privacy, Cyber Security, Recommendation.

1 Introduction

The zoonotic novel disease named coronavirus disease 2019 (COVID-19) has changed the course of the worldwide economy by putting constraints on individuals in daily commercial activities [1]. The highly contagious disease has potentially affected health facilities' capacity, even in first-world countries, where the healthcare systems are reliable with robustness [2]. To control and track the COVID-19 infection pattern, different administrations have utilized modern artificial intelligence (AI) based methods integrated with 5G technology as well as aerial drone machineries to track COVID-19 in real-time [3],[4]. As there is no definite medicine to prevent or cure the disease [5], the most effective way to avoid COVID-19 so far is not to get exposed [6]. Social distancing must be preserved between all, as recent studies [7] have shown that even an asymptomatic person may spread the disease inaudibly.

This social distancing induces the public health experts and professionals to collaborate with the technical researchers to deploy the health applications (apps) to monitor people digitally, as the manual process is quite tedious to execute. Instead of gathering the personally identifiable information (PII) of the affected individual along with contact information for the last couple of weeks through detailed interviews, the health-related apps in smartphones could be an effective substitute which have already been conceived, built, and even implemented in several countries [8].

Also, a majority of the people can use those apps using their smartphones not only in developed countries but also in the low- and middle-income countries (LMICs) [9]; proper app usability has to be guaranteed by comparing in terms of development as well as confidentiality along with popularity among the end-users, and last but not least, user-friendly interfaces.

However, as the PII is stored in those apps, potential exposure of the PII may violate the user's privacy. Moreover, the re-identification of a person could be executed by utilizing only a few demographic data of that PII. Therefore, an individual may become target for a potential cyber-attack or threat.

This paper enlightens the readers regarding the cyber security and privacy terminologies, reviews related apps through Google Play Stores, analyzes users' comments and views, suggests recommendations to mitigate trust concerns amongst the Governments, Developers and the End-Users. The studies in this paper will not only be beneficial for the authorities, but also for the mass population.

2 Definition of Terminologies

Before discussing the health-related apps and their features, fundamental trust issues concerning cyber security and privacy must be presented in short. The first one is the concept of the semi-honest model, the second one is the activity of a malicious actor, and the last one is the possibility of re-identification of a person to track and carry on cyber-attack or threat.

In a real world, when a user is using smartphone apps during any type of epidemic situation for public health activities, some PII is saved into the application storage. Those app data can indicate where the users are travelling or meeting with.

Now, after those epidemic situations go away, still the PII remains saved in that particular storage which is undesirable by the user. For this reason, the user may want the health app keeping the data for a specific timeframe, and removal of those data afterwards. Moreover, users may want a fully trustable

*Corresponding Author Email Address: mrh.cse@uap-bd.edu

model or a full honest model having no hackers or malicious actors to misuse the user data. However, it is quite impossible to create a full honest model because we cannot assume that all the actors in a security model behave in a completely honest manner [10].

But that necessarily does not imply that a vast number of malicious actors are always active to harm the unsuspecting users all the time. Because even though they may wish to harm or cheat, they in fact, act rather in a semi-honest way [10]. Therefore, we are proposing for a semi honest model to get rid of this problem of having trust.

In a malicious model, there is no an ideal stable condition. All participants are attacking each other and several kinds of malicious behaviors are present. It is quite hard to control and stop the malicious actors.

Moreover, there may be threat actors who want to create a security breach and hamper the safety of others, either intentionally or unintentionally. Those threat actors can be divided mainly in two types, malicious actors and nefarious actors. Malicious actors are the ones who try to hamper the system whenever they get the chance. Nefarious actors, on the other hand, are the ones who are always present online and try to break the systems. In real-life, nefarious actors present in a privacy model are quite rare. Some malicious actors can still be present in a privacy model. Some examples of threat actors in a privacy model are given below:

Cyber-terrorist: Threat actors who attack via technology in cyber-space are called cyber-terrorist. They may attack for political reason, creating public panic, spreading propaganda and so forth.

Cybercriminals: Cybercriminals are mainly profit-driven and represent a worldwide threat for a long time. The target of the Cybercriminals is to sell the sensitive data, such as PII, hold for ransom, and otherwise absorb for financial gain. Cybercriminals may work individually or in a group to achieve the target [11].

Now, a general misconception regarding tracking and tracing is eradicated as follows:

Tracking: The term indicates the way of travelling a path or location at the moment. Tracking gathers insights in real-time. A tracking app can detect an individual's exact location at any given moment by utilizing the geo-data through GPS coordinates or radio cell location. It can even build an extensive movement profile if it can track a person been where and when, in addition.

Tracing: On the other side of the coin, the term defines searching the path in reverse from its any given point to where it began. Tracing collects insights in retrospect. A tracing app can be employed to trace physical close contacts between individuals. Bluetooth technology makes digital devices communicating with one another over a minimal distance. It has the capability of measuring the distance between smartphones by sensing the strength of the radio signals, and therefore, sense the social encounters between individuals, also known as proximity tracing.

Finally, the demographic variables and the process of de-identification, and the data policies as well as laws are discussed as below:

Demographic variables: These are defined as the independent variables as these are immutable. Demographic variables could be either categorical, such as race, gender, psychiatric diagnosis, marital status, or continuous, such as age, income, years of education, family size and so forth [12].

De-identification:- It is the process of making datasets anonymized before being shared. It is a common practice in research and data sharing environments to preserve a person's privacy. However, from the numerous anonymous datasets, a person can be re-identified using a demographic variable, which create a big concern about the privacy and ethical use of those data. Recently the collection and subsequent sale of Facebook data to Cambridge Analytica has made an enormous trust issue.

Reporters have re-identified the political personnel in an anonymized web browsing history dataset, comprises three million German citizens, back in 2016. The incident revealed their medical information as well as their sexual preferences.

The Australian Department of Health publicly released de-identified medical records for 10% of the population exclusively for researchers few months ago, but those got re-identified one and half months later [13],[14]. Studies also had revealed that the de-identified hospital discharge data could be re-identified by utilizing the basic demographic attributes along with the year of birth, diagnostic codes, ethnicity and gender. Researchers also exclusively detect individuals in the anonymized subway data in Riga, bike sharing rides in London, taxi travelling patterns in New York City, and mobile phone as well as credit card datasets [13],[14].

To prevent such privacy hampering, the European General Data Protection Regulation (GDPR) and the California Consumer Privacy Act (CCPA) ensure that each individual in a dataset needs to be protected by being anonymous, as data protection laws around the world consider anonymous data as not PII.

3 Related Works

To secure their people from COVID-19, governments around the world have authorized the usage of a smartphone app designed and implemented by the local technical enterprises with/without the collaboration with the global tech giants. In this section, we will go by the regions, i.e., continents around the world.

The following Table 1 is going to summarize the merits and demerits of several health apps spread over the numerous countries under the regions/continents.

From Africa, the continent has seen its country Ghana implementing the GH COVID-19 Tracker [15] by crowd sourcing data. Crowd-sourced data collection is a sharing method of making a data-set with the support of a massive group of the crowd and using a more secured semi-honest model to improve Crowd-sourcing. Also, Nigeria and South Africa have developed their own apps [16],[17] with not enough documentation to be discussed.

Next from Asia, more specifically, South Asia, Bangladesh has built an app, namely, Corona Tracer BD [18], which has gathered mixed feelings from the end-users. The nicely constructed user interface has been appreciated, but the issue of heavy usage of Bluetooth along with redirection to web browser all the time have raised frown among the end-users.

On the other hand, India has developed an application named Aarogya Setu [19]. This application has got very good documentation [20]. Although there was no mention of disposal of data after the pandemic in the initial development, the updated privacy policy [21] states that all PII collected will be stored on the mobile device for one month from the date of the collection, and if it has not already been uploaded to the server, will be permanently deleted from the App. All PII uploaded to the server will be permanently deleted from the server after one and half

months being uploaded if not tested positive, two months in case of being positive and later tested negative for COVID-19.

Moreover, Aarogya Setu [19] app alerts the individuals while an infected person is nearby through Bluetooth as well as GPS. Several Data Mining techniques, namely, Classification, Association Rule Mining, and Clustering have been implemented to discover COVID-19 spreading patterns [20]. As PII of numerous users of the app is stored on one server, this design potentially allows the potential malicious actors to hack the PII of users.

Meanwhile, from Asia, more specifically from Southeast Asia, MySejahtera [22] in Malaysia needs to mention good documentation describing its data privacy. Another app from Malaysia, MyTrace [23] accepts a community-driven approach. The participating devices share the proximity information when the app can identify another device close by with the same app installed. As this app is based on the DP3T (Decentralized Privacy-Preserving Proximity Tracing) algorithm [24], it does not need any permission to access location.

From the Asia and the Pacific, Singapore has implemented TraceTogether app with an adequate privacy statement [25]. As the user given the required consent, the app shares Bluetooth signals with encryption and anonymity with devices close by having same app. The data regarding Bluetooth are automatically erased after 25 days to prevent hacking. Storing limited data, such as users' contact/mobile number, users' identification details, a random anonymized User ID, the app never shows those to the public. No GPS location is collected, nor any information regarding WiFi or mobile network. Data about devices near users do not reveal any personal identity, as whenever the users are close to another device with the same app installed, both devices utilize Bluetooth technology to share a momentary ID generated by encrypting the user ID with a private key maintained by the Ministry of Health (MOH), Singapore, which could be decrypted by the MOH only. The right to be forgotten as per GDPR is preserved. The Temporary ID inside the users' device being exchanged with other nearby devices are regularly refreshed to prevent tracking.

Next from Asia, particularly from the Middle-East area, Bahrain uses an application named BeAware [26]. This application needs to have good documentation mentioning the data privacy issue. Tetamman [27] in Saudi Arabia always uses GPS and Bluetooth to cause power leakage, i.e., battery drain. It takes much control over users' smartphones as well. In Israel, Hamagen (or "Protector" in Hebrew) [28] cross-validates the GPS chronology of the smartphones of the patients with a bona fide geographic data stored in the Ministry of Health (MOH).

Meanwhile, from Europe, Czech Republic is using an application named e-Rouška [29]. It has an adequate documentation [30] with videos which are self-explanatory. But, the medium of instruction is Czech language. Therefore, the linguistic barrier hampers the spreading of the vital information, which should rather be kept in an international language, namely, English. In Hungary, VírusRadar [31] is a mobile app which implemented for Apple iOS and also for Android. It provides the topmost security standards, total control over PII, and ensures privacy protection as well. It is generally using the Bluetooth Low Energy (BLE) protocol to detect faceless encrypted contacts [32] which are highly secured.

After that, from Northern Europe, in Iceland, the app called Rakning C-19 [33] gathers the GPS location of the individuals' smartphone and saves the PII locally inside the device. If an individual is diagnosed COVID-19 positive, then the Health Directorate asks to exchange the location data only for contact tracing and identifying the people need to be in quarantine. On the other hand, Smittestopp app [34] of Northern Europe, more specifically, from Denmark, always keeps GPS and Bluetooth turned on and empties the energy. The frequently asked questions (FAQ) section is quite useful, but it is not adequate in terms of proper documentation and the data usage policy. Linguistic barrier is a concern as well.

Meanwhile, from North America, USA has developed several apps for each state. Among those, DC CAN, COVID Alert NY and CA Notify are praiseworthy [35]-[37]. They lack efficient notification system or multi-app conjunction, but simple in design and break down data with high energy efficiency. On the other hand, Canada has built COVID Alert app [38] that preserves privacy by not tracking location via GPS. However, rapid drainage of battery makes it cumbersome to use.

Next, from South America, Brazil has made Coronavírus – SUS [39] and Colombia uses CoronApp [40]. The documentation of the CoronApp could be found in [41]. Nothing has been mentioned about data privacy and further disposal of data, so it needs to mention the data privacy of an individual. Also, both apps need to be built in English for documentation as well as tutorial videos to assist expatriates.

Finally, from Oceania, Australia is using an app, namely, COVIDsafe [42] with an excellent documentation [43]. New Zealand, on the other hand, employs NZ Covid Tracer App [44] to mitigate their pandemic situation. This is based on user interaction. Although it has a poor design, it empowers the users of not exchanging credentials and thus doing nothing. It has a better data privacy, but it is not that effective compared to other contact tracing apps.

Table 1 Trust in Health Apps: Merits and Demerits

Region	**App features by region, country and name**			
	Country Name	***App Name***	***Merits***	***Demerits***
Africa	Ghana	GH COVID-19 Tracker [15]	Crowd-sourcing	Security Model
	South Africa	COVID Alert South Africa [16]	No fake notification due to 6 digit pin	No explicit data policy, Tardy notification
	Nigeria	Rapid Trace [17]	Live COVID-19 News and Status Check	Not enough documentation
Asia	Bangladesh	Corona Tracer BD [18]	Nicely designed User Interface	Redirection to Web Browser
	India	Aarogya Setu [19]	Well documented privacy policy	Central server allows potential hacking of PII
	Malaysia	My-Sejahtera [22]	Not enough information	Data Policy

Region	App features by region, country and name			
	Country Name	***App Name***	***Merits***	***Demerits***
		MyTrace [23]	Community-driven approach, DP3T	State surveillance may go wrong
	Singapore	TraceTo-gether [25]	Secure Server	Users can delete the app anytime
	Bahrain	BeAware [26]	Not enough information	Not enough documentation
	Saudi Arabia	Tetamman [27]	Not enough information	Power leakage
	Israel	Hamagen [28]	Crosscheck GPS data with MOH data	Not enough documentation
Europe	Czech Republic	e-Rouŝka [29]	Self-explanatory	Linguistic barrier
	Hungary	VírusRadar [31]	High security	Not enough information
	Iceland	Rakning C-19 [33]	Supervised by Health Directorate	Not enough information
	Denmark	Smittestopp [34]	Helpful FAQ information	Battery drainage
North America	United States of America	DC CAN [35]	Energy efficient	App Location Service issues
		COVID Alert NY [36]	Breaks down data for the whole state as well as local county	Not usable in conjunction with other COVID-19 apps
		CA Notify [37]	Simple design	Notification issue
	Canada	COVID Alert [38]	Does not use GPS or track location	Fast drainage of batteries
South America	Brazil	Coronavírus – SUS [39]	Well documented terms and conditions	Language barrier
	Colombia	CoronApp [40]	Well documented	No English version
Oceania	Australia	COVIDsafe [42]	Well documented	Not enough information
	New Zealand	Covid Tracer [44]	Maximum security unless user misuse	User dependent action

4 Recommendations

The following recommendations have been made to assist the Governments, the App Developers and the End-Users.

For the Governments:

i. Linguistic barrier is a major concern in European and South American countries. Many foreign personals living in those countries may not speak or read the native language, so having app made in the native language causes inconvenience. This also applies for foreign volunteers working in developing countries.
ii. Aware mass level people regarding security model such that they know that not all actors are malicious and there are very few nefarious actors. Also, a pure honest model is not possible, so caveat emptor (Latin, meaning "let the buyer beware") is the best policy in a semi-honest model.
iii. Moreover, even though the re-identification is mathematically possible, proper data management can reduce the threat significantly. So, it is the duty of the Government to educate the population so that the panic reduces.

For the App Developers:

i. Applications which are being used in different countries are not creating documentations properly. If an application has proper documentation, then people will feel more comfortable to use that application because they already know how the application in exactly working.
ii. To increase the trust issues, the app developers should make a proper documentation and a self-explanatory video to let the people know about the working procedure of the application.
iii. Furthermore, as every contact tracing application is using a centralized database to store data, if the distributed ledger is used, it will be safer for the data stored. If done so, in case of malicious attacks, the actor will be able to retrieve maybe a part of the database rather than the whole database.
iv. Therefore, Blockchain technology can play a vital role in this regard. It ensures maximum security with a shared ledger system, which makes it the best match to address the issues raised by the centralized systems.

For the End-Users:

i. The end-users should learn regarding the cyber security and privacy terminologies explained by the Government and the App Developers.
ii. They should be aware of their rights, know the data usage policy, ask questions before being forced to use any app, read app documentations and demand if not provided. Overall, they need to be conscious, not gullible.
iii. Cooperate the Government to take decisions regarding apps by volunteering for the pre-release. Also, suggest the requirements to the App Developers, so that there is no gap between supply and demand.
iv. In Democracy, the people have the authority. Therefore, they should trust and get trust from the Government and the App Developers. There should be clarity in each step to enhance trust issues.

5 Conclusion

To conclude, the Governments need to educate their citizens regarding cyber security and privacy. Moreover, data policy should be explicit and available to all. The App Developers should work with the Government to publish the data usage policy and assure the End-Users. It is also highly essential to study an individual's trust issues using digital health monitoring technologies including health apps. If in the near future, the trust issues are not solved, it will cost more, as people will be reluctant to use health apps and make a pandemic to come a much worse one.

Further studies and implementations have to be carried out as per the suggestions presented in the recommendations section. Afterwards we can ensure a better strategy to prepare for a future zoonosis or such disease.

References

[1] Gvili, Y., 2020. Security analysis of the COVID-19 contact tracing specifications by Apple Inc. and Google Inc. *IACR Cryptol. ePrint Arch.*, *2020*, p.428.

[2] Pillai, S., Siddika, N., Apu, E.H. and Kabir, R., 2020. COVID-19: Situation of European countries so far. *Archives of medical research*, *51*(7), pp.723-725.

[3] Hussein, M.R., Apu, E.H., Shahabuddin, S., Shams, A.B. and Kabir, R., 2020. Overview of digital health surveillance system during COVID-19 pandemic: public health issues and misapprehensions. *arXiv preprint arXiv:2007.13633*.

[4] Hussein, M.R., Shams, A.B., Apu, E.H., Mamun, K.A.A. and Rahman, M.S., 2020. Digital Surveillance Systems for Tracing COVID-19: Privacy and Security Challenges with Recommendations. *arXiv preprint arXiv:2007.13182*.

[5] Lai, C.C., Shih, T.P., Ko, W.C., Tang, H.J. and Hsueh, P.R., 2020. Severe acute respiratory syndrome coronavirus 2 (SARS-CoV-2) and coronavirus disease-2019 (COVID-19): The epidemic and the challenges. *International journal of antimicrobial agents*, *55*(3), p.105924.

[6] Hussein, M.R., Shams, A.B., Rahman, A., Raihan, M.S., Mostari, S., Siddika, N., Kabir, R. and Apu, E.H., 2020. Real-time credible online health information inquiring: a novel search engine misinformation notifier extension (SEMiNExt) during COVID-19-like disease outbreak. DOI: 10.21203/rs.3.rs-60301/v2 *PPR: PPR257400*.

[7] Yu, X. and Yang, R., 2020. COVID-19 transmission through asymptomatic carriers is a challenge to containment. *Influenza and Other Respiratory Viruses*, 14(4), pp.474-475.

[8] Ahmed, N., Michelin, R.A., Xue, W., Ruj, S., Malaney, R., Kanhere, S.S., Seneviratne, A., Hu, W., Janicke, H. and Jha, S.K., 2020. A survey of covid-19 contact tracing apps. *IEEE Access*, 8, pp.134577-134601.

[9] Jalabneh, R., Zehra Syed, H., Pillai, S., Hoque Apu, E., Hussein, M.R., Kabir, R., Arafat, S.M. and Azim Majumder, M., 2020. Use of mobile phone apps for contact tracing to control the COVID-19 pandemic: A literature review. Doi.org/10.1016/j.arcmed.2020.05.015.

[10] Goldreich, O., 2009. Foundations of cryptography: volume 2, basic applications. *Cambridge University Press*.

[11] Ablon, L., 2018. Data thieves: The motivations of cyber threat actors and their use and monetization of stolen data. *RAND*.

[12] El Emam, K., Brown, A. and AbdelMalik, P., 2009. Evaluating predictors of geographic area population size cut-offs to manage re-identification risk. *Journal of the American Medical Informatics Association*, 16(2), pp.256-266. https://doi.org/10.1197/jamia.M2902

[13] Rocher, L., Hendrickx, J.M. and De Montjoye, Y.A., 2019. Estimating the success of re-identifications in incomplete datasets using generative models. *Nature Communications*, 10(1), pp.1-9. https://doi.org/10.1038/s41467-019-10933-3

[14] Sweeney, L., 2000. Simple demographics often identify people uniquely. *Health (San Francisco)*, 671(2000), pp.1-34.

[15] GH COVID-19 Tracker, Available at: https://www.coronatracker.com/about, last accessed on: August 20, 2020.

[16] COVID Alert South Africa, *Department of Health – South Africa*, available at: https://play.google.com/store/apps/details?id=za.gov.health.covidconnect&hl=en_US&gl=US, last updated on: December 21, 2020 and last accessed on: January 26, 2021.

[17] Rapid Trace, *Cadnetwork Enterprise, Nigeria*, available at: https://www.rapidtrace.com.ng, last updated on: January 01, 2021 and last accessed on: January 21, 2021.

[18] Corona Tracer BD, *Mobile game & application project, ICT Division, Bangladesh*, available at: https://play.google.com/store/apps/details?id=com.shoho z.tracer&hl=en_US&gl=US, last updated on: July 21, 2020 and last accessed on: January 04, 2021.

[19] Aarogya Setu, NIC eGOV Mobile Apps. Available at: https://play.google.com/store/apps/details?id=nic.goi.aarogyasetu&hl=en, last updated on: July 8, 2020 and last accessed on: August 23, 2020.

[20] Sharma, U., 2020. Understanding aarogya setu: navigating privacy during a pandemic proves to be tricky. *LSE Covid 19 Blog*.

[21] Aarogya Setu Privacy Policy, available at: https://web.swaraksha.gov.in/ncv19/privacy, last updated on: July 8, 2020 and last accessed on: August 28, 2020.

[22] MySejahtera, Government of Malaysia, available at: https://play.google.com/store/apps/details?id=my.gov.onegovappstore.mysejahtera&hl=en, last updated on: August 10, 2020 and last accessed on: August 29, 2020.

[23] MyTrace, Government of Malaysia, available at: https://play.google.com/store/apps/details?id=my.gov.onegovappstore.mytrace&hl=en, last updated on: April 26, 2020 and last accessed on: August 29, 2020.

[24] Nanni, M., Andrienko, G., Barabási, A.L., Boldrini, C., Bonchi, F., Cattuto, C., Chiaromonte, F., Comandé, G., Conti, M., Coté, M. and Dignum, F., 2021. Give more data, awareness and control to individual citizens, and they will help COVID-19 containment. *Ethics and Information Technology*, pp.1-6.

[25] TraceTogether Privacy Safeguards, A Singapore Government Agency Website, A collaboration between Ministry of Health, SG United and GovTech. available at: https://play.google.com/ store/apps/details?id=my.gov.onegovappstore.mytrace& hl=en, last updated on: July 20, 2020 and last accessed on: August 30, 2020.

[26] BeAware Bahrain, Information & eGovernment Authority, available at: https://play.google.com/store/apps/details?id=bh.bahrain. corona. tracker&hl=en, last updated on: August 17, 2020 and last accessed on: August 31, 2020.

[27] Tetamman, *Ministry of Health, Kingdom of Saudi Arabia*, available at: https://play.google.com/store/apps/details?id=com.tetam an.home&hl=en, last updated on: August 25, 2020 and last accessed on: September 15, 2020.

[28] Hamagen ("Shield" in Hebrew), The Health Ministry, Israel, available at: Ihttps://play.google.com/store/apps/details?id=com. hamagen&hl=en, last updated on: August 27, 2020 and last accessed on: September 12, 2020.

[29] eRouška - part of smart quarantine, *Ministry of Health of the Czech Republic*, available at: https://play.google.com/store/apps/details? id=cz.covid19cz.erouska&hl=en, last updated on: July 26, 2020 and last accessed on: September 9, 2020.

[30] eRouška, *Ministry of Health of the Czech Republic*, available at: https://erouska.cz/en, last accessed on: September 9, 2020.

[31] VírusRadar, *Government Informatics Development Agency*, Hungary, available at: https://play.google.com/store/apps/details ?id=hu.gov.virusradar&hl=en, last updated on: May 15, 2020 and last accessed on: September 6, 2020.

[32] Nextsense, "VirusRadar – a mobile app for Covid-19 contact tracing implemented in Hungary as a donation," available at: https://www.nextsense.com/ns-newsarticle-virusradar-a-mobile-contact-tracing-implemented.nspx, last updated on: May 14, 2020 and last accessed on: September 6, 2020.

[33] Rakning C-19, *The Office of the Medical Director of Health, Iceland*, available at: https://play.google.com/store/apps/details ?id=is.landlaeknir.rakning&hl=en, last updated on: July 19, 2020 and last accessed on: September 3, 2020.

[34] Smittestop ("Stop infection" in Danish), *Ministry of Health and the Elderly, Denmark*, available at: https://play.google.com/store/apps/ details?id=com.netcompany.smittestop_exposure_notific ation&hl=en, last updated on: August 14, 2020 and last accessed on: September 4, 2020.

[35] DC CAN, DC Exposure Notifications, *Washington DC, USA*, available at: https://play.google.com/store/apps/details?id=gov.dc.cov id19.exposurenotifications, last updated on: January 13, 2021 and last accessed on: February 09, 2021.

[36] COVID Alert NY, *New York State Department of Health, New York, USA*, available at: https://play.google.com/store/apps/details?id=gov.ny.hea lth.proximity, last updated on: November 30, 2020 and last accessed on: February 06, 2021.

[37] CA Notify, CA *Dept of Technology, California, USA*, available at: https://play.google.com/store/apps/details?id=gov.ca.cov id19.exposurenotifications, last updated on: January 14, 2021 and last accessed on: January 31, 2021.

[38] COVID Alert - Let's protect each other, *Health Canada*, available at: https://play.google.com/store/apps/details?id=ca.gc.hcsc. canada.stopcovid&hl=en&gl=US, last updated on: January 20, 2021 and last accessed on: February 03, 2021.

[39] Coronavírus - SUS, *Governo do Brasil, Brazil*, available at: https://play.google.com/store/apps/details?id=br.gov.data sus.guardioes&hl=en&gl=US, last updated on: October 27, 2020 and last accessed on: February 07, 2021.

[40] CoronApp - *Colombia*, available at: https://play.google.com/store/ apps/details?id=co.gov.ins.guardianes&hl=en, last updated on: September 2, 2020 and last accessed on: September 7, 2020.

[41] A healthy isolation, Tips for being at home, *The Government of Colombia*, available at: https://coronaviruscolombia.gov.co/ Covid19/aislamiento-saludable/coronapp.html, last accessed on: September 12, 2020.

[42] COVIDSafe, *Australian Department of Health*, available at: https://play.google.com/store/apps/details?id=au.gov.hea lth.covidsafe&hl=en, last updated on: August 14, 2020 and last accessed on: September 9, 2020.

[43] How COVIDSafe works, COVIDSafe app, *Australian Government: Department of Health*, available at: https://www.health.gov.au/resources/apps-and-tools/covidsafe-app#how-covidsafe-works, last updated on: August 24, 2020 and last accessed on: September 9, 2020.

[44] NZ COVID Tracer, *Ministry of Health NZ (New Zealand)*, available at: https://play.google.com/store/apps/details?id=nz.govt.he alth. covidtracer&hl=en, last updated on: September 7, 2020 and last accessed on: September 13, 2020.

SciEn
Journal of Engineering Advancements Vol. 02(01) 2021, pp 41-47 https://doi.org/10.38032/jea.2021.01.006

Depressed People Detection from Bangla Social Media Status using LSTM and CNN Approach

*Tabassum Ferdous Mumu, Ishrat Jahan Munni, Amit Kumar Das**

Department of Computer Science and Engineering, East West University, Dhaka, Bangladesh

Received: January 28, 2021, Revised: February 23, 2021, Accepted: February 25, 2021, Available Online: March 06, 2021

ABSTRACT

At present, depression is the main reason for suicidal death. Depression also causes different kinds of diseases. Nowadays, people are deeply involved in social media and like to share their feelings on social media. So, it becomes easy to analyze depression through social media. In this paper, a combination of two CNN (Convolutional Neural Network) and LSTM (Long Short-Term Memory) models has been proposed to make a hybrid CNN-LSTM model, CNN has performed for the image to create a matrix, and LSTM has given the result from the given matrix. In this paper, datasets are prepared based on depression and non-depression-related status. The proposed method has been applied to that dataset. The best result has been obtained using a hybrid neural network with the word embedding technique using the Bengali Facebook status dataset. We have used the SVM (Support Vector Machine) model to predict a small dataset of Bengali Facebook status and count vectorizer to count the word in the document. Finally, this paper has built up a model that makes strength and support for deep learning architecture.

Keywords: Depression, CNN-LSTM, SVM, Word Embedding, Neural Network.

1 Introduction

Depression is a silent killer. Depression is a serious and common medical illness, and it negatively impacts how someone feels, thinks, and behaves [1]. With the help of technology and skills, humans are now at a different level [2]. But between the rapid growth, people forget to trend their mental health. That's the world we currently live in. In a developing country like Bangladesh, things are more severe than one can look at. In Bangladesh, people do not have time to think about any type of mental illness where basic needs are lacking. This is a serious issue that takes many lives over the years. According to the CDC report (Centers for Disease Control), one of the leading causes of suicide is depression [3]. Even if the world is becoming more open-minded about human behavior and mental illness, Bangladesh is still lagging in this sector. In many countries like Bangladesh, mental illness is at a tolerable level. People with mental illness are not treated nicely. That's why depression becomes a significant issue because people cannot share their problems with others who lack trust in cognitive cases.

Nowadays, people become more and more expressive on social media than ever. It's called virtual self-disclosure. Self-disclosure can be done on various platforms of Social media. Sometimes, people think offline nobody can optically discern them; they are at liberty to express their genuine emotion. It helps some people to cope-up with the stressful life. They want to express most of the virtual life emotions that they cannot express in real life. Applications such as Twitter, Facebook, Instagram, and many other platforms write and multimedia type contents and express their emotions, feelings, and sentiments about different subjects, topics, or issues online [4]. Expressing emotion online leads to detecting a person's emotions, such as happiness, anger, depression, sadness, fear, surprises.

This work aims to find out if a person is having any kind of depression or not using a machine learning approach utilizing social media status related to depression. The authors tried to scale the depressive status based standard scale of depression. There have two types of data set one is contained depressive status, and another is non-depressive status. This research used two main algorithms, i.e., LSTM and CNN. Differentiate between depressive and not depressive status TF-IDF (Term Frequency- Inverse Document Frequency) was used, and CNN and LSTM were used to train the model. For comparing results, logistic regression was also used to train the model. There are two different accuracies from different model training.

The study is to simply find depressive status from social media that can disclose the early stages of depression. While successful first treatment can lead to a positive result, untreated depression can lead to even life loss. The study is limited to extrovert social media users only. Because many people silently cope up with their depression. They don't express it on social media, but that does not mean that they are not depressed.

Depression is a mood disorder that causes different persistent feelings like sadness and loss of interest in life. Its effects are feeling, thinking, behavior and might result in a range of physical and emotional types of problems. Normal activities can be quite troublesome, and sometimes the range of feeling come to like life is not worth living [5]. According to WHO (World Health Organization), depression is the leading cause of disability worldwide [6]. Depression is an ongoing problem, not a passing one. It can last a week, a month, a year, or a decade. Depression is not just for a particular age of people. Every age group can have depression. CDC report says depression is twice as common among women as men. According to the American Psychological Association, around 9% of men have depression in the USA. Even children at age 3-17 age also have depression [6]. So, it is a significant problem now around the world.

Many factors can play a role in the causes of depression. The main problem is that it is just the problem of living, not the real enemy. So, it is hard to fight off. There is much reason for people

*Corresponding Author Email Address: amit.csedu@gmail.com

to feel depressed. Even a lack of nutrition can cause depression [7].

Causes can range from biological to circumstantial. Some key reasons are horrible family history, early childhood trauma, less active brain, medical conditions, drug use, etc. Substance use problems can also cause depression. Like low esteem, mental illness, stressful events, etc. [8]. Taking about Bangladesh, the main problem is a lack of awareness about depression. According to WHO, 6 million Bangladeshi suffer from depression [9]. According to the Global School-Based Student Health Survey (2014) data, 13-17 years of children in Bangladesh, 7% attempted suicide in the last 12 months, while 8% made a suicide plan, and 5% considered trying it. The same report shows that 8% of children cannot sleep because of Depression [8].

Depression can be treated and prevented. The better option is prevention than treatment. A better understanding of depression can avoid that problem and can also help the treatment. Taking therapy, anti-depression medication is the primary treatment for depression. More income, a better relationship, and tablets are more commonly suggested treatment [9]. It is necessary to end the silence and overcome the fear of talking with someone professional so depression can avoid. Major Depression is hard to cure, but it is also preventive. In this research collection of data is based on different types of depression but just some random popular depressive status. Major Depression and minor Depression are hard to recognize solely based on status. That's why there is no level the depression only considers as a depressive status.

Depression is a significant public health concern all over the world. While successful early treatment can lead to a positive result, untreated depression can lead to even the cause of life. It is proved from many researchers that discloser of depression, or we can say emotion can prevent the worst scenario, can release stresses. Social media is the best platform for people to disclose their emotions in this new area. Self-discloser is in social media is a stress reliever for modern people nowadays. So, one can get the hype of their emotion through social media. We cannot guarantee that everything in social media is real. In our study, we collect some status to detect depression and at least warn their loved ones that maybe he/she is depressed.

Measurement of Depression is a depression scale that identifies if any person is alright or he/she has to undergo some treatment to cure depression. The method is to ask some questions, and the result will be according to the answer. This question is almost accurate in finding people's mental states. This scaling purpose is to recognize people at risk of developing the disorder only. The depression scale determines the severity of the depression, and the professionals will determine what type of treatment is more appropriate [2]. Depression scale can be classified by researchers and also by patients. One of the completed ranges by researchers is HAM-D (Hamilton depression) rating scaling. It is a widely used and oldest version. It takes 20-30 minutes to administer. That's why many people prefer The BDI (Beck Depression Inventory). It is a patient scale rated scale. It has high specificity and sensitivity. Currently, HAM-D and BDI are the best-validated scales [10].

For our research, the paid attention to GDS (Geriatric Depression Scale). It is designed to minimize the impact of depression symptoms. It has a yes/no format and has good sensitivity.

2 Related Works

As an Asian region, people use Facebook than twitter most of the time, so Billah and Hassan [11] locked their target on Bengali Facebook status. They tried to predict the depression from Facebook status. The collection of data is randomly on Facebook and even has suicide victim's data. Naive Bayes, Linear SVC, Logistic Regression, Multinomial Naive Bayes, and other classifiers are used. Five types of features are used in their model. Because of the lack of data model provided the best 77.96% accuracy. Traditional machine learning procedures are only used for the first Bangla attempt and small dataset. The researchers proposed that they could achieve up to 100% accuracy if they used the neural network.

Islam et. al. [4], with the help of SVM, DT (Decision Tree), KNN (K-Nearest Neighbors) performed depression analysis. They aimed to perform depression analysis on Facebook data collected from online sources. First, they proposed emotional, temporal, linguistic styles for their data collection. With their chosen classification techniques, they study each factor independently. They used the NCapture tool for data collection. Their research applied 21 types of attributes for detecting Depression from LIWC (Linguistic Inquiry and Word Count) software. They achieved accuracy between 60 to 80%.

Ramalingam et. al. [12] developed an SVM model to detect depression. They argued that men and women are classified differently according to depression. Their dataset consists of different sets of inputs like text, speech, and image—applied different classifiers to classify them correctly. The model contains several classifiers in groups. They achieved an accuracy of 82.2% in the case of males and 70.5 in the case of females.

Uddin et. al. [13] research topic is mostly similar to ours. They used a special type of RNN (Recurrent Neural Network), GRU (Gated Recurrent Units), to detect Bangla language depression status. They collected 500 tweets and 210 depressive statuses using the survey. They tried to prove that questionnaires and academic interviews are not the only way to detect depression. Because their dataset only contains 1,176 data, they achieved 75.7% accuracy with GRU, but with LSTM, they gained 88.6%accuracy.

Choudhury et. al. [2] in their research measure depression of university undergraduates for the purpose to help them if they needed any treatment for their depression. Their main objective was to find the main reasons for depression and whether depression can be predicted successfully. They found that most university students are suffering from different types of depression. But in this country, depression is not a major enough issue for the university to provide a psychiatrist for students. They took a survey from university students. They used six algorithms Gradient Boost, Deep learning, Generalized Linear Model, KNN, Random Forest, and SVM, to train and test the dataset. They found that deep learning is the best method among them, with the lowest number of false negatives, followed by the Gradient Boost algorithm. From the Generalized Linear model, they get their highest accuracy, which is 74.17%.

3 Materials and Methods

People of Bangladesh face different kinds of problems. For all of these, they suffer from depression. Bangladesh is a developing country, so poverty is the main reason for depression. Nowadays, the younger generation also faces love problems. Some people even get depressed regarding their studies.

Bangladesh contains a larger population than its land, so people face job problems.

On the other hand, there are a lot of non-depression sentences. Daily people post their status, which is not under depression. This study aims to implement a combined deep learning classifier to enhance the performance of language modeling and text classification to detect depression using the dataset of Bengali Facebook status.

In the framework, datasets are transformed into word vectors using word embedding. Then the word vector is fed into the CNN layer. In the max-pooling layer, it makes a sequential layer to feed into the LSTM layer.

3.1 Data Collection

Bangla language is comparatively more complicated to recognize than English. Most of the analysis is done in the English dataset. So, finding many datasets is not possible for analysis, and experiments used two different datasets: depressive and non-depressive. But it was challenging to find depressive Bangla datasets, as the presence of depressive Bangla datasets is less frequent. From existing paper 1177 depressive and non-depressive status was collected [13]. A better performance needs more dataset. The self-developed dataset contains Bangla status from different sources like Facebook, Twitter, YouTube comment sections. There is also some translated Bangla status in the dataset. The authors collected some non-depressive data from GitHub and Kaggle. The datasets are labeled like depressive datasets as '1' and non-depressive as '0'. The primary dataset contains 5053 depressives, and the 2110 non-depressive dataset total dataset is 7163. As for deep learning, the large dataset is required authors thought about this dataset is incomplete. That's why the dataset is still in the updated phase. Sample of datasets are given in Table 1.

Table 1 Sample data set

Depressive Data	Non- Depressive
ভাল থাকুক তারা যাদের জন্য আমি আজ মৃত প্রায়।	করোনা নিয়ে সবাইকে সচেতন হতে হবে
অভিশপ্ত এই জীবন। আত্মহত্যা ছাড়া আর কোন উপায় নাই আমার কাছে।	আহারে কাজের কোন শেষ নাই
ভবিষ্যত সম্পূর্ণ অন্ধকার।	ভালো কথার ভাত নাই।।।এইটাই বুঝলাম
অভিশপ্ত আমি আজ। এটাই আমার প্রাপ্য. সারা পৃথিবী পেয়ে আজ তোমাকে হারালাম।	সামান্য কিছু টাকার কাছে আজ মানবতার পরাজয়।
প্রতিকূলতার সাথে আর পেরে উঠছি না আমি। আমি এক অস্তগামী সূর্য। সংসার এর মায়া ত্যাগ করার সময় চলে আসছে। কিনা করলাম তোর মত স্বার্থপর এর জন্য। আর তুই কি দিলি? তোর মত স্বার্থপর এর কোনদিন ভাল হবে না।	নিরাপদে থাকুন
নিজের পাপে জর্জরিত আমি। জগতেই পাই আজ নরক যন্ত্রণা। আমার এই কদাকার রুপ আমি কাউকে দেখাবো না	পরিবার নিয়ে সুখে আছি

3.2 Data Pre-processing

An input text has filtered using pre-processing to enhance a proposed model's performance by eliminating unnecessary features to process row posts before acknowledging word embedding. Pre-process of the dataset was needed. To make the dataset clean and eligible for testing, used Natural language toolkit (NLTK) [14] for pre-processing datasets. The genetic kit is a platform that is used to build Python programs that work in statistical NLP (Neuro-Linguistic Programming) with language data to apply. It includes libraries for processing text for tokenization, sorting, grouping, stemming, tagging, and semblance reasoning. We have used NLTK to remove punctuation, stop-words according to the given text document. But it did not remove all the punctuation that is used as emoticons signs. Bangla dataset contains many misspelling and incomplete words. Some spelling seems to be different from each other, but they are the same. For this type of word, stemming was done. Removed all the URLs with white-space from the dataset, and then we got our required dataset.

3.3 Proposed Neural Network

3.3.1 CNN

CNN is known as an artificial neural network that is used in recognize image and processing. It is designed especially for the processing of pixel data. Height, weight, the depth that three types of dimensions are organized in the CNN layer. CNN layer contains two components: one is feature extraction, and another is classification. In feature extraction, convolution series and pooling operation are done. And in classification, a fully connected will do their work [15]

CNN can predict using the spatial structure as its input. First, from the input data, it produces a feature map by using a filter. A convolution layer is created after padding the feature map. Then the pooling layer is performed to decrease the parameter size and execution in the network. Max polling is mostly used as a pooling layer. It reduces the size of the feature map by choosing the maximum value from every window. It does not lose any kind of important information. In a fully connected layer, flatten is performed to convert 3D or 2D data into 1D. Fully connected shows the output from the last layer of the neural network. Finally, CNN shows a sequential sentence as the result of output [16].

3.3.2 LSTM

LSTM is an artificial neural network used for the classification process and predicts the result of output in lines of sentences. For sequential series, LSTM is used. LSTM is a special type of RNN because RNN cannot maintain information for a long time, so LSTM is established. A vanishing gradient is one of the main problems of RNN that is solved by using LSTM.

LSTM mechanism contains three gates: Forget, Input, and Output gate [17]. Three gates perform differently for a sequential series. Forget gate removes cell information that is not required anymore. The input gate takes a sequential input and updates the information of the cell. Finally, the output gate gives the result of the output for the LSTM module. For each of the gates, LSTM uses an equation. All the equations are given below:

$$f_t = \sigma\,(W_f\, x_t + U_f\, h_{t-1} + b_f)$$

$$i_t = \sigma\,(W_i\, x_t + U_i\, h_{t-1} + b_i)$$

$$o_t = \sigma\,(W_o\, x_t + U_o\ h_{t-1} + b_o)$$

$$u_t = tanh\,(W_u\, x_t + U_u\ h_{t-1} + b_u)$$

$$c_t = f_t\, \Theta\, c_{t-1} + i_t\, \Theta\, u_t$$

$$h_t = o_t\, \Theta\, tanh(c_t)$$

Here, f_t represents the gate, i_t as input gate, and output gate is o_t. Θ represents the multiplication of elements step by step. The logistic sigmoid function is used for each gate. Here, u_t represents the *tanh* function. The memory cell information contains in c_t, and at last, h_t represents the hidden state. Three gates contain a bias vector. LSTM is key to cell state. LSTM maintains the information from the previous cell.

3.3.3 LSTM and CNN

Our model is based on the hybrid model of CNN and LSTM [18]-[28]. The workflow of our proposed model is given in Fig. 1.

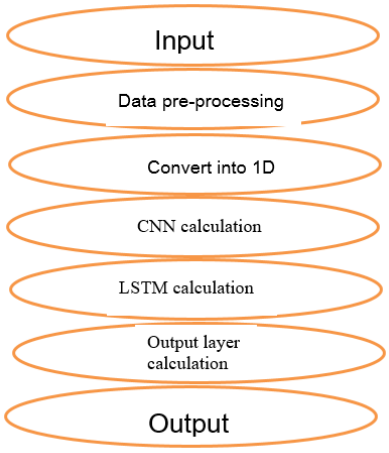

Fig. 1 Workflow of the proposed model

3.3.4 Training Model

To identify the presence of depression in social media, combined the strengths of the neural network architectures of CNN and LSTM and applied a hybrid CNN-LSTM model to classify text data. In recent years CNN was used in many text classification research, and LSTM is known for the text classification neural network. That's why the authors thought of mixing these two algorithms (see Fig. 2) to get a better result. The model takes an input and then a single number representing the probability that the tweet indicates depression. The experiment followed the Hybrid framework for detecting depression using the LSTM-CNN method.

After pre-processing the dataset, the dataset is ready for implementation the model. Keras was used as a neural network framework and Tensorflow as a backend library. Keras is designed for deep neural networks, as authors used deep neural algorithms for model training. For the model training, the Bangla word2 vector is used, which contains the Bangla language vocabulary. This word2 vector is used to create an embedding matrix. As a CNN word with 2D images, the text has to convert in 2D vector array for text classification. That's why the embedding layer was used—this embedding matrix fed into the embedding layer for further execution. The embedding layer was used to minimize the cost of the loss function. Here we consider the difference between other layers with this embedding layer; then, the main difference is that the output is not like a mathematical function of the input—this pre-trained word vector was constructed for further use on the CNN model.

For this model, CNN was used as a front-end layer followed by LSTM layers and the dense output layer. CNN model was for feature mapping, and for the feature extraction, the LSTM model was used. Authors used CNN as CNN is known for taking original data to create feature maps from it. The dataset is a 1D structure. The structure was fed as input (see Fig. 2). CONV1D took the input to interpret the data into smaller square sizes. The MAXPOOLING layer then explained the result by reducing its size into an abstract dimension. The flatten layer took this output data to convert it into a vector fed into other layers for further resulting prediction. CNN was done with extracting data to transform into a vector. For the internal state to building up, LSTM was used. The sequential output was fed into the LSTM layer. LSTM is an artificial neural network architecture used in deep learning to classify processes and predict output in sentences. LSTM predicted from the previous cell, and the 3 resulting models were created.

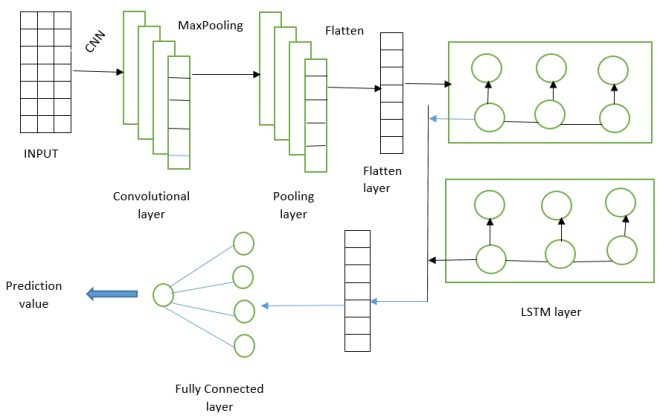

Fig. 2 Mixed mechanism of LSTM and CNN

We tried to minimize our cross-entropy error for the model. Given a training sample x (i) and its true label $y\,(i) \in \{1, 2, \cdots, k\}$ where k is the number of possible labels and the estimated probabilities ye (i) $j \in [0, 1]$ for each label $j \in \{1, 2, \cdots, k\}$, the error is defined as:

$$L(x\,(i)\,, y(i)\,) = X\ k\ j=1\ 1\{y\,(i) = j\}\ log(ye\,(i)\ j\,)$$ [18]

where 1\{condition\} is an indicator such that 1\{condition is true\} = 1 otherwise 1\{condition is false\} = 0. [18]

TF-IDF vectorizer and count vectorizer of SVM used for depression prediction. TF-IDF transformer provided a matrix of the count. On the other hand, the count vectorizer transformed text into a sparse matrix of n-grams counts. Tf-Idf transformed and counted Vectorizer both perform well for prediction. That's why the authors used them both as a combined matrix. TF-IDF vectorizer showed higher accuracy than count Vectorizer, as is expected because TF-IDF balanced out with term frequency and its inverse document frequency. For the training model of TF-

IDF Vectorizer and count Vertorizer, four types of the classifier were used. Those were Naïve Bayes, SVM, Logistic Regression, and Random Forest. From the training of those classifiers, the best accuracy of TF-IDF was SVM. That's why SVM was the chosen classifier for the prediction.

SVM is a supervised machine learning algorithm for classification problems. It performs well for two classifier problems. As the authors used two types of data, depressive and non-depressive so SVM is the best selection for prediction. When a sentence is given to predict depressive or non-depressive, the count vectorizer split the word from the sentence and counts the word's value. According to the word count from the given dataset, it shows prediction. If the number of depressive words is more significant than the non-depressive word, it shows depression or vice versa.

4 Experimental Results

4.1 Performance Evaluation

With the small dataset in hand, the LSTM and CNN model only got 81.05% accuracy. For comparison, the model we also trained the model with Logistic Regression and got 81.49% accuracy. To get this accuracy, we have done multiple tuning, and after that, we have selected the tuning value. The parameter setting for the tuning is given in Table 2.

Table 2 The list of values that are used in work

Hyper-parameter	Value
Embedding Dim	300
Hidden Units of LSTM	128
The activation function of LSTM	Sigmoid
Batch Size	10
No of CNN Layers	1
No of Convolution filter	32
Activation function	RELU
Max pool size	2
Regularization	Dropout operation
Dropout rate	0.2
Learning rate	0.1

TF-IDF and count vector models with different classifiers got us different accuracy for TF-IDF Vectorizer and counted Vectorizer as shown in Fig. 3. The best efficiency of the TF-IDF vectorizer was 67.62%, and the count vectorizer was 75.05%. That's why this TF-IDF and count vector model is unable to predict correctly. Sometimes it gets the wrong result.

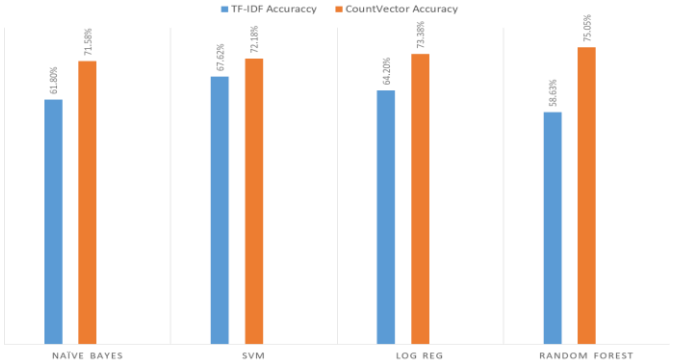

Fig. 3 Accuracy graph of TF-IDF Vectorizer and Count Vectorizer

4.2 Comparison of Proposed Model

Comparing with the international journal [11] helped determine the model's efficiency. The ground of comparison was different algorithms and accuracy. They have chosen Naive Bayes, Multinomial Naive Bayes, Logistic Regression, and Linear SVC as their main algorithms with 1000 Bangla dataset. While we achieved 81.05% with LSTM and CNN, this proposed research is different from this research. Still, the authors tried to compare the deep learning model training accuracy with ML model training accuracy. That's the main reason for the selection of this particular research paper.

That comparison research showed that only 53.93% could be achieved with unigram and emoticon while unigram, emoticon, and depressive word lists showed different accuracy for different algorithms. With our TF-IFD vectorizer, and count vector accuracy of TF-IDF is much better than this proposed method as shown in Fig. 4. Different batch sizes, feature sizes, and different classifiers are responsible for different accuracy.

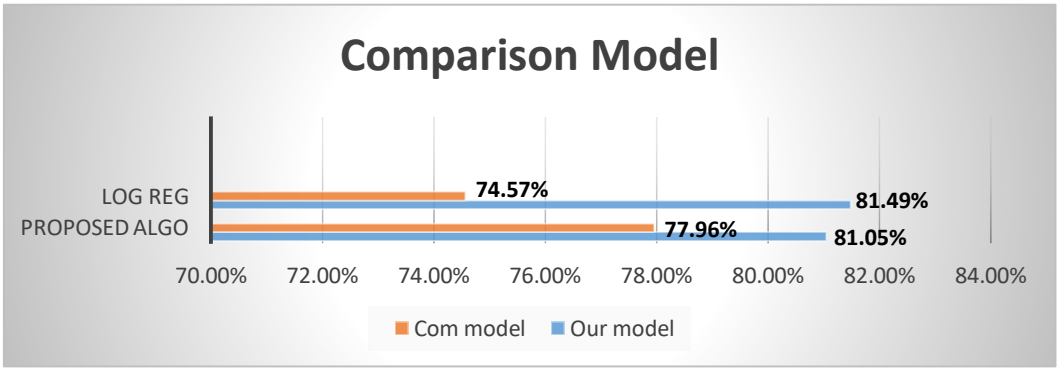

Fig. 4 Comparison model (Series 1: LSTM-CNN, Series 2: Comparison research)

5 Discussion

The authors used the CNN-LSTM hybrid model to execute their system. As far [29], a paper has already been completed with this hybrid model using English Dataset. But the new thing in this paper is that the authors used the same hybrid model using the Bangla dataset. But as the Bangla dataset is not available so much, the authors have created a small dataset for execution. After executing the hybrid model using the Bangla dataset, it performed well in detecting depression. In this modern era, most people are found in depression because of work stress and some other problem.

On the other hand, social media is a common way to express their emotion to decrease their sorrow or expand their happiness. So, it is easy to find out someone's emotional status or daily status through social media. This kind of data is most famous for the proposed system. Sometimes treatment can be given through social media. The authors have executed a system that can predict depressive and non-depressive status. After knowing that the person is in extreme level depression, some sort of treatment can be done through social media. This procedure can reduce the cause of death due to depression.

6 Conclusion

This paper tried to implement a hybrid algorithm to recognize depression in social media using Bangla datasets. Natural Toolkit was used for pre-processing the dataset. The dataset contains both depressive and non-depressive Facebook Bengali status. Word vector was used, which is full of the vocabulary of all Bangla words. This word vector helps to create an embedding matrix. In the embedding layer, an embedding matrix creates to feed into the CNN model. After getting a sequential result that is fed into the LSTM model, Support Vector Machine was used for prediction with a short number of datasets at the end of all processes. Count vectorizer showed the best performance than TF-IDF tokenizer. TF-IDF is unable to give precise results because of the small data set. Proposed better algorithms than LSTM and better datasets could achieve more efficiency. We used LSTM and CNN for our model, but in the future, the work would build the model using better RNN. After detecting depression, then the program will suggest, according to the result, if they need any counseling or not.

References

[1] "What Is Depression?" https://www.psychiatry.org/patients-families/depression/what-is-depression (accessed Jun. 06, 2020).

[2] Choudhury, A.A., Khan, M.R.H., Nahim, N.Z., Tulon, S.R., Islam, S. and Chakrabarty, A., 2019, June. Predicting depression in Bangladeshi undergraduates using machine learning. In 2019 IEEE Region 10 Symposium (TENSYMP) (pp. 789-794). IEEE. DOI: 10.1109/TENSYMP46218.2019.8971369.

[3] "Can Depression Really Kill You?" https://www.verywellmind.com/can-depression-kill-you-1067514 (accessed Jun. 06, 2020).

[4] Islam, M.R., Kabir, M.A., Ahmed, A., Kamal, A.R.M., Wang, H. and Ulhaq, A., 2018. Depression detection from social network data using machine learning techniques. Health Information Science and Systems, 6(1), pp.1-12. DOI: 10.1007/s13755-018-0046-0.

[5] "Depression (major depressive disorder) - Symptoms and causes - Mayo Clinic." https://www.mayoclinic.org/diseases-conditions/depression/symptoms-causes/syc-20356007 (accessed Jun. 06, 2020).

[6] "What is mental illness? - MindFreedom International (MFI)." https://mindfreedom.org/kb/voices-for-choices/voices-for-choices-what-is-mental-illness/ (accessed Jun. 06, 2020).

[7] "Depression: What it is, symptoms, causes, treatment, types, and more." https://www.medicalnewstoday.com/articles/8933 (accessed Jun. 06, 2020).

[8] "World Health Organization, Depression: Let's talk." http://www.searo.who.int/bangladesh/enbanwhd2017/en/ (accessed Jun. 06, 2020).

[9] Selim, N., 2010. Cultural dimensions of depression in Bangladesh: a qualitative study in two villages of Matlab. Journal of Health, Population, and Nutrition, 28(1), p.95.

[10] Anderson, J.E., Michalak, E.E. and Lam, R.W., 2002. Depression in primary care: Tools for screening, diagnosis, and measuring response to treatment. British Columbia Medical Journal, 44(8), pp.415-419.

[11] Billah, M. and Hassan, E., Depression Detection from Bangla Facebook Status using Machine Learning Approach. International Journal of Computer Applications, 975, p.8887. DOI: 10.5120/ijca2019919314.

[12] Ramalingam, D., Sharma, V. and Zar, P., 2019. Study of depression analysis using machine learning techniques. Int. J. Innov. Technol. Explor. Eng, 8(7C2), pp.187-191.

[13] Uddin, A.H., Bapery, D. and Arif, A.S.M., 2019, July. Depression Analysis from Social Media Data in Bangla Language using Long Short Term Memory (LSTM) Recurrent Neural Network Technique. In 2019 International Conference on Computer, Communication, Chemical, Materials and Electronic Engineering (IC4ME2) (pp. 1-4). IEEE. DOI: 10.1109/IC4ME247184.2019.9036528.

[14] "NLTK Book." https://www.nltk.org/book/ (accessed Jun. 05, 2020).

[15] "Understanding of Convolutional Neural Network (CNN) — Deep Learning." https://medium.com/@RaghavPrabhu/understanding-of-convolutional-neural-network-cnn-deep-learning-99760835f148 (accessed Jun. 14, 2020).

[16] "An intuitive guide to Convolutional Neural Networks." https://www.freecodecamp.org/news/an-intuitive-guide-to-convolutional-neural-networks-260c2de0a050/ (accessed Jun. 14, 2020).

[17] "Long Short Term Memory | Architecture Of LSTM. " https://www.analyticsvidhya.com/blog/2017/12/fundamentals-of-deep-learning-introduction-to-lstm/ (accessed Jun. 14, 2020).

[18] Zhou, C., Sun, C., Liu, Z. and Lau, F., 2015. A C-LSTM neural network for text classification. arXiv preprint arXiv:1511.08630. Available: http://arxiv.org/abs/1511.08630.

[19] Rakib, O.F., Akter, S., Khan, M.A., Das, A.K. and Habibullah, K.M., 2019, December. Bangla word prediction and sentence completion using GRU: an extended version of RNN on N-gram language model. In

2019 International Conference on Sustainable Technologies for Industry 4.0 (STI) (pp. 1-6). IEEE.

[20] Emon, E.A., Rahman, S., Banarjee, J., Das, A.K. and Mittra, T., 2019, June. A deep learning approach to detect abusive bengali text. In 2019 7th International Conference on Smart Computing & Communications (ICSCC) (pp. 1-5). IEEE.

[21] Hossain, M.M., Labib, M.F., Rifat, A.S., Das, A.K. and Mukta, M., 2019, June. Auto-correction of English to Bengali Transliteration System using Levenshtein Distance. In 2019 7th International Conference on Smart Computing & Communications (ICSCC) (pp. 1-5). IEEE.

[22] Drovo, M.D., Chowdhury, M., Uday, S.I. and Das, A.K., 2019, June. Named Entity Recognition in Bengali Text Using Merged Hidden Markov Model and Rule Base Approach. In 2019 7th International Conference on Smart Computing & Communications (ICSCC) (pp. 1-5). IEEE.

[23] Biswas, E. and Das, A.K., 2019, June. Symptom-Based Disease Detection System In Bengali Using Convolution Neural Network. In 2019 7th International Conference on Smart Computing & Communications (ICSCC) (pp. 1-5). IEEE.

[24] Das, A.K., Ashrafi, A. and Ahmmad, M., 2019, February. Joint Cognition of Both Human and Machine for Predicting Criminal Punishment in Judicial System. In 2019 IEEE 4th International Conference on Computer and Communication Systems (ICCCS) (pp. 36-40). IEEE.

[25] Tuhin, R.A., Paul, B.K., Nawrine, F., Akter, M. and Das, A.K., 2019, February. An automated system of sentiment analysis from Bangla text using supervised learning techniques. In 2019 IEEE 4th International Conference on Computer and Communication Systems (ICCCS) (pp. 360-364). IEEE.

[26] Islam, J., Mubassira, M., Islam, M.R. and Das, A.K., 2019, February. A speech recognition system for Bengali language using recurrent Neural network. In 2019 IEEE 4th international conference on computer and communication systems (ICCCS) (pp. 73-76). IEEE.

[27] Bhuiyan, M., Rahman, A., Ullah, M. and Das, A.K., 2019. iHealthcare: Predictive model analysis concerning big data applications for interactive healthcare systems. Applied Sciences, 9(16), p.3365.

[28] Labib, M.F., Rifat, A.S., Hossain, M.M., Das, A.K. and Nawrine, F., 2019, June. Road accident analysis and prediction of accident severity by using machine learning in Bangladesh. In 2019 7th International Conference on Smart Computing & Communications (ICSCC) (pp. 1-5). IEEE.

[29] Tadesse, M.M., Lin, H., Xu, B. and Yang, L., 2020. Detection of suicide ideation in social media forums using deep learning. Algorithms, 13(1), p.7. DOI: 10.3390/a13010007.

SciEn
Journal of Engineering Advancements Vol. 02(01) 2021, pp 48-57 https://doi.org/10.38032/jea.2021.01.007

Plant Disease Detection through the Implementation of Diversified and Modified Neural Network Algorithms

*Fatema Nihar, Nazmun Nahar Khanom, Syed Sahariar Hassan, Amit Kumar Das**

Department of Computer Science and Engineering, East West University, Dhaka, Bangladesh

Received: January 28, 2021, Revised: February 25, 2021, Accepted: March 01, 2021, Available Online: March 12, 2021

ABSTRACT

In the era of artificial systems, disease detection is becoming easier. For detecting disease, monitoring the plants 24 hours, visiting the agricultural office, or asking for help from a specialist seem difficult. This situation demands a user-friendly plant disease detection system, which allows people to detect whether the plant is diseased or not in an easier way. If the plant is diseased, a treatment plan will also be notified. In this way, people can easily save time, money, and, most importantly, plants. In this study, the researchers have collected data of vegetables from a field and applied multiple diversified Neural Network Algorithms such as CNN, MCNN, FRCNN, and, along with that, also proposed a new modified neural network architecture (ModCNN), which has produced 97.69% accuracy. The authors have also classified the bean leaf diseases into four categories according to their symptoms, which will help to identify diseases accurately.

Keywords: Artificial, Agriculture, Monitoring, Disease Detection, Neural Network.

1 Introduction

As days go by, people face different types of problems regarding plant disease. Some may know the reason and treatment, but most people do not. People tend to browse online to find out the answers. However, what if the answer can be found just by uploading a photo? In this way, people will not only know the cause, types of the disease but also will be able to know about the treatment. This process will be time, cost-effective and allow people to interact more and gain valuable information about plants.

At present, it is comprehensible to design such a system that can interact with people more effectively. Different types of organizations such as Bangladesh Rice Research Institute, Sher-E-Bangla Agricultural University, etc., are researching continuously to discover new findings for different kinds of crops. The objective of this research is to detect plant diseases. Moreover, this research study has classified the bean leaf disease into four categories: low, mid, high, and fully infected. It will specify how much the disease has spread through the leave, and it will notify the user to take fruitful steps. These will help the agriculture field advance towards development, and the researchers will contribute more. Several studies related to this topic have been done before. In paper [1], the authors have used 50,000 images to classify plant disease.

In contrast, in paper [2], the authors have combined three color components in a three-layer convolutional network to address plant disease accurately. In another paper [3], the authors have also worked with 14 different crops and deliver the highest accuracy in finding the disease. Therefore, it has been seen that this research study provides slightly less accuracy than some of the other research studies. Nevertheless, in this study, the researchers differentiated the diseases and identified the disease more specifically. The researchers have built their own CNN architecture that gives higher accuracy among the algorithms the authors have used so far.

In paper [4], the authors have used a cloud-based platform to track the disease easily for farmers. In paper [5], the authors have detected early leaf disease to ensure efficient crop production. In paper [6], the authors have worked with 14 different crops with distinct 25 diseases, which gives high accuracy results.

There are other related works as well, which intend to perform disease detection and provide good results.

2 Background

In paper [1], the authors have classified and recognized plant disease. At most, 50,000 images have been used in the database. CNN, with GoogLeNet architecture, has been implemented here with augmented training datasets. Plant pathologists' and farmers' participation will improve the process for collecting the images, image labeling, and other parts of the plants such as root, stems, and so on that will produce different future results.

In paper [2], the authors have depicted vegetable leaf disease's recognition process combining three-color components using a three-channel convolutional network (TCCNN) model.

In paper [3], the authors have used deep learning models to identify plant disease. To train the architectures, Keras with Theano backend have been used. In this paper, the authors have used VGG16, Inception v4, ResNet with 50,101,152 layers, and DenseNets with 121 layers for the model.

In paper [4], the authors have implemented the CNN model and a cloud-based platform to identify and track farmers' plant disease. In the future, using different factors such as soil, pesticide treatment, temperature, rainfall, etc., will improve the accuracy of the model and will help to enable disease forecasting.

In paper [5], the authors have detected early leaf disease for the efficient production of crops. CNN and Learning Vector Quantization (LVQ) algorithms have been implemented with three channels (RGB components) based filters.

In paper [6], the authors have used AlexNet, GoogLeNet architecture with a transfer learning approach for building the model for detecting the disease of plants using leaves images.

*Corresponding Author Email Address: amit.csedu@gmail.com Published by: SciEn Publishing Group

Image collection using realistic methods will produce different results in the future.

In paper [7], the authors have implemented architectures of CNN, such as AlexNet, AlexNetOWTBn, Overfeat, VGG, and GoogLeNet, to build the model for detection and diagnosis of the disease of the plants. Automated pesticide prescription systems will allow the farmers to purchase the appropriate pesticides in the future.

In paper [8], the authors have diagnosed the early detection of apple leaf diseases by implementing GoogLeNet Inception architecture and Rainbow Concatenation, INAR-SSD (Single-shot multi-box detection with Rainbow Concatenation and inception module).

In paper [9], the authors have developed a multilayer convolutional neural network (MCNN) to predict healthy or diseased mango tree leaves. At most, 1070 real-time healthy or diseased Mango tree leaf images and 1130 images from plant village datasets have been used. The authors have detected fungal disease-Anthracnose of Mango tree leaves. Their proposed model has given 97.13% accuracy, which is higher than the other approaches. In the future, working with other plants with economic importance will produce different results.

In [10], [11], [12], [13] and [14] the authors have applied Faster R-CNN with FCM-KM fusion for the rapid rice blast, bacterial blight, and blight disease detection. The authors have also used the 2DFM-AMMF algorithm for noise reduction and faster 2D-Otsu segmentation. The authors have applied a max and min distance algorithm for the optimization of FCM-KM. The average accuracy found from the proposed model is 97.2%. In the future, automated rice disease detection using mobile will allow real-time monitoring and pest identification.

In the paper [15], the authors have used K-means clustering and support vector machine algorithms to predict and classify soybean leaf disease. The diseased leaves are divided into Septoria leaf blight, downy mildew, and frog eye. Four thousand seven hundred seventy-five images of plant village datasets have been taken. The average classification accuracy found from the model is almost 90%. In the future, using real-time images will bring a difference to the result.

3 Main Focus of the Article

Numerous researches have been done to detect plant diseases, but the researchers have applied either existing algorithms or proposed algorithms. The main goal behind this is to increase accuracy as much as possible to produce an accurate result. In paper [1], the author has applied CNN with GoogleNet architecture on a database that contains 50,000 images of 171 diseases affecting 21 plant species. Still, the author has only used corn disease due to its' widest variety of conditions. The author has been able to achieve only 87% accuracy. Still, their future task of involving farmers and plant pathologists in image collection has been one of the inspirations behind this study. In paper [5], the authors have applied CNN with the Learning Vector Quantization algorithm on 500 images of Tomato with four symptoms of diseases and have achieved only 86% accuracy. However, while going through the detection phase, the authors have faced issues such as some of the images being labeled in the wrong classes due to their similarities. In this study, the researchers have used CNN, MCNN, FRCNN, and ModCNN to detect the diseases according to classes accurately. Paper [1] and paper [5] have worked as good influences. This study focuses on proposing a new algorithm to produce the highest accuracy to detect plant diseases accurately and involve people from all occupations in this process.

The data, which will be collected from the user, will be processed thoroughly to predict the disease. The data collected from the user can be the image of the plant. This disease prediction will help to reduce costs in the future, minimize treatment costs and unexpected expenses.

Using the prediction outcome, people do not need to wait for any agricultural officers or expert opinions. Instead, they can immediately start taking preventive measures and treatment actions if required. Nevertheless, for advanced cases of plants, experts' advice is highly recommendable. Therefore, this study's proposed prediction model helps people save plants and provide better services. It also reduces the time of diagnosis and unnecessary cost of treatment.

4 Methods and Materials

4.1 Image processing in plant disease detection

Through the image processing method, many different types of photos of plants (data) can be diagnosed. These data can be structured or not. However, using this method to detect plant disease and provide information is excellent research to help the agricultural arena. Many people live their livelihood through farming without knowing what type of disease the plant has, what kind of pesticide or treatment to cure the plant. Though there are many agricultural departments and officers to train the farmers, not everybody visits those places to train himself or herself. During bad weather or pandemic, people stay at home to be safe. In this type of situation, people can only use their electronic devices to detect plant disease as nowadays everyone uses a cellphone. In this way, life gets more comfortable, and people can be more productive.

By performing Image processing on an image, one can easily extract the required information about the image. It is one kind of signal processing method, where the image will be the input, and the output can be an image or some characteristics related to that image. As nowadays, the uses of image processing are rapidly increasing, it is also becoming more efficient and valuable to researchers. It is one of the core areas of the research involving three steps.

- Step 1: Using acquisition tools, import the image
- Step 2: Manipulate and analyze the image
- Step 3: Show output where the result is either an altered image or report found in image analysis

In image processing, two kinds of methods are generally used, and they are Analogue and Digital. Analog image processing is mainly used for hard copies such as photographs and printouts, while the digital image processing technique manipulates digital images through computers. All kinds of data undergo three general phases while implementing digital techniques.

- Phase One: The image will be pre-processed
- Phase Two: After enhancing, the image will be displayed
- Phase Three: Extract the required information about the image

Digital Image Processing mainly involves three parts.

- Collection of images.
- Processing of image.
- Analysis of image.

At the basic level, there are three components in a digital image processing system.

To process images, a computer system.

- An Image Digitizer.
- A Display Device to display image.

There are several essential steps of image processing required to process an image and predict accurate results.

- Step 1: Image Acquisition.

To produce a digital image, one or more image sensor is needed. Apart from that, different kinds of light-sensitive cameras including, radar, range sensors, ultrasonic cameras, tomography devices, etc., are also required.

- Step 2: Image Enhancement.

It is mainly used to improve the image's visual quality to bring out the details hidden inside the image. There are also two types of techniques: The transform domain method and the spatial domain method.

The spatial domain Method performs directly on the pixels where the transform domain method only plays on the Fourier transform of an image and transforms it back to the spatial domain.

- Step 3: Image Restoration.

It is used to remove the noise from the original version of the image. Noise can occur due to camera shaking, less light, etc. In this case, filters are used to remove the noise. Here, after taking a corrupted or noisy image, one can easily estimate the clean original image. Corruption can occur in many different forms like motion blurriness, noises, and missed camera focus.

- Step 4: Morphological Processing.

It can extract components of images that are useful to represent and describe the shape. It is also used for edge detection. It is like a convolution process.

- Step 5: Segmentation.

It partitions the image into a set of pixels. It involves two techniques: Local Segmentation, Global Segmentation.

In Local Segmentation, sub-images are mainly segmented. These images are like small windows in a whole image. The number of pixels that are available to local segmentation is always less than global segmentation.

In Global Segmentation, segmentation of a whole image is performed. The goal of this is to simplify or change the representation part of an image into something else, which can be easily analyzed and will be meaningful too.

- Step 6: Object Recognition.

It recognizes different parts of an image, such as color, shape, and texture. It can comprehend an object's physical properties and apply semantic attributes to that particular object, which also involves the realization of usage, prior experience with that specific object, and how it relates to the others.

- Step 7: Representation.

One can represent an object by its boundary (its external characteristics) or internal characteristics (texture).

- Step 8: Description.

The object boundary may be described by its length, orientation, or number of concavities.

- Step 9: Image Compression.

It is mainly performed to save disc space by representing an image with a minimum number of bits. There are two kinds of image compression, and they are Lossy compression, Lossless compression.

In Lossy compression, some of the information is lost, and in Lossless compression, the image that will be re-constructed will be the same as the original version of the image. In the Lossless compression method, two techniques are being used: run-length coding and Huffman coding.

- Step 10: Color Image Processing.

Within 100 shades of grey, the human eye can only distinguish hundreds of thousands of different colors. The image contains more information. Using this information, one can simply analyze images such as object identification, extraction.

In the image processing approach, the image can be easily analyzed in the post-processing part. Images can be stored in computer memory, and the initial cost can vary.

The architecture of the Proposed System

In this study, Fig. 1 presents the proposed user-friendly plant disease detection system architecture, which has focused on three phases.

- Phase One: The data collected with the unique interaction of electronic devices.
- Phase Two: Analyze and process the data given by individual users for future disease prediction.
- Phase Three: Detect plant disease along with providing necessary information

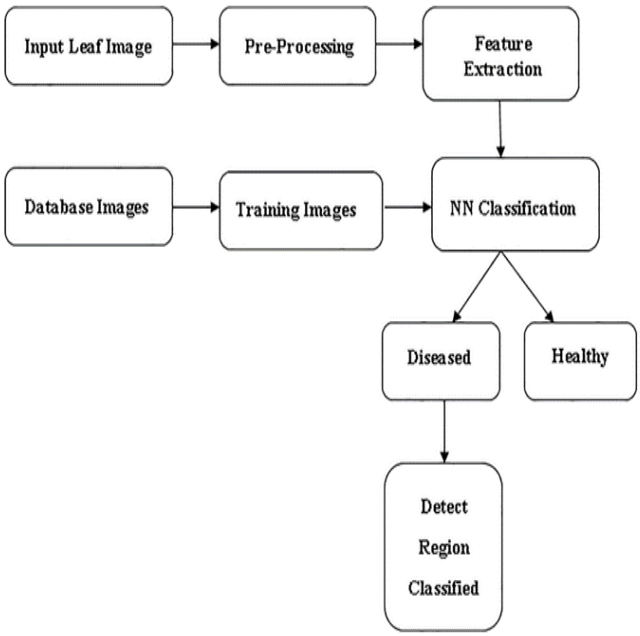

Fig. 1 Three phases of user-friendly plant disease detection system

Here, in Fig. 1,

Input Leaf Image -> Pre-Processing- > Feature Extraction -> NN Classification -> Diseased / Healthy.

Diseased -> Detect Region Classified.

Database Images -> Training Images -> NN Classification.

The system will collect data through a user interface. Users can use electronic devices to input data. The data can be an image of the plant, such as the leaf of the plant. After collecting the image, it will be compiled with the trained model the authors already have. I t will classify whether the plant is diseased or not. If it is healthy, it will be informed to the users. However, if it is not, then treatment plans and suggestions will be shown to the users. In this research, the researchers have used only two types of plants: Tomato and beans. In the case of Tomato, it will only show the two statuses (healthy, diseased). But, in the case of beans, it will show two types of state (healthy, diseased); in diseased, there are also three classifications (low affected, medium affected, and profoundly affected). The authors already have the data on the temperature of each area from previous years. So, based on those data, necessary actions will be suggested to the users. The data (image, output, and temperature-related data) will be stored in a cloud-based database such as Google Drive.

Fig. 2 Implementation of a user-friendly plant disease detection system.

Fig. 2 represents the implementation phase of the plant disease detection system.

At first, it welcomes the user to this 'Plantology' Application. It analyzes a given image and, after detection, provides output such as 'Fully Diseased Bean leaf, search if there is more than 30% of leaves are similar. If it is, then remove the plant; otherwise, remove the diseased leaf. Please water the plants, and the temperature is high; this time, the insects will increase the virus infections'.

4.2 Brief system architecture

4.2.1 Convolutional Neural Network (CNN)

This algorithm addresses classification problems and helps to recognize images. It is also used in identifying videos, recommendation systems, etc. There are four layers in this network.

Layer One: Convolution.

The features metric has been generated randomly in the convolutional layer and multiplied using the matric with the input image pixel-by-pixel values. Then, all the values are added and divided with the total number of feature pixels. Here, the feature pixel is generated randomly, and the weight is passed down for forwarding propagation. After that, the weight will be updated after Backpropagation. In this way, after completing the calculation, the final metric is found.

Layer Two: ReLu.

Rectifier Linear Unit is also known as ReLu, which works as one of CNN's activation functions. ReLu mainly helps remove the negative values from the result gained from Convolution Layer, which helps get only the primary feature value from the image. The ReLu equation can be explained when the input is less than zero; the output is equal to zero. When the input is greater than or equal to zero, the output is similar to the input.

Layer Three: Pooling.

There are many kinds of pooling functions, such as max pooling, average pooling, mean pooling, etc. For this algorithm, max pooling is widely used, and it has mainly 2×2 or 3×3 window size, where it only gives the maximum values from the metrics to generate only the most essential values from the data. It helps to shrink the input metrics. After passing the pooling layer, the final parameter is found, and that will be sent to the next layer.

Layer Four: Fully Connectedness (also known as Fully Connected Layer).

It converts the input metrics into a 1D array or a single list.

CNN can be sequential or functional. On CNN, some hidden layers are called convolutional layers, and they make a CNN. There can also be non-convolutional layers, but the base of a CNN is mainly the convolutional layers. This layer receives input, transforms it somehow, and shows the output after that. This output will be the input for the next layer. With this convolution layer, this transformation that passes through is called a convolution operation. Convolution layers can easily detect images and patterns, such as edges and images also. While using the convolutional layer, one needs to specify the number of filters that the layers will work with. These filters mainly detect the patterns. ReLu or Rectified Linear Activation Function transforms the summation of the weighted input from a particular node to the activation part and shows the output. To make training more comfortable and achieving better performance, it is highly needed. The pooling layer simplifies the data by reducing dimensionality. This also reduces training time and overfitting problems. In the fully connected layers, every neuron is connected to the next. In this stage, it mainly looks for those features, which accurately describe the particular classes. The result shows a probability with a single vector that is embodied in depth.

This algorithm is being used in different areas such as vehicle recognition systems, natural language processing tasks, computer vision, drug discovery, game playing, etc.

4.2.2 Multi-Layer Convolutional Neural Network (MCNN)

MCNN works just like CNN, it is just different from most of the other CNN architectures, and it consists of multilayers of the convolutional layer. It is also one of the deep learning models that are used for solving complex problems.

In the model described in the paper [8], they have been inspired by AlexNet architecture, which has six convolutional layers with six ReLU(Rectifier Linear Unit), three max-pooling layers, one flatten layer, and two dense or fully-connected layers. The first two convolutional layers' size is (128, 3×3), the next

two convolutional layers' size is (256, 3×3), and last two convolutional layers' sizes are (384, 3×3) and (256, 3×3). In this model, the authors have used each of the max-pooling layers with a pool size of (2×2) and a dropout rate of 0.2. The flatten layer helps the result set to convert into output form, and the dense or fully-connected layer supports it to turn into a 1D array or single list and uses SoftMax as the activation function.

4.2.3 Faster Region-based Convolutional Neural Network (FRCNN)

FRCNN is implemented to detect the object. It uses a search selective algorithm to discover the regions of interest and passes those to a ConvNet. Then it searches the areas that may be an object by uniting similar types of pixels and textures into multiple rectangular boxes. The search selective algorithm is calculated based on the feature map's output, which is found in the previous step.

After that, the ROI (region of interest) pooling layer is implemented to ensure that the standard and pre-defined output sizes are all accurate. Then, valid outputs are passed down to fully connected layers to be considered as inputs. In the final step, two output vectors are implemented to portend the observed object with a SoftMax classifier and modify bounding box localizations along with a linear regressor. Before training, the images have been annotated using the label box. After training, it produces a significant result with annotation.

In FRCNN, RPN (region proposal network) is used to reduce computation costs and detect images faster than before. RPN uses a feature map as input, which is generated by the network. It slides a 3X3 sliding window over that map with the help of K anchor boxes. Besides, it performs this operation for each window. One gets an anchor box every time after each of the training phase finishes. Anchor box helps to improve the output of the detection and reduces cost. As for the training phase, one may consider the sliding window with a different scale and aspect ratio. In this case, anchor boxes help a lot, as it is scale and translation invariant.

After that, one will calculate loss using the loss function. There are also two kinds of loss functions here. One is Classification Loss, and the other is Regression Loss. To train the RPN, randomly 256 anchors will be selected and considered as a mini-batch. Then, the loss function will be computed using this.

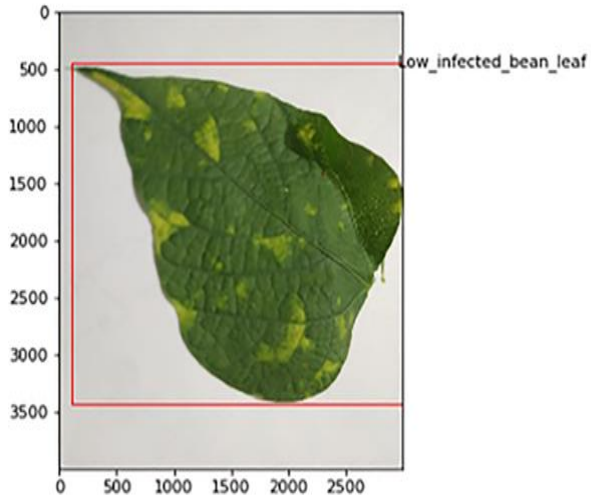

Fig. 3 The labeled image of the low infected leaf of bean

Fig. 3 indicates the labeled image of the low infected leaf of the bean.

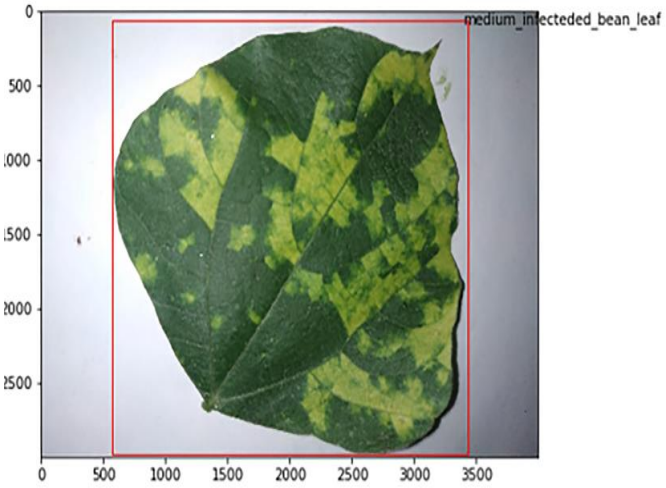

Fig. 4 The labeled image of the medium infected leaf of bean

Fig. 4 indicates the labeled image of the medium infected leaf of the bean.

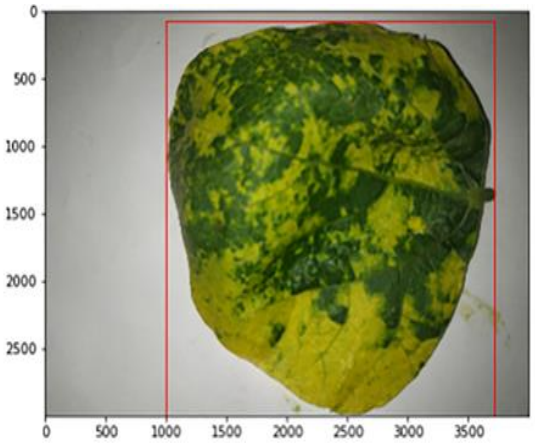

Fig. 5 The labeled image of the highly infected leaf of bean

Fig. 5 represents the labeled image of the highly infected leaf of bean

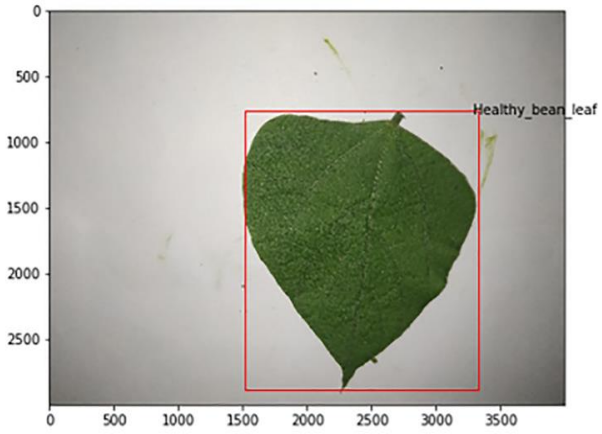

Fig. 6 The labeled image of the fully infected leaf of bean

Fig. 6 depicts the labeled image of a fully infected leaf of the bean.

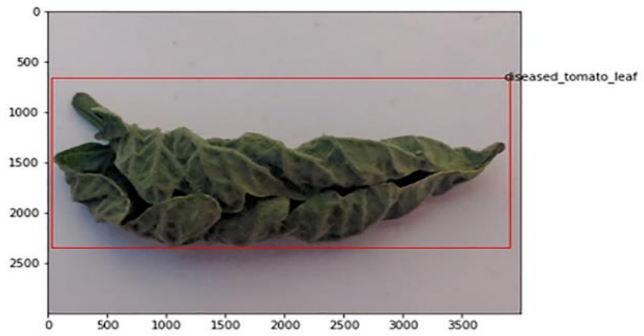

Fig. 7 The labeled image of the healthy leaf of bean

Fig. 7 represents the labeled image of the healthy leaf of bean

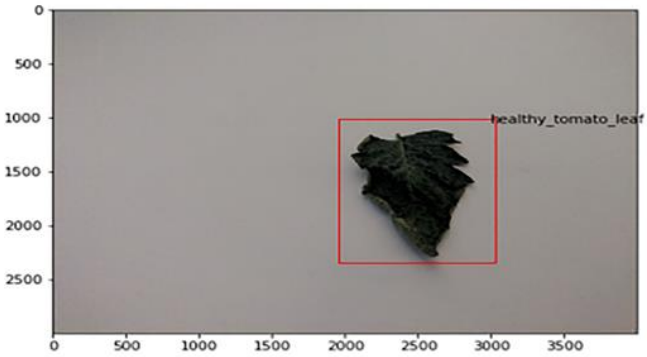

Fig. 8 The labeled image of the infected leaf of Tomato

Fig. 8 shows the labeled image of the infected leaf of Tomato

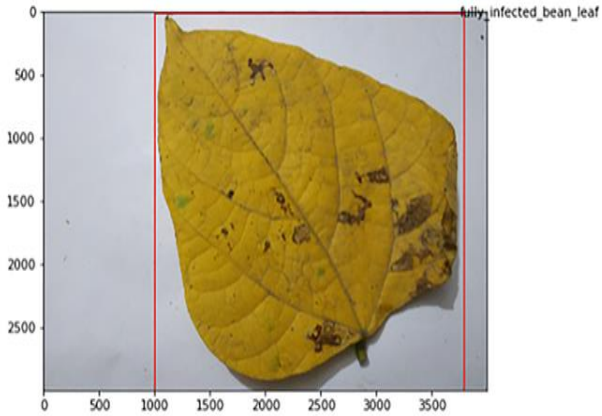

Fig. 9 The labeled image of the healthy leaf of the Tomato

Fig. 9 indicates the labeled image of a healthy leaf of Tomato.

4.2.4 Modified Convolutional Neural Network (ModCNN)

This model is a sequential model that consists of a few layers. The architecture of this model is shown in Fig. 10. In this model, at first, there are two convolution layers with the size of (32, 3X3). Then comes the max-pooling layer with size (2X2). Again, comes two convolution layers with the size of (64, 3X3). Then, a max-pooing layer with size (2X2). Now comes one convolution layer with the size of (128, 3X3). Again, comes a max-pooling layer with size (2X2). At this stage, there will come a flattened layer. In the final stage, there will be two fully connected layers with a SoftMax activation function. This model will be implemented to process the images and detecting them accurately.

There are various optimizers, but the authors have used Adam optimizer, which manipulates the learning rate by changing momentum. For loss function, binary cross-entropy has been used, which generates multiple classes' loss function. The learning rate is 0.05, and after the learning rate, the batch size was 32. In the study, the researchers have used 25 epochs. Though different numbers of epochs have been used through the research, at last, 25 epochs have succeeded in achieving the highest accuracy in both the training & testing phase, which are respectively 98.52% and 97.69%.

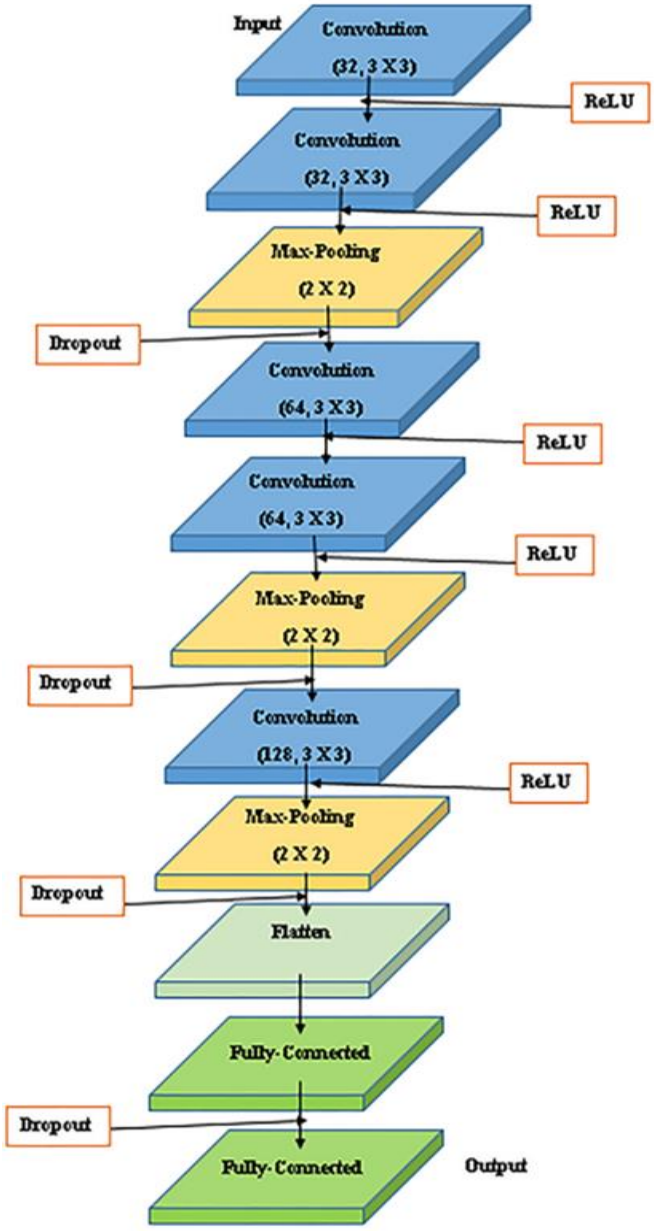

Fig. 10 The architecture model of the proposed ModCNN algorithm

4.3 Environmental setup

The authors have conducted this research using Anaconda Navigator (Jupyter Notebook) version 3.2 and have used python as a programming language. The laptop used to conduct this research and compile codes has 8 GB Ram, 4 GB Graphics, 256

GB SSD, and the Intel is CORE i5. In the backend, h5py, Keras 2.0.3, NumPy, OpenCV-python, and sklearn have been used.

4.4 Dataset and disease description

In this research, two plant leaves have been used, and they are bean and Tomato. The images of leaves have been collected from Sher-E-Bangla Agricultural University under the supervision of Dr. Md. Belal Hossain, Professor, Department of Plant Pathology (Faculty of Agriculture). While collecting the images, white background has been used. There are a total of 1043 images of bean and tomato leaves. In the case of beans, there are 596 images where 213 images are healthy leaves, and 383 images are diseased leaves (71 images of low infected, 76 images of medium infected, 187 images of highly infected, and 49 images of fully infected). In the case of Tomato, there are a total of 447 images where there are 302 healthy images of leaves and 145 diseased images. The Tomato has 'Leaf Curl disease,' and the bean has 'Mosaic Virus.' But, while evaluating, the tomato leaf will only show whether it's diseased or healthy, but the bean leaf will show four stages when it's diseased (low, medium, high, and fully infected).

In this study, the researchers have worked with two diseases; one is tomato curl leaf, and the other is the bean mosaic virus disease. In tomato leaf curl disease, the leaf becomes curl due to the leaf curl virus's effect. In this case, the plant grows severely unbalanced, the size of the leaf decreases, excision in flowers, and so on. An insect named Aphid works as a carrier of this virus. On the other side, for bean leaf, when the mosaic virus occurs, the leaf shows some light green spots. The more virus affects the leaves, and the spots become bigger. In this case, the whitefly insect is the carrier of the mosaic virus.

At a temperature of 25 -35 degrees, Celsius is suitable for both carriers to outspread the Tomato and Bean leaves' virus. If the insect is reduced from the plant, the outspread of the virus will also decrease. For that reason, at that temperature, the plants must be watered, and pesticides must be used. The virus-affected leaf should be removed from the plant to protect the other leaves from the virus. If the temperature is <25%, the leaf is affected by the virus, and then the plant can be saved by removing the affected leaves. However, if it goes more than 40%, the plant has to be cut down to protect other plants near it from the virus. In this study, the authors have built a modified CNN model that gives 97.69% testing accuracy in predicting Tomato and bean leaf diseases. The researchers have also collected temperature-related data of the Dhaka division from the previous years, which also shows the average temperature of each month. The model will take input of an image of either Tomato or bean leaf that will predict if it is diseased or not. If the leaf is diseased, then the model will take the month from the system automatically. It will check the temperature-related data of that month for that year, and if the temperature is higher than 35-degree coleus at that time, the model will suggest watering the plants and using insecticide. If the situation becomes more dangerous or gets out of hand, the user will be advised to visit any specialist for further treatments.

5 Results and Discussions

5.1 Comparison of Performances

There will be a comparison of detailed analysis among this study with some of the other authors' studies related to plant disease detection using various deep learning models.

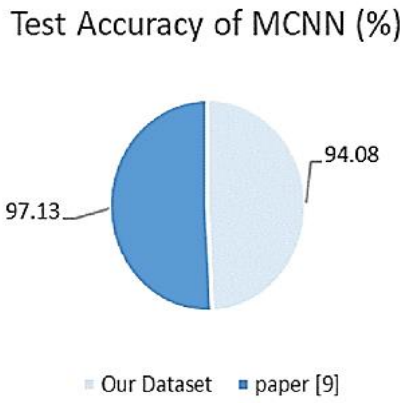

Fig. 11 Test accuracy of MCNN (%) between this study & paper [9]|

Comparison based on test accuracy in the MCNN algorithm between this study and paper [9]| has been represented in Fig. 11. This study has achieved 94.08% test accuracy white paper [9]| has scored 97.13%. In this case, paper [9]| has provided better performance than this study.

Comparison based on test accuracy in the FRCNN algorithm between this study and paper [10] has been indicated in Fig. 12. This study has achieved 60% test accuracy while paper [10] has scored 98.26%. In this case, paper [10] has provided better performance than this study.

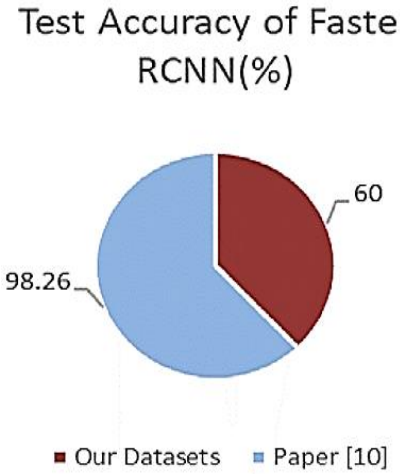

Fig. 12 Test accuracy of FRCNN (%) between this study & paper [10]

Comparison based on test accuracy in the case of CNN, MCNN, FRCNN, and Modified CNN algorithm among this paper and the other papers from the related work has been represented in Fig. 13. This paper has achieved 97.69% test accuracy using the proposed modified CNN, while paper [3] has scored 99.75%. In this case, both of the papers have shown promising performances as both of them have used different types of algorithms and have still managed to score more than 95%.

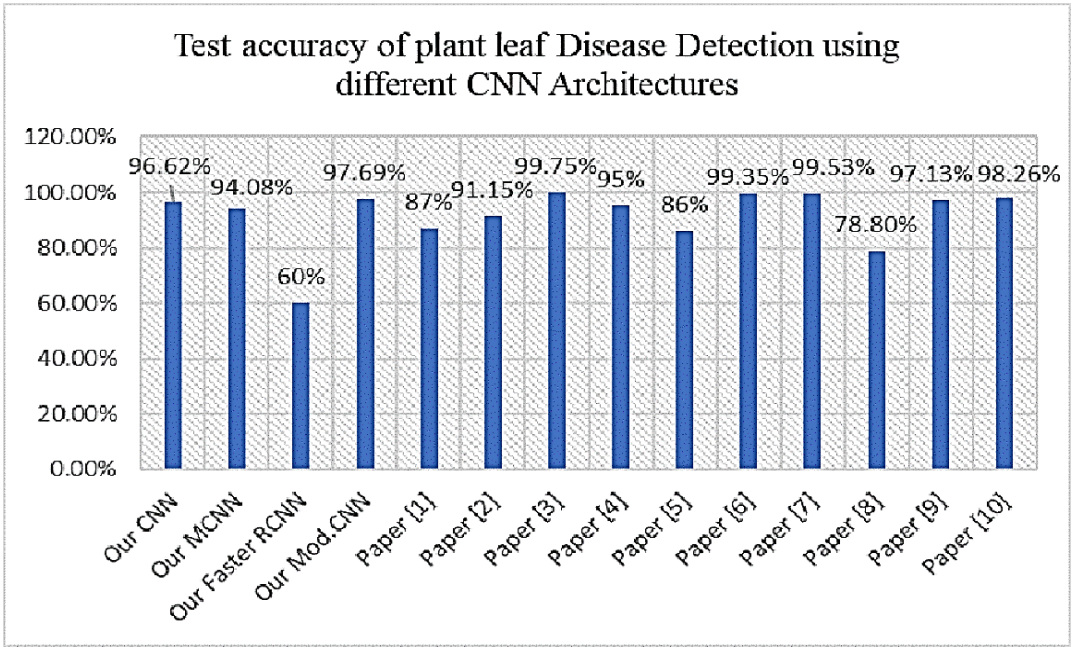

Fig. 13 Test accuracy of plant leaf disease detection using different CNN architectures

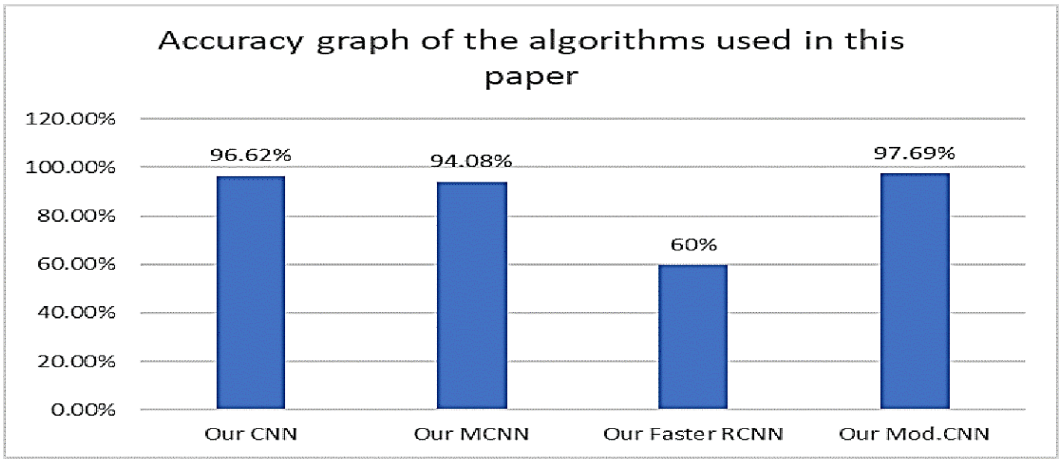

Fig. 14 Accuracy graph of the algorithms used in this study

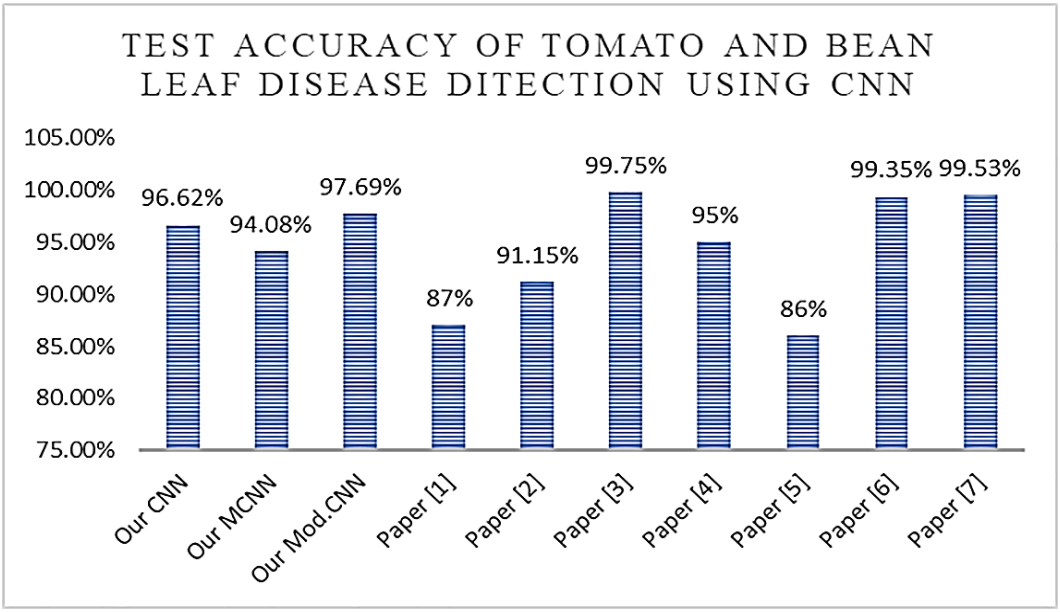

Fig. 15 Test accuracy of tomato and bean leaf disease detection using CNN

Table 1 Comparison table of used methods along with the test accuracy of related works

References	Used methods	Datasets	Test Accuracy (%)
[1]	CNN	Corn Leaf	87
[2]	TCCNN	Tomato leaf	91.15
[3]	CNN	14 different plant leaves from Plant village	99.75
[4]	CNN	Plant village datasets	95
[5]	CNN with LVQ	Tomato leaf	86
[6]	CNN	14 different corps from plant village	99.35
[7]	CNN	25 different plants	99.53
[8]	CNN	Apple leaf	78.8
[9]	MCNN	Mango leaf	97.13
[10]	Faster RCNN	Rice leaf	98.26

Comparison based on the test accuracy of tomato and bean leaf disease detection using different types of CNN among this paper and the other papers from the related work has been shown in Fig. 15. This paper has achieved 97.69% test accuracy using the proposed modified CNN, while paper [3] has scored 99.75%. In this case, both of the papers have shown outstanding performances as both of them have used different types of CNN and have still managed to score more than 95%.

The comparison based on some other papers from the related works has been indicated in

Table 1. The factors which are considered here are used methods, datasets, and test accuracy in percentage. From

Table 1, it is clear that paper [3] has scored the highest test accuracy. It has used 14 different plant leaves from the plant village and achieved 99.75% accuracy by implementing CNN.

Table 2 indicates that the proposed ModCNN model provides the highest accuracy in both training & testing phases among the models used for the dataset.

Table 2 Comparison table of accuracy based on the used methods to detect tomato & bean leaf diseases

Accuracy		
	Train Accuracy	**Test Accuracy**
CNN	98.21 %	96.62%
MCNN	98.51%	94.08%
ModCNN	98.52%	97.69%
Faster RCNN	66%	60%

6 Conclusion and Future Work

6.1 Limitations

Now, at this point, different types of questions can arise, such as why the accuracy is lower. Well, due to some limitations, the authors have encountered this type of situation.

While collecting data, the authors have faced image pre-processing steps due to image capture conditions as all of the images have been collected directly from the field, then sent to the pre-processing stage. In the pre-processing stage, some of the images were almost similar. Therefore, it was complicated to differentiate them to assign them to a particular class label. But it will not be an issue for the farmers who will use this model. The researchers have faced these kinds of problems for training the model, but in the farmer's case, they don't have to give an accurate image of their plant as the researchers did. They can provide raw data from the field, and the model which have been implemented and trained by the researchers will predict the disease accurately. The farmers don't have to train the model and go through the testing phase like the researchers, so at the user end, they will not face these kinds of problems in the future.

From the result of the algorithms used in our study, Mod-CNN has provided the highest accuracy result though there is a limitation of collecting lots of data. For the other algorithms, such as FRCNN, which has produced the lowest test accuracy result. Nevertheless, it has been found that if there is a low amount of data, then FRCNN is not preferable for creating those models. If some developers or researchers want to expand this study, it will be better to get more data to increase the accuracy result for FRCNN. But for Mod-CNN, they can use our model and work with other crops and vegetables.

However, after facing all these issues, the authors have tried hard and achieved 97.69% accuracy and intend to increase accuracy in the future.

6.2 Future Work

This study's future work is to develop a user interface on android using a cloud-based storage system and apply other algorithms to improve the performances. This will add a new dimension and open another way in the agricultural arena to improve the system by including more interactive features. Twenty-four hours of the monitoring system for the plants through live video recording and live monitoring systems can be developed to notify the user via the internet system if there are any slight chances of infection in the leaf. In this way, the user can take any required action instantly.

6.3 Conclusions

The proposed system for detecting plant disease will improve the agricultural system's development, which will accurately predict whether a plant is infected or not. If not, it will be notified, but if affected, then the treatment plan will also be provided to help the user save the plant as soon as possible. This system allows the user to diagnose diseases earlier to take reasonable preventive measures beforehand and save plants. This is a time-effective approach as the users can easily do it within a short amount of time without visiting anywhere. It is cost-effective, as it does not require any money to diagnose the disease. This system shows a better and promising future in the agricultural arena, and people need this system to save the plants from leading a happy, healthy, and comfortable life.

7 References

[1] Barbedo, J.G., 2018. Factors influencing the use of deep learning for plant disease recognition. *Biosystems engineering*, 172, pp.84-91.

[2] Zhang, S., Huang, W. and Zhang, C., 2019. Three-channel convolutional neural networks for vegetable leaf disease recognition. *Cognitive Systems Research*, *53*, pp.31-41.

[3] Too, E.C., Yujian, L., Njuki, S. and Yingchun, L., 2019. A comparative study of fine-tuning deep learning models for plant disease identification. *Computers and Electronics in Agriculture*, *161*, pp.272-279.

[4] Singh, K.K., 2018, November. An artificial intelligence and cloud based collaborative platform for plant disease identification, tracking and forecasting for farmers. In *2018 IEEE International Conference on Cloud Computing in Emerging Markets (CCEM)* (pp. 49-56). IEEE.

[5] Sardogan, M., Tuncer, A. and Ozen, Y., 2018, September. Plant leaf disease detection and classification based on CNN with LVQ algorithm. In *2018 3rd International Conference on Computer Science and Engineering (UBMK)* (pp. 382-385). IEEE.

[6] Mohanty, S.P., Hughes, D.P. and Salathé, M., 2016. Using deep learning for image-based plant disease detection. *Frontiers in plant science*, *7*, p.1419.

[7] Dalakouras, A., Wassenegger, M., Dadami, E., Ganopoulos, I., Pappas, M.L. and Papadopoulou, K., 2020. Genetically modified organism-free RNA interference: exogenous application of RNA molecules in plants. *Plant physiology*, *182*(1), pp.38-50.

[8] Jiang, P., Chen, Y., Liu, B., He, D. and Liang, C., 2019. Real-time detection of apple leaf diseases using deep learning approach based on improved convolutional neural networks. *IEEE Access*, *7*, pp.59069-59080.

[9] Singh, U.P., Chouhan, S.S., Jain, S. and Jain, S., 2019. Multilayer convolution neural network for the classification of mango leaves infected by anthracnose disease. *IEEE Access*, *7*, pp.43721-43729.

[10] Zhou, G., Zhang, W., Chen, A., He, M. and Ma, X., 2019. Rapid detection of rice disease based on FCM-KM and faster R-CNN fusion. *IEEE Access*, *7*, pp.143190-143206.

[11] Bhuiyan, M., Rahman, A., Ullah, M. and Das, A.K., 2019. iHealthcare: Predictive model analysis concerning big data applications for interactive healthcare systems. *Applied Sciences*, *9*(16), p.3365.

[12] Cynthia, S.T., Hossain, K.M.S., Hasan, M.N., Asaduzzaman, M. and Das, A.K., 2019, December. Automated detection of plant diseases using image processing and faster R-CNN algorithm. In *2019 International Conference on Sustainable Technologies for Industry 4.0 (STI)* (pp. 1-5). IEEE.

[13] Paul, S., Joy, J.I., Sarker, S., Ahmed, S. and Das, A.K., 2019, December. An Unorthodox Way of Farming Without Intermediaries Through Blockchain. In *2019 International Conference on Sustainable Technologies for Industry 4.0 (STI)* (pp. 1-6). IEEE.

[14] Islam, S., Khan, S.I.A., Abedin, M.M., Habibullah, K.M. and Das, A.K., 2019, July. Bird species classification from an image using vgg-16 network. In *Proceedings of the 2019 7th International Conference on Computer and Communications Management* (pp. 38-42).

[15] Kaur, S., Pandey, S. and Goel, S., 2018. Semi-automatic leaf disease detection and classification system for soybean culture. *IET Image Processing*, *12*(6), pp.1038-1048.

SciEn
Journal of Engineering Advancements Vol. 02(01) 2021, pp 58-63 https://doi.org/10.38032/jea.2021.01.008

Explicit Travelling Wave Solutions to Nonlinear Partial Differential Equations Arise in Mathematical Physics and Engineering

Muktarebatul Jannah, Md. Tarikul Islam, Mst. Armina Akter*

Department of Mathematics, Hajee Mohammad Danesh Science and Technology University, Dinajpur, Bangladesh

Received: January 23, 2021, Revised: March 11, 2021, Accepted: March 13, 2021, Available Online: March 30, 2021

ABSTRACT

To describe the interior phenomena of the mysterious problems around the real world, non-linear partial differential equations (NLPDEs) plays a substantial role, for which construction of analytic solutions of those is most important. This paper stands for a goal to find fresh and wide-ranging solutions to some familiar NLPDEs namely the non-linear cubic Klein-Gordon (cKG) equation and the non-linear Benjamin-Ono (BO) equation. A wave variable transformation is made use to convert the mentioned equations into ordinary differential equations. To acquire the desired precise exact travelling wave solutions to the above-stated equations, the rational (G'/G)-expansion method is employed. Consequently, three types of equipped solutions are successfully come out in the forms of hyperbolic, trigonometric and rational functions in a compatible way. To analyse the physical problems arisen relating to nonlinear complex dynamical systems, our obtained solutions might be most helpful. So far we know, these achieved solutions are different than those in the literature. The applied method is efficient and reliable which might further be used to find different and novel solutions to many other NLPDEs successfully in research field.

Keywords: The rational (G'/G)-expansion method, nonlinear partial differential equation, complex transformation, exact solution.

1 Introduction

In this new era, nonlinear phenomena have arisen in a wide range in the area of extensive physical science and mathematics. The nonlinear mechanism of nature can be depicted by NLPDEs. For this reason, with the rapid development of nonlinear sciences, it has debuted with a lot of importance in physical science and mathematics and many research works have been done to analyse these equations. A special case, the closed form solutions of NLPDEs bears significant role to delineate many models concerning the underlying mechanisms of real world. Subsequently, research on this topic is becoming as a matter of attraction in the field of nonlinear science day by day. With this importance, for the analytical solutions of NLPDEs, many traditional techniques have been emerged and implemented to solve various kinds of problems such as the Adomian decomposition method [1]-[2], the tanh function method [3]-[4], the simplest equation method [5]-[6], the Jacobi elliptic function method [7]-[8], the expansion function method [9]-[10], the modified simple equation method [11]-[12], the (G'/G)-expansion method [13]-[14], the cosh function method [15]-[16], the homotopy perturbation method [17]-[18], the multiple exp-function method [19]-[20], the Bernoulli sub-ODE method [21]-[22], the homotopy analysis method [23]-[24], the variational iteration method [25]-[26], the modified tanh-coth method and the extended Jacobi elliptic function method [27], the He homotopy perturbation method [28]-[29], the homogeneous balance method [30], the inverse scattering method [31], the Backlund transformation method [32]-[33], the extended modified direct algebraic method [34]-[37]. In this paper, we have described the rational (G'/G)-expansion method [38]-[41].

2 Explanation of the Technique

Consider the following NLPDE:

$$F(u, u_x, u_t, u_{xx}, u_{tt}, u_{tx} \cdots) = 0 \quad (1)$$

where $u = u(x,t)$ and the subscripts in u represents partial derivatives. Followings are the main steps of the rational (G'/G)-expansion method:

First step: Introduce the transformation

$$u(x,t) = U(\xi), \xi = x \pm vt \quad (2)$$

where v stands for the wave velocity. This transformation reduces Eq. (1) to the ordinary differential equation with respect to ξ,

$$Q(U, U', U'', U''', \cdots) = 0 \quad (3)$$

Second step: Take anti-derivative of Eq. (3) as much as possible; the integral constant may be considered as zero for seeking solitary wave solutions.

Third step: Consider the solution of Eq. (3) as follows:

$$U(\xi) = \frac{\sum_{i=0}^{n} a_i (G'/G)^i}{\sum_{i=0}^{n} b_i (G'/G)^i} \quad (4)$$

with unknown constants a_i and $b_i (i = 0,1,2, \cdots, n)$ in which at least one of a_n and b_n is non-zero. $G = G(\xi)$ satisfies the ordinary differential equation,

$$G''(\xi) + \lambda G'(\xi) + \mu G(\xi) = 0 \quad (5)$$

where λ and μ are real parameters. Eq. (5) has turned into

$$\frac{d}{d\xi}(G'/G) = -(G'/G)^2 - \lambda (G'/G) - \mu \quad (6)$$

Then we have the general solutions of Eq. (5) (or equivalent to Eq. (6)) as follows:

*Corresponding Author Email Address: tarikul_hstu@yahoo.com Published by: SciEn Publishing Group

$$(G'/G) = -\frac{\lambda}{2} + \frac{\sqrt{\lambda^2-4\mu}}{2}\left(\frac{Asinh\left(\left(\sqrt{\lambda^2-4\mu}/2\right)\xi\right)+Bcosh\left(\left(\sqrt{\lambda^2-4\mu}/2\right)\xi\right)}{Acosh\left(\left(\sqrt{\lambda^2-4\mu}/2\right)\xi\right)+Bsinh\left(\left(\sqrt{\lambda^2-4\mu}/2\right)\xi\right)}\right), \quad \lambda^2 - 4\mu > 0 \tag{7}$$

$$(G'/G) = -\frac{\lambda}{2} + \frac{\sqrt{4\mu-\lambda^2}}{2}\left(\frac{-Asin\left(\left(\sqrt{4\mu-\lambda^2}/2\right)\xi\right)+Bcos\left(\left(\sqrt{4\mu-\lambda^2}/2\right)\xi\right)}{Acos\left(\left(\sqrt{4\mu-\lambda^2}/2\right)\xi\right)+Bsin\left(\left(\sqrt{4\mu-\lambda^2}/2\right)\xi\right)}\right), \quad \lambda^2 - 4\mu < 0 \tag{8}$$

$$(G'/G) = -\frac{\lambda}{2} + \frac{B}{A+B\xi}, \quad \lambda^2 - 4\mu = 0 \tag{9}$$

where A and B are real parameters.
Fourth step: Determine n by applying homogeneous balance to Eq. (3) for the degree of $U(\xi)$ as n. Then

$$deg\left[\frac{d^nU(\xi)}{d\xi^m}\right] = n + m, \quad deg\left[U^m\left(\frac{d^lU(\xi)}{d\xi^l}\right)^p\right] = mn + p(n + l).$$

Fifth step: Eq. (3) with Eqs. (4), (5) makes a polynomial (G'/G). Set each coefficient to zero and solve them by the computer software Maple to calculate the values of a_i, b_i, μ and v.
Sixth step: Inserting the values determined in fifth step along with the outcomes given in Eqs. (7)-(9) into solution Eq. (4) provides the solutions of Eq. (1).

3 Implementation of the Technique

Herein, the suggested scheme is applied to examine the exact analytic solutions to the considered equations.

3.1 The cKG equation

The cKG equation is

$$u_{xx} + u_{yy} - u_{tt} + au + bu^3 = 0 \tag{10}$$

The wave variable transformation $u(x, y, t) = U(\xi), \xi = x + y - ct$ reduces Eq. (10) into the following equation:

$$(2 - c^2)U'' + aU + bU^3 = 0 \tag{11}$$

Due to homogeneous balance method, Eq. (11) gives $n = 1$ and Eq. (4) turns into the form

$$U(\xi) = \frac{a_0+a_1(G'/G)}{b_0+b_1(G'/G)} \tag{12}$$

Inserting Eq. (12) into Eq. (11) provides a polynomial in (G'/G). Set the coefficients to zero and solved by computational software Maple. Accordingly, the following outcomes for a_0, a_1, b_0, b_1 and c are obtained:
Set-1:

$$a_0 = \pm\frac{b_1}{2}\sqrt{\frac{a(-\lambda^2+4\mu)}{b}}, \quad a_1 = 0, \quad b_0 = \frac{b_1\lambda}{2}, \quad c = \pm\sqrt{\frac{2(a+4\mu-\lambda^2)}{-\lambda^2+4\mu}} \tag{13}$$

Set-2:

$$a_0 = \mp(2b_1\mu - \lambda b_0)\sqrt{\frac{a}{b(-\lambda^2+4\mu)}},$$

$$a_1 = \pm(2b_0 - b_1\lambda)\sqrt{\frac{a}{b(-\lambda^2+4\mu)}}, \tag{14}$$

$$c = \pm\sqrt{\frac{2(a+4\mu-\lambda^2)}{(-\lambda^2+4\mu)}}$$

Set-3:

$$a_0 = \frac{b_1\left(-2\mu+\lambda\left(\frac{\lambda}{2}\pm\frac{1}{6}\sqrt{-12\mu+3\lambda^2}\right)\right)\sqrt{-3ab}}{b\sqrt{-12\mu+3\lambda^2}},$$

$$a_1 = \pm\frac{\sqrt{-3ab}}{3b}b_1, \tag{15}$$

$$b_0 = \left(\frac{\lambda}{2}\pm\frac{1}{6}\sqrt{-12\mu+3\lambda^2}\right)b_1,$$

$$c = \pm\sqrt{\frac{2(a+4\mu-\lambda^2)}{(-\lambda^2+4\mu)}}$$

Set-4:

$$a_0 = -\frac{b_1\left(-2\mu+\lambda\left(\frac{\lambda}{2}\pm\frac{1}{6}\sqrt{-12\mu+3\lambda^2}\right)\right)\sqrt{-3ab}}{b\sqrt{-12\mu+3\lambda^2}},$$

$$a_1 = \pm\frac{\sqrt{-3ab}}{3b}b_1, \tag{16}$$

$$b_0 = \left(\frac{\lambda}{2}\pm\frac{1}{6}\sqrt{-12\mu+3\lambda^2}\right)b_1,$$

$$c = \pm\sqrt{\frac{2(a+4\mu-\lambda^2)}{(-\lambda^2+4\mu)}}$$

Eq. (12) along with Eq. (13) becomes

$$U_1(\xi) = \sqrt{\frac{a}{b}}\frac{\sqrt{-\lambda^2+4\mu}}{\lambda+2(G'/G)}, \tag{17}$$

Where,

$$\xi = x + y \mp \sqrt{\frac{2(a+4\mu-\lambda^2)}{-\lambda^2+4\mu}}t.$$

Utilizing the solutions in Eqs. (7)-(9) from Eq. (17), we make available the following solutions to Eq. (10) in the following three different forms:
Case 1: When $\lambda^2 - 4\mu > 0$,
Eq. (12) along with Eq. (13) becomes

$$U_{1_1}(\xi) = i\sqrt{\frac{a}{b}}\frac{Acosh\left(\left(\sqrt{\lambda^2-4\mu}/2\right)\xi\right)+Bsinh\left(\left(\sqrt{\lambda^2-4\mu}/2\right)\xi\right)}{Asinh\left(\left(\sqrt{\lambda^2-4\mu}/2\right)\xi\right)+Bcosh\left(\left(\sqrt{\lambda^2-4\mu}/2\right)\xi\right)} \tag{18}$$

where,

$$\xi = x + y \mp \sqrt{\frac{2(a+4\mu-\lambda^2)}{-\lambda^2+4\mu}}t$$

For $A = 0$ and $B \neq 0$, we get

$$U_{1_2}(\xi) = i\sqrt{\frac{a}{b}}\, tanh\left(\left(\sqrt{\lambda^2 - 4\mu}/2\right)\xi\right) \tag{19}$$

Assigning $A \neq 0$ and $B = 0$ yields

$$U_{1_3}(\xi) = i\sqrt{\frac{a}{b}}\, coth\left(\left(\sqrt{\lambda^2 - 4\mu}/2\right)\xi\right) \tag{20}$$

Case 2: For $\lambda^2 - 4\mu < 0$,

$$U_{1_4}(\xi) = \sqrt{\frac{a}{b}}\frac{Acos\left(\left(\sqrt{4\mu-\lambda^2}/2\right)\xi\right) + Bsin\left(\left(\sqrt{4\mu-\lambda^2}/2\right)\xi\right)}{-Asin\left(\left(\sqrt{4\mu-\lambda^2}/2\right)\xi\right) + Bcos\left(\left(\sqrt{4\mu-\lambda^2}/2\right)\xi\right)} \tag{21}$$

where,

$$\xi = x + y \mp \sqrt{\frac{2(a+4\mu-\lambda^2)}{-\lambda^2+4\mu}}t.$$

Appling $A = 0$ and $B \neq 0$, provides

$$U_{1_5}(\xi) = \sqrt{\frac{a}{b}}\, tan\left(\left(\sqrt{4\mu-\lambda^2}/2\right)\xi\right) \tag{22}$$

Using $A \neq 0$ and $B = 0$ gives

$$U_{1_6}(\xi) = -\sqrt{\frac{a}{b}}\, \cot\left(\left(\sqrt{4\mu-\lambda^2}/2\right)\xi\right) \tag{23}$$

Case 3: If $\lambda^2 - 4\mu = 0$, the method yields stationary wave solutions and thus have not been documented.

Using the similar procedure for the all-other sets of solutions, as we have applied for set-1, we obtain the hyperbolic solutions for $\lambda^2 - 4\mu > 0$, the trigonometric solutions for $\lambda^2 - 4\mu < 0$, and $\lambda^2 - 4\mu = 0$ gives the stationary wave solutions.

3.2 The BO equation

Consider the BO equation

$$u_t + hu_{xx} + uu_x = 0 \tag{24}$$

Using the transformation $u(x,t) = U(\xi)$, $\xi = x - ct$, Eq. (24) reduces to the ODE

$$-cU' + hU'' + UU' = 0 \tag{25}$$

Integrating Eq. (25) gives

$$r - cU + hU' + \frac{1}{2}U^2 = 0, \tag{26}$$

where r is the integral constant. Appling homogeneous balance to U^2 and U' produces $n = 1$ for which the solution (4) becomes

$$U(\xi) = \frac{a_0 + a_1(G'/G)}{b_0 + b_1(G'/G)} \tag{27}$$

where at least one of a_1 or b_1 is non zero.

Inserting Eq. (27) into Eq. (26) makes a polynomial in (G'/G). Setting the coefficients to zero and calculating by computer software Maple provides the following values for a_0, a_1, b_0, b_1 and c:

$$\begin{aligned} a_0 &= \frac{b_1}{2h}\left\{(c + h\lambda)\left(c \pm \sqrt{c^2 - 2r}\right) - 2r\right\}, \\ a_1 &= b_1\left(c \pm \sqrt{c^2 - 2r}\right), \\ b_0 &= \frac{b_1}{2h}\left(h\lambda \pm \sqrt{c^2 - 2r}\right), \end{aligned} \tag{28}$$

Eq. (27) together with the values in Eq. (28) reduces to

$$U(\xi) = \frac{\left\{(c + h\lambda)\left(c \pm \sqrt{c^2 - 2r}\right) - 2r\right\} + 2h\left(c \pm \sqrt{c^2 - 2r}\right)(G'/G)}{\left(h\lambda \pm \sqrt{c^2 - 2r}\right) + 2h(G'/G)} \tag{29}$$

where $\xi = x - ct$.

Eq. (29) with the aid of Eqs. (7)-(9) serves the following exact solutions to Eq. (24) in three types as hyperbolic, trigonometric and rational:

Case 1: If $\lambda^2 - 4\mu > 0$,

$$U_1(\xi) = \frac{\left\{(c + h\lambda)\left(c \pm \sqrt{c^2 - 2r}\right) - 2r\right\} + 2h\left(c \pm \sqrt{c^2 - 2r}\right)\left(-\frac{\lambda}{2} + \frac{\sqrt{\lambda^2 - 4\mu}}{2} \times \frac{Asinh\left(\left(\sqrt{\lambda^2 - 4\mu}/2\right)\xi\right) + Bcosh\left(\left(\sqrt{\lambda^2 - 4\mu}/2\right)\xi\right)}{Acosh\left(\left(\sqrt{\lambda^2 - 4\mu}/2\right)\xi\right) + Bsinh\left(\left(\sqrt{\lambda^2 - 4\mu}/2\right)\xi\right)}\right)}{\left(h\lambda \pm \sqrt{c^2 - 2r}\right) + 2h\left(-\frac{\lambda}{2} + \frac{\sqrt{\lambda^2 - 4\mu}}{2} \times \frac{Asinh\left(\left(\sqrt{\lambda^2 - 4\mu}/2\right)\xi\right) + Bcosh\left(\left(\sqrt{\lambda^2 - 4\mu}/2\right)\xi\right)}{Acosh\left(\left(\sqrt{\lambda^2 - 4\mu}/2\right)\xi\right) + Bsinh\left(\left(\sqrt{\lambda^2 - 4\mu}/2\right)\xi\right)}\right)} \tag{30}$$

where $\xi = x - ct$.

If $A = 0$, $B \neq 0$, then

$$U_{1_1}(\xi) = \frac{\left\{(c + h\lambda)\left(c \pm \sqrt{c^2 - 2r}\right) - 2r\right\} + 2h\left(c \pm \sqrt{c^2 - 2r}\right)\left(-\frac{\lambda}{2} + \frac{\sqrt{\lambda^2 - 4\mu}}{2} \times coth\left(\left(\sqrt{\lambda^2 - 4\mu}/2\right)\xi\right)\right)}{\left(h\lambda \pm \sqrt{c^2 - 2r}\right) + 2h\left(-\frac{\lambda}{2} + \frac{\sqrt{\lambda^2 - 4\mu}}{2} \times coth\left(\left(\sqrt{\lambda^2 - 4\mu}/2\right)\xi\right)\right)} \tag{31}$$

Again, for $A \neq 0$, $B = 0$,

$$U_{1_2}(\xi) = \frac{\left\{(c + h\lambda)\left(c \pm \sqrt{c^2 - 2r}\right) - 2r\right\} + 2h\left(c \pm \sqrt{c^2 - 2r}\right)\left(-\frac{\lambda}{2} + \frac{\sqrt{\lambda^2 - 4\mu}}{2} \times tanh\left(\left(\sqrt{\lambda^2 - 4\mu}/2\right)\xi\right)\right)}{\left(h\lambda \pm \sqrt{c^2 - 2r}\right) + 2h\left(-\frac{\lambda}{2} + \frac{\sqrt{\lambda^2 - 4\mu}}{2} \times tanh\left(\left(\sqrt{\lambda^2 - 4\mu}/2\right)\xi\right)\right)} \tag{32}$$

Case 2: For $\lambda^2 - 4\mu < 0$,

$$U_2(\xi) = \frac{\left\{(c + h\lambda)\left(c \pm \sqrt{c^2 - 2r}\right) - 2r\right\} + 2h\left(c \pm \sqrt{c^2 - 2r}\right)\left(-\frac{\lambda}{2} + \frac{\sqrt{4\mu - \lambda^2}}{2} \times \frac{-Asin\left(\left(\sqrt{4\mu - \lambda^2}/2\right)\xi\right) + Bcos\left(\left(\sqrt{4\mu - \lambda^2}/2\right)\xi\right)}{Acos\left(\left(\sqrt{4\mu - \lambda^2}/2\right)\xi\right) + Bsin\left(\left(\sqrt{4\mu - \lambda^2}/2\right)\xi\right)}\right)}{\left(h\lambda \pm \sqrt{c^2 - 2r}\right) + 2h\left(-\frac{\lambda}{2} + \frac{\sqrt{4\mu - \lambda^2}}{2} \times \frac{-Asin\left(\left(\sqrt{4\mu - \lambda^2}/2\right)\xi\right) + Bcos\left(\left(\sqrt{4\mu - \lambda^2}/2\right)\xi\right)}{Acos\left(\left(\sqrt{4\mu - \lambda^2}/2\right)\xi\right) + Bsin\left(\left(\sqrt{4\mu - \lambda^2}/2\right)\xi\right)}\right)} \tag{33}$$

where $\xi = x - ct$.

Assign $A = 0$, $B \neq 0$, then

$$U_{2_1}(\xi) = \frac{\left\{(c + h\lambda)\left(c \pm \sqrt{c^2 - 2r}\right) - 2r\right\} + 2h\left(c \pm \sqrt{c^2 - 2r}\right)\left(-\frac{\lambda}{2} + \frac{\sqrt{4\mu - \lambda^2}}{2} \times cot\left(\left(\sqrt{4\mu - \lambda^2}/2\right)\xi\right)\right)}{\left(h\lambda \pm \sqrt{c^2 - 2r}\right) + 2h\left(-\frac{\lambda}{2} + \frac{\sqrt{4\mu - \lambda^2}}{2} \times cot\left(\left(\sqrt{4\mu - \lambda^2}/2\right)\xi\right)\right)} \tag{34}$$

Fix $A \neq 0$, $B = 0$, then

$$U_{2_2}(\xi) = \frac{\left\{(c + h\lambda)\left(c \pm \sqrt{c^2 - 2r}\right) - 2r\right\} + 2h\left(c \pm \sqrt{c^2 - 2r}\right)\left(-\frac{\lambda}{2} + \frac{\sqrt{4\mu - \lambda^2}}{2} \times \left(-tan\left(\left(\sqrt{4\mu - \lambda^2}/2\right)\xi\right)\right)\right)}{\left(h\lambda \pm \sqrt{c^2 - 2r}\right) + 2h\left(-\frac{\lambda}{2} + \frac{\sqrt{4\mu - \lambda^2}}{2} \times \left(-tan\left(\left(\sqrt{4\mu - \lambda^2}/2\right)\xi\right)\right)\right)} \tag{35}$$

Case 3: When $\lambda^2 - 4\mu = 0$,

$$U_3(\xi) = \frac{\left\{(c + h\lambda)\left(c \pm \sqrt{c^2 - 2r}\right) - 2r\right\} + 2h\left(c \pm \sqrt{c^2 - 2r}\right)\left(-\frac{\lambda}{2} + \frac{B}{A + B\xi}\right)}{\left(h\lambda \pm \sqrt{c^2 - 2r}\right) + 2h\left(-\frac{\lambda}{2} + \frac{B}{A + B\xi}\right)} \tag{36}$$

where $\xi = x - ct$.
Put $A = 0, B \neq 0$,

$$U_{3_1}(\xi) = \frac{\{(c + h\lambda)(c \pm \sqrt{c^2 - 2r}) - 2r\} + 2h(c \pm \sqrt{c^2 - 2r})\left(-\frac{\lambda}{2} + \frac{1}{\xi}\right)}{(h\lambda \pm \sqrt{c^2 - 2r}) + 2h\left(-\frac{\lambda}{2} + \frac{1}{\xi}\right)} \quad (37)$$

Choose $A \neq 0, B = 0$, then

$$U_{3_2}(\xi) = \frac{\{(c + h\lambda)(c \pm \sqrt{c^2 - 2r}) - 2r\} + 2h(c \pm \sqrt{c^2 - 2r})\left(-\frac{\lambda}{2}\right)}{(h\lambda \pm \sqrt{c^2 - 2r}) + 2h\left(-\frac{\lambda}{2}\right)} \quad (38)$$

4 Results, discussion and graphical representations

To analyse the problems clearly and to describe the solutions of the phenomena, a graphical representation of the solutions can be an effective tool to brief the commentaries. On account of this, we provide different types of physical appearances of the solutions bearing the actual form of solitary waves (Fig. 1-Fig. 6). The plots are of kink shape soliton, cuspone, periodic solutions etc. Fig. 1 stands for kink type soliton of solution (17) for $\lambda = 3, \mu = 2, c = 1, a = 1, b = 1, x = 0$ in the interval $-10 \leq y \leq 10$ and $-10 \leq t \leq 10$. Fig. 2 characterizes cuspon which is depicted for solution (17) for $\lambda = 3, \mu = 3, c = -1, a = 1, b = 1, x = 0$ within $-10 \leq y \leq 10$ and $-10 \leq t \leq 10$. Fig. 3 indicates periodic soliton generated from the solution (17) for $\lambda = 3, \mu = 3, c = 1, a = 1, b = 1, x = 0$ in $-10 \leq y \leq 10$ and $-10 \leq t \leq 10$. Fig. 4 indicates cuspon plotted for solution (17) for $\lambda = 3, \mu = 2, c = -1, a = 1, b = 1, x = 0$ for the interval $-10 \leq y \leq 10$ and $-10 \leq t \leq 10$. Fig. 5 designates singular kink type soliton emerged from the solution (29) for $\lambda = 4, \mu = 2, c = -5, h = -5, r = 1$ within $-10 \leq x \leq 10$ and $-10 \leq t \leq 10$. Fig. 6 represents kink soliton from the solution (29) for $\lambda = 7, \mu = 3, c = -5, h = -5, r = -1$ in the intervals $-10 \leq x \leq 10$ and $-10 \leq t \leq 10$. Fig. 7 designates cuspon emerged from solution (29) for $\lambda = 3, \mu = 4, c = 5, h = -1, r = -1$ for $-10 \leq x \leq 10$ and $-10 \leq t \leq 10$. Fig. 8 designates singular kink type soliton emerged from the solution (29) for $\lambda = -3, \mu = 0, c = 5, h = -3, r = 1$ in the interval $-10 \leq x \leq 10$ and $-10 \leq t \leq 10$.

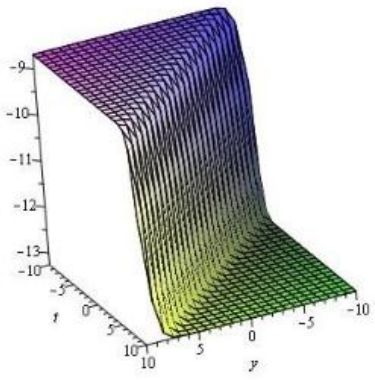

Fig. 1

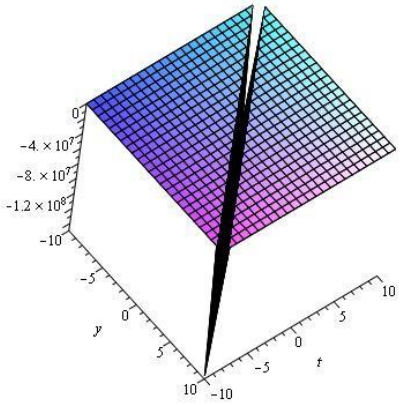

Fig. 2

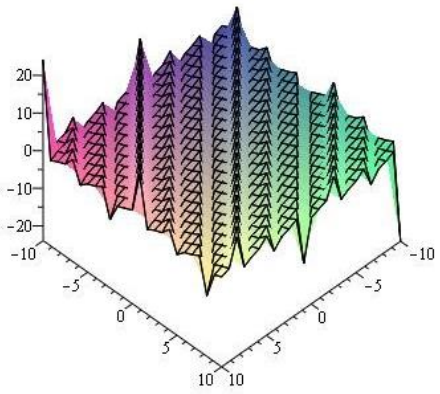

Fig. 3

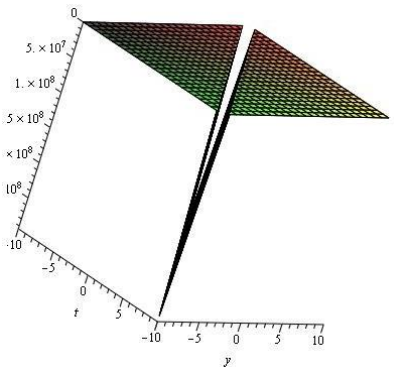

Fig. 4

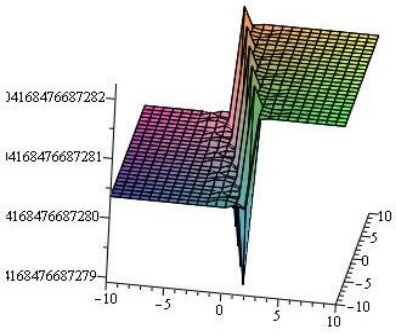

Fig. 5

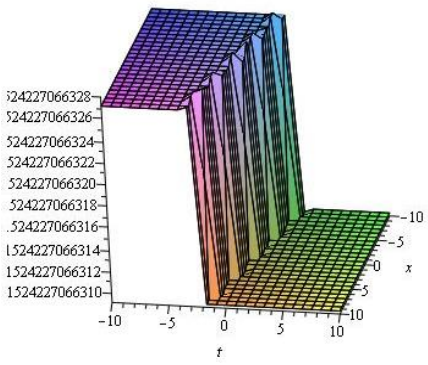

Fig. 6

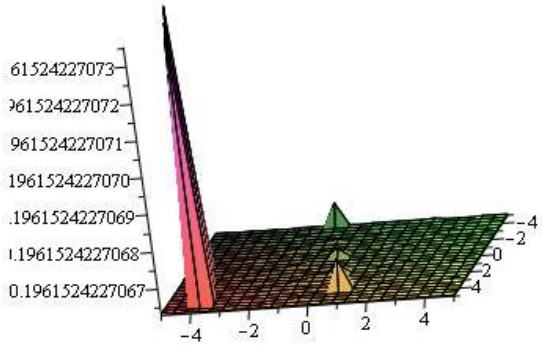

Fig. 7

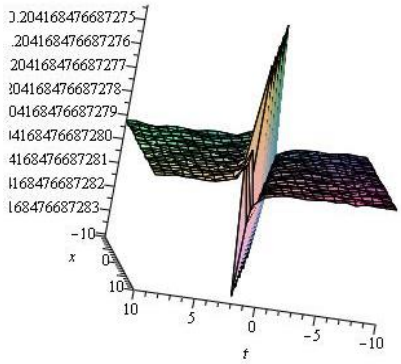

Fig. 8

5 Conclusions

The determination of this article was to investigate closed form analytic solutions to the cKG and BO equations by employing the rational (G^'/G)-expansion method. Consequently, different and advanced travelling wave solutions to the considered equations have successfully been furnished, on comparison to other methods available in the literature. Our derived solutions might effectively be helpful to depict the interior behaviors of internal mechanisms of nature world like describing shallow water waves, acoustic waves etc. The gained hyperbolic, trigonometric and rational function solutions together with the physical appearances show the efficiency and the reliability of our employed method which might be used in further research works to find fresh and further general solutions of any other NLPDEs in different fields.

References

[1] Wazwaz, A.M., 2002. Partial differential equations: methods and applications. AA Balkema.

[2] Helal, M.A. and Mehanna, M.S., 2006. A comparison between two different methods for solving KdV–Burgers equation. Chaos, *Solitons & Fractals*, 28(2), pp.320-326.

[3] Parkes, E.J. and Duffy, B.R., 1996. An automated tanh-function method for finding solitary wave solutions to non-linear evolution equations. *Computer Physics Communications*, 98(3), pp.288-300.

[4] Abdou, M.A., 2007. The extended tanh method and its applications for solving nonlinear physical models. *Applied mathematics and computation*, 190(1), pp.988-996.

[5] Kudryashov, N.A., 1990. Exact solutions of the generalized Kuramoto-Sivashinsky equation. *Physics Letters A*, 147(5-6), pp.287-291.

[6] Kudryashov, N.A., 2005. Simplest equation method to look for exact solutions of nonlinear differential equations. *Chaos, Solitons & Fractals*, 24(5), pp.1217-1231.

[7] Xu, G., 2006. An elliptic equation method and its applications in nonlinear evolution equations. *Chaos, Solitons & Fractals*, 29(4), pp.942-947.

[8] Parkes, E.J., Duffy, B.R. and Abbott, P.C., 2002. The Jacobi elliptic-function method for finding periodic-wave solutions to nonlinear evolution equations. *Physics Letters A*, 295 (5-6), pp.280-286.

[9] He, J.H. and Wu, X.H., 2006. Exp-function method for nonlinear wave equations. *Chaos, Solitons & Fractals*, 30(3), pp.700-708.

[10] Naher, H., Abdullah, F.A. and Akbar, M.A., 2012. New traveling wave solutions of the higher dimensional nonlinear partial differential equation by the Exp-function method. *Journal of Applied Mathematics*, 2012.

[11] Khan, K., Akbar, M. A. and Alam, M. N., 2013. "Travelling wave solutions of the nonlinear Drinfel'd-Shokolov-Wilson equation and modified Benjamin-Bona-Mahony equations," *Journal of the Egyptian Mathematical Society*, 21, pp. 233-240.

[12] Islam, M.H., Khan, K., Akbar, M.A. and Salam, M.A., 2014. Exact traveling wave solutions of modified KdV–Zakharov–Kuznetsov equation and viscous Burgers equation. *SpringerPlus*, 3(1), pp.1-9.

[13] Wang, M., Li, X. and Zhang, J., 2008. The (G′ G)-expansion method and travelling wave solutions of nonlinear evolution equations in mathematical physics. *Physics Letters A*, 372(4), pp.417-423.

[14] Ebadi, G. and Biswas, A., 2011. The G′ G method and topological soliton solution of the K (m, n) equation. *Communications in Nonlinear Science and Numerical Simulation*, 16(6), pp.2377-2382.

[15] Biswas, A., 2009. Solitary wave solution for the generalized Kawahara equation. *Applied Mathematics Letters*, 22(2), pp.208-210.

[16] Biswas, A., Petković, M.D. and Milović, D., 2010. Topological and non-topological exact soliton solution of the power law KdV equation. *Communications in Nonlinear Science and Numerical Simulation*, 15(11), pp.3263-3269.

[17] Chun, C. and Sakthivel, R., 2010. Homotopy perturbation technique for solving two-point boundary value problems–comparison with other methods. *Computer Physics Communications*, 181(6), pp.1021-1024.

[18] Sakthivel, R., Chun, C. and Lee, J., 2010. New travelling wave solutions of Burgers equation with finite transport memory. *Zeitschrift für Naturforschung A*, 65(8-9), pp.633-640.

[19] He, J.H. and Wu, X.H., 2006. Exp-function method for nonlinear wave equations. *Chaos, Solitons & Fractals*, 30(3), pp.700-708.

[20] Ma, W.X., Huang, T. and Zhang, Y., 2010. A multiple exp-function method for nonlinear differential equations and its application. *Physica Scripta*, 82(6), p.065003.

[21] Zheng, B., 2011. A new Bernoulli sub-ODE method for constructing traveling wave solutions for two nonlinear equations with any order. *UPB Sci. Bull., Series A*, 73(3), pp.85-94.

[22] Zheng, B., 2012. Soling a nonlinear evolution equation by a proposed Bernoulli sub-ODE method. *In Int. Conf. Image Vis. Comput.*

[23] Abbasbandy, S., 2010. Homotopy analysis method for the Kawahara equation. *Nonlinear Analysis: Real World Applications*, 11(1), pp.307-312.

[24] Molabahrami, A. and Khani, F., 2009. The homotopy analysis method to solve the Burgers–Huxley equation. *Nonlinear Analysis: Real World Applications*, 10(2), pp.589-600.

[25] Molliq, Y., Noorani, M.S.M. and Hashim, I., 2009. Variational iteration method for fractional heat-and wave-like equations. *Nonlinear Analysis: Real World Applications*, 10(3), pp.1854-1869.

[26] Mohyud-Din, S.T., Noor, M.A. and Noor, K.I., 2009. Modified Variational Iteration Method for Solving Sine-Gordon Equations, *World Applied Sciences Journal*, 6(7), pp. 999-1004.

[27] Lee, J. and Sakthivel, R., 2014. Exact travelling wave solutions of a variety of Boussinesq-like equations.," *Chinese Journal of Physics*, 52(3), pp. 939-957.

[28] Ganji, D.D., 2006. The application of He's homotopy perturbation method to nonlinear equations arising in heat transfer. *Physics Letters A*, 355(4-5), pp.337-341.

[29] Ganji, D.D., Afrouzi, G.A. and Talarposhti, R.A., 2007. Application of variational iteration method and homotopy–perturbation method for nonlinear heat diffusion and heat transfer equations. *Physics Letters A*, 368(6), pp.450-457.

[30] Wang, M., 1995. Solitary wave solutions for variant Boussinesq equations. *Physics letters A*, 199(3-4), pp.169-172.

[31] Ablowitz, M.J., Ablowitz, M.A., Clarkson, P.A. and Clarkson, P.A., 1991. Solitons, nonlinear evolution equations and inverse scattering (Vol. 149). *Cambridge University Press*, UK.

[32] Rogers, C. and Shadwick, W.F., 1982. Bäcklund transformations and their applications. *Academic Press*, New York.

[33] Jianming, L., Jie, D. and Wenjun, Y., 2011, January. Bäcklund transformation and new exact solutions of the Sharma-Tasso-Olver equation. *In Abstract and Applied Analysis* (Vol. 2011). Hindawi.

[34] Seadawy, A.R., 2015. Fractional solitary wave solutions of the nonlinear higher-order extended KdV equation in a stratified shear flow: Part I. *Computers & Mathematics with Applications*, 70(4), pp.345-352.

[35] Seadawy, A.R., 2016. Three-dimensional nonlinear modified Zakharov–Kuznetsov equation of ion-acoustic waves in a magnetized plasma. *Computers & Mathematics with Applications*, 71(1), pp.201-212.

[36] Arshad, M., Seadawy, A., Lu, D. and Wang, J., 2016. Travelling wave solutions of generalized coupled Zakharov–Kuznetsov and dispersive long wave equations. *Results in Physics*, 6, pp.1136-1145.

[37] Seadawy, A.R., El-Kalaawy, O.H. and Aldenari, R.B., 2016. Water wave solutions of Zufiria's higher-order Boussinesq type equations and its stability. *Applied Mathematics and Computation*, 280, pp.57-71.

[38] Islam, M., Akbar, M.A. and Azad, A.K., 2015. A Rational (G'/G)-expansion method and its application to the modified KdV-Burgers equation and the (2+ l)-dimensional Boussinesq equationn. *Nonlinear Studies*, 22(4).

[39] Islam, M.T., Akbar, M.A. and Azad, M.A.K., 2017. Multiple closed form wave solutions to the KdV and modified KdV equations through the rational (G′/G)-expansion method. *Journal of the Association of Arab Universities for Basic and Applied Sciences*, 24, pp.160-168.

[40] Islam, M.T., Ali, M.A. and Hasan, M.R., Closed Form Wave Solutions to the Nonlinear Partial Differential Equations via the Rational)/'(GG-Expansion Method. *International Journal for Research in Applied Science & Engineering Technology*, 6(2), pp 1519-1525.

[41] Akbar, M.A., Ali, N.H.M. and Islam, M.T., 2019. Multiple closed form solutions to some fractional order nonlinear evolution equations in physics and plasma physics. *AIMS Mathematics*, 4(3), pp.397-411.

This page is left intentionally blank

Journal of Engineering Advancements (JEA)

DOI: https://doi.org/10.38032/jea

Indexed by:

Volume 02 Issue 01

DOI: https://doi.org/10.38032/jea.2021.01

Published by: SciEn Publishing Group

Website: www.scienpg.com